# PREDICTION MODEL FOR THE ONSET OF EDGE-EFFECT DELAMINATION AT HOLES IN COMPOSITE LAMINATES

by

Doron Shalev

Dissertation submitted to the Faculty of the
Virginia Polytechnic Institute and State University
in partial fulfillment of the requirements for the degree of

DOCTOR OF PHILOSOPHY
in
Engineering Science and Mechanics

APPROVED:

K. L. Reifsnider

C. W. Smith

R. T. Haftka

R. M. Jones

R. A. Heller

July, 1988

Blacksburg, Virginia

PREDICTION MODEL FOR THE ONSET OF EDGE-EFFECT DELAMINATION AT HOLES IN COMPOSITE LAMINATES

by

Doron Shalev

Committee Chairman: K. L. Reifsnider

Engineering Science and Mechanics

(ABSTRACT)

Composite laminates are prone to delamination at free edges, straight edges or at holes, due to the mismatch at interfaces where two adjacent plies have different fiber orientations and/or different material properties. The linear analysis of the mismatch at the edge results in a mathematical singularity. That phenomenon occurs in a boundary layer and has to be treated mathematically and physically as such. In the literature it is called the "Boundary Layer Effect" or simply the "Edge Effect". It is of great importance to recognize and be able to predict delamination locations at edges prone to such events. The goal of this research was to create a model capable of providing such a prediction. In an effort to generalize the model, the more complicated case of a free edge at holes in the composite laminate was chosen rather then the case of a straight free edge.

A sequel of three major efforts was completed: 1) Development of the analysis of the free-edge effect at a hole in a composite laminate, 2) Performance of an extensive experimental program to provide data for the creation of the prediction model, and 3) On the basis of the analysis,

establishment of the model, and comparison with the experimental results.

The prediction model consists of two major products of the analysis, the order of the singularity and the strain energy release rate. Both are useful in locating the interface most prone to delaminate and the point along the hole circumference where it initiates.

Two material systems (AS4/3501-6 and AS4/1808) and two stacking sequences $[(0/45/0/-45)_s)_4]$ and $[(0/45/90/-45)_s]_4$, quasi-orthotropic and quasi-isotropic respectively, were quasi-statically tested under tension and compression. The specimens were X-rayed after each loading stage in order to locate the initiation of delaminations. The fact that both materials consisted of the same type of fibers, was an excellent opportunity to examine the performance of the matrix and its influence on the process of delamination. Matrix dependent behavior was successfully examined and studied through the experiments and the prediction model. Results showed good correlation and high sensitivity to the type of matrix material involved.

## ACKNOWLEDGEMENTS

This study was supported in part by the United States Air Force Office of Scientific Research under grant no. 85.0087. Acknowledgment is expressed and appreciated. Large support, fruitful guidance and interesting discussions are acknowledged to the chairman of my committee Prof. Reifsnider. Thanks to C. R. Bakis who guided me through the fascinating world of experiments. Special thanks to Dr. A. Unger of Israel Aircraft Industry who navigated me toward that turning point in my life. Finally, I thank my wife *Esti* and "my three sons" (not the TV show), *Naftaly*, *Eilon* and *Gad* for major support and I take the opportunity to apologize for being too committed to that work rather than to them.

Thanks Joe Kennedy, for making me a happy person during the last year

TABLE OF CONTENTS

LIST OF ILLUSTRATIONS

## LIST OF TABLES

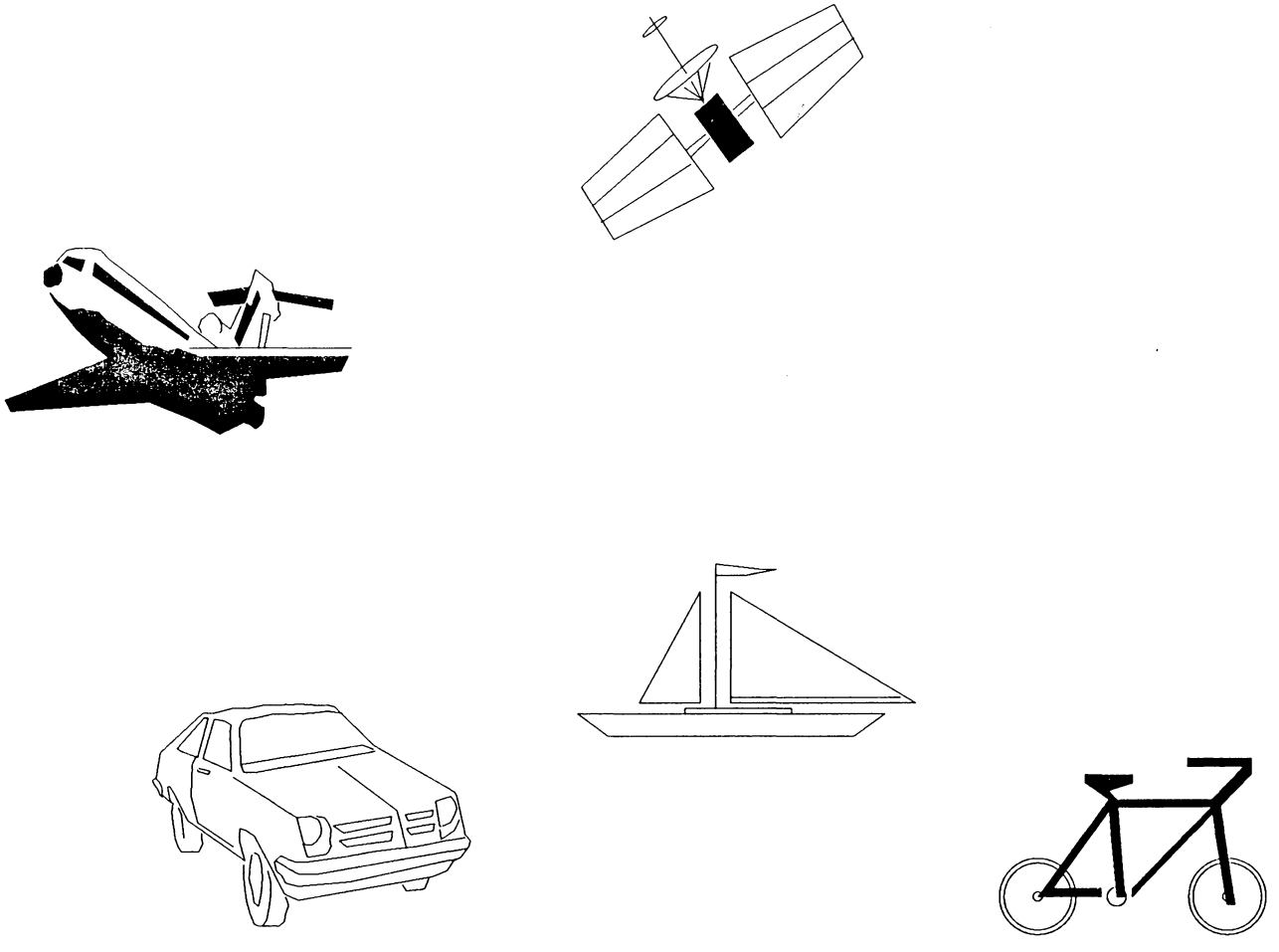

Composites Everywhere - Prone to Delamination !!!

# Chapter 1

# INTRODUCTION

It is known that a wide range of properties and performance can be achieved through the utilization of composite laminates in structures, since it is possible to adjust the ply orientations, stacking sequence, and thickness. At the edge of the laminate, however, high values of stresses are often obtained due to ply deformation mismatching, which may lead to delamination. That delamination can be controlled by artificial means such as stitching, tufting, or constraining the edge by caps.

A more natural procedure is available through optimization of fiber orientation, weaving, and layer sequencing in the vicinity of the edge in order to reduce edge effects, or even by reversing the situation by changing tension conditions to compression. In order to utilize the above mentioned improvements, a tool is needed to provide the means to locate and qualify locations prone to delaminate, so that we can make the necessary changes. This tool should consist of a prediction model and the supporting analysis.

In the search for such a criterion, some parameters involved in the analysis are investigated as major factors which control the phenomenon. These parameters are the order of stress singularity, the free edge stress intensity factors, and energy considerations associated with the energy release rate.

Even though a singularity is the result of a mathematical procedure within a boundary layer, and not a physical parameter, its order

reflects a local trend and rate. Thus, comparing the order of the singularity at different locations results in the method of rating the vulnerability to delamination in those positions.

There are three major steps in the investigation of the problem of delaminations at free edges. First, a proper way to analyze the phenomenon of the edge effect at holes should be developed. Than, a prediction model should be built upon that analysis. Finally, it is essential to compare the analysis-based model with the result of appropriate experiments. The next few sections will examine the present situation in conjunction with the above-mentioned steps, and then preview the scope of the current investigation.

## 1.1 Survey of the state of the art

As mentioned above, two major aspects of the current research are surveyed in the literature. (1) the analysis of edge effects at composite laminates at free edges and at holes, and (2) the development and utilization of a prediction model for the onset of delamination.

### 1.1.1 The edge effect in composite laminates

The behavior of the stress field at edges of composite laminates due to the deformation mismatching has been the subject of extensive investigation during the last two decades. Pipes and Pagano (1970) used a finite difference method to solve the relevant elasticity equations, whereas Wang and Crossman (1977) employed a finite element approach to

investigate this phenomenon. Recently, an approximate method was presented by Lagace (1987) using the force balance method in conjunction with minimization of energy. Due to the approximate nature of the approaches involved in the previous studies, it was not possible to determine the order of singularity of the stresses at the free edges. Wang and Choi (1982) derived an analytical solution, following a Lekhnitskii (1963) formulation, and obtained the exact order of singularity at the edge of the laminate. Their derivation involves a special form of Lekhnistkii's stress potentials which explicitly includes a parameter identified as the order of the singularity. However, their solution for the stresses is approximate, and due to mathematical difficulties the method was only applied to the analysis of special types of laminates at the straight free edge, as was done by the previously mentioned researchers.

### 1.1.2 Models for delamination prediction

The significance of the ability to predict the onset of delaminations in composites, as discussed above, drove many investigators to postulate methods and models to provide such a tool.

The simple idea of looking at high values of stresses or strains at the region of influence of the phenomenon was applied by various investigators. Klang and Hyer (1985) used the finite element method to calculate the distribution of strains looking for the maximum as a criterion for initiation of delamination. Kim and Soni (1984) looked at the distribution of the out-of-plane interlaminar stress, then averaged

that stress along a fixed distance called the critical length taken as one ply thickness, assuming failure to occur when the average value reached some interlaminar tensile strength. That critical stress is very difficult to determine and so was taken as the transverse strength of the composite material.

Pagano and Pipes (1972) searched for a fast and simple way to look for initiation, provides an engineering tool, easy apply. In doing so, they looked at the transverse planner stresses resulting from classical lamination theory, and the moments these stresses apply on the interfaces. Then stresses were calculated utilizing these moments, and the most vulnerable interface was predicted simply by comparison of those stresses.

O'Brien (1982) looked at the energy release rate at the interfaces at free edges of the laminate. The calculation of the energy release rate was based on the stiffness loss due to delamination, calculated by means of classical lamination theory. The expression for the energy release rate is as follows,

$$G = \frac{\varepsilon^2 t}{2} (E_{lam} - E^*)$$

where, $\varepsilon$ is the nominal axial strain at the undelaminated laminate, t is the laminate thickness, $E_{lam}$ is the axial laminate stiffness calculated from classical lamination theory. $E^*$ is axial stiffness of the laminate when completely delaminated along one or more interfaces, calculated by the stiffnesses of the separated, delaminated parts weighted by the number of plies in each sublaminate.

## 1.2 Scope of investigation

The overall process of the current research is presented in fig. 1 which shows the logical flow-chart to be followed. The two main branches, as reflected in the flow-chart, are the analytical path and the experimental one. The following is a brief discussion of the intentions and methods employed in both.

As previously described, none of the analyses of the free edge effect except the one done by Wang and Choi (1982) included the mathematical singularity as it appears at the free edge. Indeed, comparison of the results of the different approaches shows discrepancies, sometimes resulting in an opposite stress sign indicating tension instead of compression as it should be. None of the analyses deals with the problem of the free edge at a hole. In the present work, the approach of Wang and Choi (1982) is followed for the analysis of a laminated plate with an elliptical hole. The proposed method is general and can be applied to any type of composite laminate with an elliptical hole. For the special case when the effect of the hole is disregarded, the general method is applicable to the special types of laminates treated by Wang and Choi (1982). The analysis leads to an over-determined system of equations which shows ill-conditioned behavior. This mathematical obstacle is overcome by adopting the Singular Value Decomposition Method, Stewart (1973), to determine the real rank of the matrix when it is less than full rank.

Since the mathematical singularity plays an important role in the analysis, it has to find its way to the prediction model, too. That is, in the formulation of the strain energy release rate, and the order of

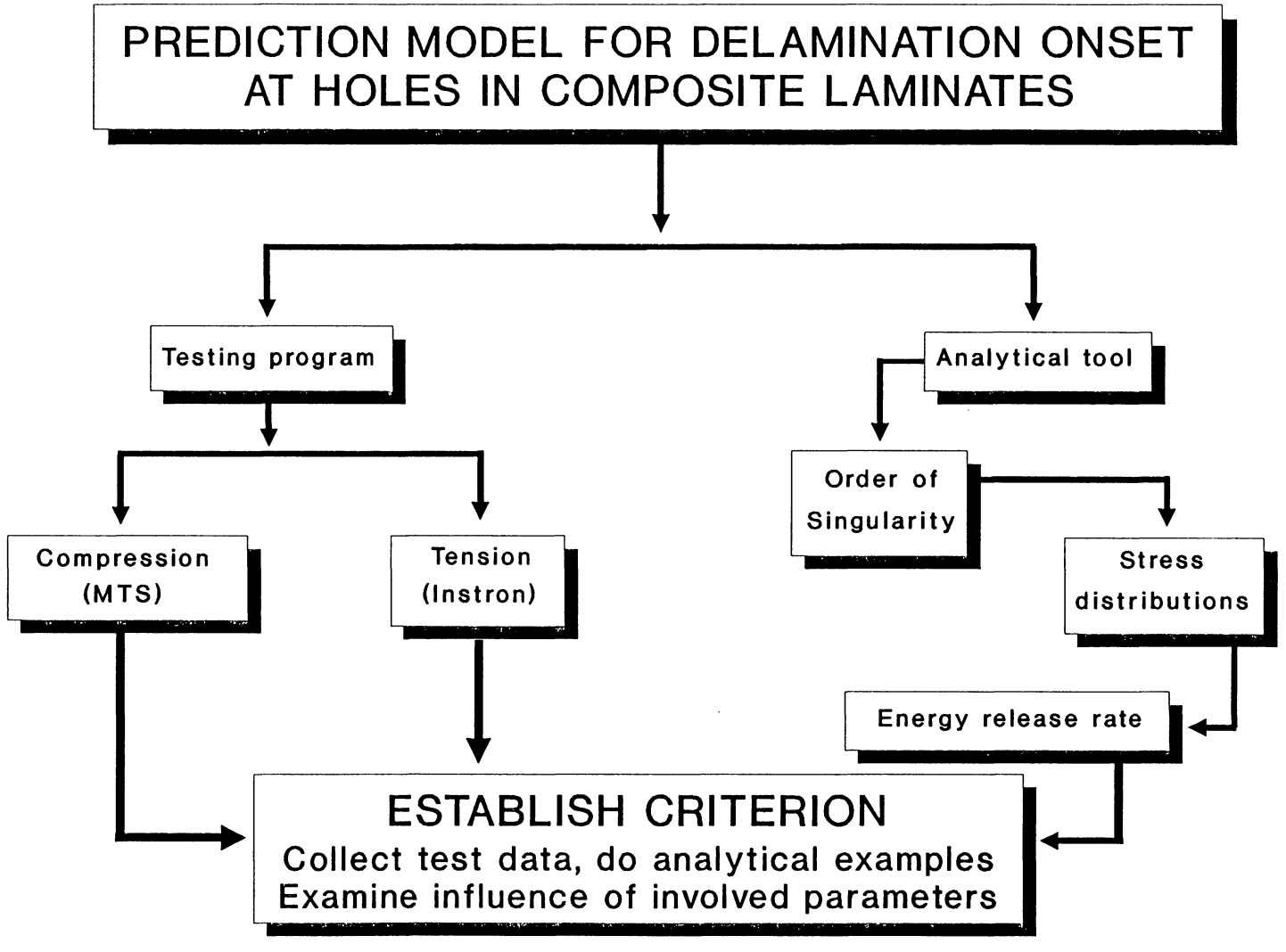


Figure No. 1.: Research methodology; flow-chart

the singularity as a stand-alone parameter as well. The importance of the order of singularity as a physical parameter rather then merely as a mathematical one will be discussed and explained within the context of the boundary layer effect.

Finally, a series of experiments is to be presented, analyzed, and examined in conjunction with the prediction model. In order to meet as many objectives as possible, the testing program consists of various types of materials with different matrix systems and different stacking sequences, as well as different loading (tension and compression).

# Chapter 2

## ANALYSIS OF THE EDGE EFFECT AT ELLIPTICAL HOLES IN COMPOSITE PLATE

The development of a solution for the free edge effect at holes in a composite plate is described in this chapter. The governing equations consist of differential equations and therefore are decomposed into homogeneous and particular parts. The derivation of the homogeneous solution is identical to the method of Wang and Choi (1982). The particular solution satisfies the governing equations, free edge conditions, the interfacial continuity relations, and the upper and lower traction-free surface requirements and represents the influence of the hole. The effect of an elliptical hole is incorporated by adopting Lekhnitskii's solution for anisotropic plates containing an elliptical cavity. By conversion of the composite laminate into an anisotropic plate via classical lamination theory (Jones (1975)), the strains were evaluated from Lekhnitskii's solution. The corresponding stresses in the different plies can thus be determined. As the analysis is based on a set of eigenvalues and includes some numerical integration, the accuracy of the results was assessed and demonstrated by selecting various numbers of eigenvalues and points of integration. Results are given which exhibit the effect of the hole's edge on the behavior of stresses within the boundary layer and, for special cases, throughout the laminate.

## 2.1 Basic formulation

### 2.1.1 Solution methodology

Consider a composite laminate containing an elliptical cutout as shown in fig. 2. A system of Cartesian coordinates is introduced whose origin is located at the bore edge at the examined interface and its orientation follows the scanning azimuth in a way that $x_1$ axis is always radially oriented away from the center of the hole. Every lamina is assumed to be elastic and anisotropic, obeying the generalized Hooke's law:

$$\{\varepsilon\} = [S]\{\sigma\} \tag{1}$$

in which $\{\varepsilon\}$ are the strain components of the $m^{th}$ ply,

$$\{\varepsilon\} = [\varepsilon_{11}, \varepsilon_{22}, \varepsilon_{33}, 2\varepsilon_{23}, 2\varepsilon_{13}, 2\varepsilon_{12}]^T$$

The solution methodology follows Lekhnitskii's (1963) approach for anisotropic plates as used by Wang and Choi (1982). The problem is treated as a boundary layer problem. It is somewhat similar to the aerodynamic problem of viscous flow around an airfoil. In the aerodynamic problem, we consider a streaming flow past a slender body. The fluid viscosity is taken to be relatively small and the shearing stresses developed are very small. It is known that except for a thin layer adjacent to the solid body, the transverse velocity gradients are negligibly small throughout the flow field. However, within that thin

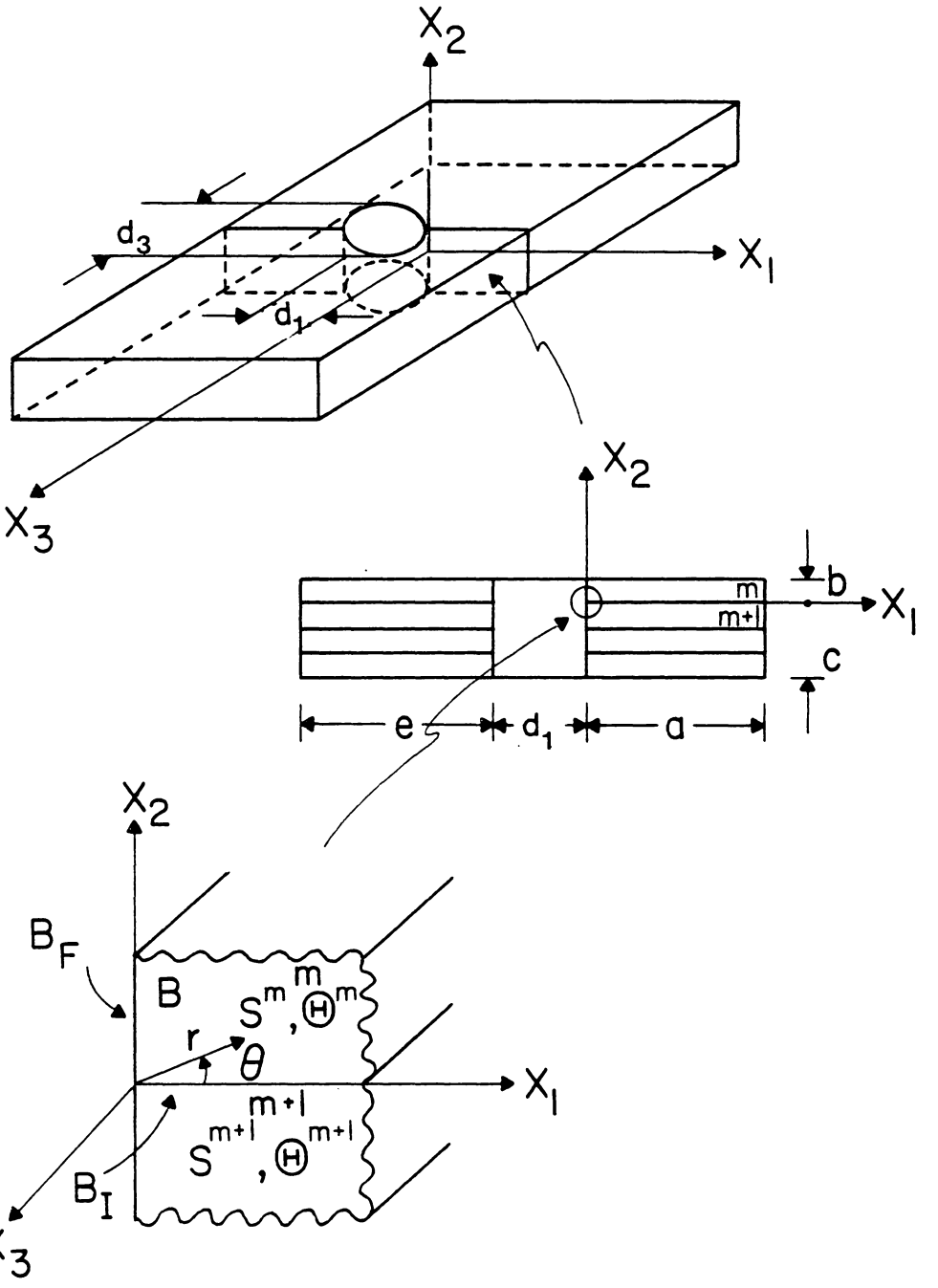


Figure No. 2: Geometry and coordinates of composite laminate with embedded elliptical hole

boundary layer, large shearing velocities are produced resulting in large shear stresses. The importance of this concept is that it allows us to apply the more complicated equations related to the boundary only within that thin layer, and some appreciable simplifying assumptions can reasonably be made. In the aerodynamics case, these are the viscous motion equations. In our case, the boundary layer is a relatively thin region at the vicinity of the edge. At the free edge the stress field is singular and thus its values are infinite. Within the boundary layer stresses change rapidly from the edge to the other side of the region where they agree with results from classical lamination theory, Jones (1975), and anisotropic plates, Lekhnitskii (1963). Within the boundary layer, changes with respect to $x_1$ and $x_2$ are considered to be larger than changes with respect to $x_3$. Thus, within that region we may simplify the problem and neglect variations with respect to $x_3$ requiring compatibility with the above mentioned solutions which take changes with respect to $x_3$ into account such as the solution of an anisotropic plate with cavity, Lekhnitskii (1963). Several assumptions should be noted:

1. The composite laminate is of finite width.
2. The laminate is long enough such that end effects can be neglected.
3. Due to the neglect of variations with respect to $x_3$ we may assume a state of generalized plane deformation within the boundary layer.

The equilibrium equations, in the absence of body forces, are given by

$$\sigma_{ij,j} = 0 \qquad i,j = 1,2,3 \qquad (2)$$

Due to assumption 3, derivatives with respect to $x_3$ are omitted, reducing (2) to

$$\sigma_{11,1} + \sigma_{12,2} = 0 \qquad \text{(a)}$$

$$\sigma_{21,1} + \sigma_{22,2} = 0 \qquad \text{(b)} \qquad (3)$$

$$\sigma_{31,1} + \sigma_{32,2} = 0 \qquad \text{(c)}$$

The small strain tensor is given in terms of the displacements $u_i$ by

$$\varepsilon_{ij} = \frac{1}{2}(u_{i,j} + u_{j,i}) \qquad (4)$$

Using (4) in (1) and integrating provides

$$u_1 = -\frac{1}{2} A_1 S_{33} x_3^2 - A_4 x_2 x_3 + U_1(x_1, x_2) + \omega_2 x_3 - \omega_3 x_2 + u_{10} \qquad \text{(a)}$$

$$u_2 = -\frac{1}{2} A_2 S_{33} x_3^2 + A_4 x_1 x_3 + U_2(x_1, x_2) + \omega_3 x_1 - \omega_1 x_3 + u_{20} \qquad \text{(b)} \qquad (5)$$

$$u_3 = (A_1 x_1 + A_2 x_2 + A_3) S_{33} x_3 + U_3(x_1, x_2) + \omega_1 x_2 - \omega_2 x_1 + u_{30} \qquad \text{(c)}$$

where $u_{i0}$ and $\omega_i$ are rigid-body translations and rotations, respectively. The stress in the longitudinal direction, $\sigma_{33}$ is given by,

$$\sigma_{33} = A_1 x_1 + A_2 x_2 + A_3 - \frac{S_{3j}\sigma_j}{S_{33}} \qquad (6)$$

where j=1,2,4,5,6 using the contracted Greek notation for stresses.

The derivatives of functions $U_1(x_1,x_2), U_2(x_1,x_2), U_3(x_1,x_2)$ are expressed in the form

$$U_{1,1} = \tilde{S}_{1j}\sigma_j + S_{13}(A_1x_1 + A_2x_2 + A_3) \qquad (a)$$

$$U_{2,2} = \tilde{S}_{2j}\sigma_j + S_{23}(A_1x_1 + A_2x_2 + A_3) \qquad (b)$$

$$U_{3,1} = \tilde{S}_{5j}\sigma_j + S_{53}(A_1x_1 + A_2x_2 + A_3) + A_4x_2 \qquad (c) \qquad (7)$$

$$U_{3,2} = \tilde{S}_{4j}\sigma_j + S_{43}(A_1x_1 + A_2x_2 + A_3) - A_4x_1 \qquad (d)$$

$$U_{1,2} + U_{2,2} = \tilde{S}_{6j}\sigma_j + S_{63}(A_1x_1 + A_2x_2 + A_3) \qquad (e)$$

where $\tilde{S}$ is the reduced form of S given by:

$$\tilde{S}_{ij} = S_{ij} - \frac{S_{i3}S_{j3}}{S_{33}} \qquad i,j=1,2,4,5,6 \qquad (8)$$

Following Wang (1982), we adopt Lekhnitskii's stress potentials $F,\Psi$ defined by

$$\sigma_1 = \sigma_{11} = F_{,22}; \qquad \sigma_2 = \sigma_{22} = F_{,11}; \qquad \sigma_4 = \sigma_{23} = -\Psi_{,1};$$

$$\sigma_5 = \sigma_{13} = \Psi_{,2}; \qquad \sigma_6 = \sigma_{12} = -F_{,12} \qquad (9)$$

Equation (9) satisfies (3) and when used in conjunction with (5) & (7) it creates a system of governing equations that can be expressed in terms of partial differential operators which have the form:

$$\begin{cases} L_3 F + L_2 \Psi = -2A_4 + A_1 S_{34} - A_2 S_{35} \\ L_4 F + L_3 \Psi = 0 \end{cases} \tag{10}$$

where

$$L_2 = \tilde{S}_{44}\frac{\partial^2}{\partial x_1^2} - \tilde{S}_{45}\frac{\partial^2}{\partial x_1 \partial x_2} - \tilde{S}_{55}\frac{\partial^2}{\partial x_2^2} \tag{a}$$

$$L_3 = -\tilde{S}_{24}\frac{\partial^3}{\partial x_1^3} + (\tilde{S}_{25} + \tilde{S}_{46})\frac{\partial^3}{\partial x_1^2 \partial x_2} + (\tilde{S}_{14} + \tilde{S}_{56})\frac{\partial^3}{\partial x_1 \partial x_2^2} + \tilde{S}_{15}\frac{\partial^3}{\partial x_2^3} \tag{b}$$

$$L_4 = \tilde{S}_{22}\frac{\partial^4}{\partial x_1^4} - 2\tilde{S}_{26}\frac{\partial^4}{\partial x_1^3 \partial x_2} + (2\tilde{S}_{12} + \tilde{S}_{66})\frac{\partial^4}{\partial x_1^2 \partial x_2^2} - 2\tilde{S}_{16}\frac{\partial^4}{\partial x_1 \partial x_2^3} + \tilde{S}_{11}\frac{\partial^4}{\partial x_2^4} \tag{c}$$

(11)

### 2.1.2 Boundary conditions

We consider three types of boundary conditions, as follows in the next sections.

2.1.2.1 Traction-free edge boundary conditions

Assuming that the edges of the laminate and the hole are traction-free, it follows that

$$\sigma_{11} = \sigma_{13} = \sigma_{12} = 0 \qquad x_1 = 0, \quad x_2 = 0, \quad x_3 = 0 \tag{12}$$

2.1.2.2 End conditions

We require static equilibrium with the remote loading by forming the following integrals over the cross-sectional area B as shown if fig. 2 (Lekhnitskii, 1963)

$$\iint_B \sigma_{13} dx_1 dx_2 = 0 \tag{a}$$

$$\iint_B \sigma_{23} dx_1 dx_2 = 0 \tag{b}$$

$$\iint_B \sigma_{33} dx_1 dx_2 = P_{33} \tag{c}$$

(13)

$$\iint_B \sigma_{33} x_2 dx_1 dx_2 = M_{11} \tag{d}$$

$$\iint_B \sigma_{33} x_1 dx_1 dx_2 = M_{22} \tag{e}$$

$$\iint_B (\sigma_{23} x_1 - \sigma_{13} x_2) dx_1 dx_2 = M_{12} \tag{f}$$

For cases where analysis is done at an azimuthal angle $\alpha$ different than $0^{\circ}$, the coordinate system is rotated such that the $x_3$ axis is tangent to the hole surface and creates an angle $\alpha$ with respect to the longitudinal axis of the plate. The domain in which integration is carried out is cross-sectional area $B/\cos(\alpha)$.

2.1.2.3 The cavity boundary conditions

Special treatment is required in the vicinity of the hole. This is achieved by conversion of the laminate plate cross section into an anisotropic plate via its effective elastic constants $(E_x, E_y, G_{xy}, \nu_{xy})$ calculated by classical lamination theory, Jones (1975). Analysis of such a plate with cavity subjected to various loads, is done following Lekhnitskii (1963). The resulting strains, when multiplied by the stiffness components of the relevant ply, provide the planar stress distribution in that ply. These stress distributions are applicable away from the hole where the edge effects are negligible.

2.1.3 Interfacial continuity

Continuity of tractions must be satisfied at the interface between the m and m+1 plies:

$$\sigma_{2i}^{(m)} = \sigma_{2i}^{(m+1)} \qquad i = 1,2,3; \qquad x_2 = 0 \tag{14}$$

and the displacements must be continuous:

$$u_i^{(m)} = u_i^{(m+1)} \qquad i = 1,2,3; \qquad x_2 = 0 \tag{15}$$

## 2.2 Solution of the governing equations

The solution consists of two parts, homogeneous and particular solutions. The homogeneous part can be exactly derived and provides the stress singularities at the edges. On the other hand, the particular solution can not be exactly obtained, and an approximate method is applied.

### 2.2.1 The homogeneous solution

Following Lekhnitskii (1963), the general forms of his stress potential are taken in the form

$$F(x_1,x_2) = \sum_{k=1}^{6} F_k(Z_k) \tag{a}$$

$$\Psi(x_1,x_2) = \sum_{k=1}^{6} \eta_k F_k'(Z_k) \tag{b}$$

(16)

where $Z_k = x_1 + \mu_k x_2$, $\mu_k$ are the roots of the characteristic equation as shown below, $\eta_k$ are ratios of components of the characteristic equation, and $F_k'(Z_k)$ is the derivative w.r.t. the argument $Z_k$.

Regarding the homogeneous form of Eqn. (10), we consider the

potentials F and $\Psi$ to consist of two parts denoted by indices 1 and 0 designating the homogeneous and the particular solutions, respectively. The characteristic equation of the homogeneous solution is defined by the LHS of (10). Eliminating one of the functions, say $\Psi_1$, we obtain a $6^{th}$ order equation for the remaining $F_1$,

$$(L_4L_2 - L_3^2)F_1 = 0 \qquad \text{(a)}$$

which can be decomposed into (17)

$$D_6D_5D_4D_3D_2D_1F_1 = 0 \qquad \text{(b)}$$

where

$$D_k = \frac{\partial}{\partial x_2} - \mu_k \frac{\partial}{\partial x_1}$$

Consequently, new sets of operators are obtained from (11):

$$l_2 = \tilde{S}_{55}\mu^2 - 2\tilde{S}_{45}\mu + \tilde{S}_{44} \qquad \text{(a)}$$

$$l_3 = \tilde{S}_{15}\mu^3 - (\tilde{S}_{14} + \tilde{S}_{56})\mu^2 + (\tilde{S}_{25} + \tilde{S}_{46}) - \tilde{S}_{24} \qquad \text{(b)} \qquad (18)$$

$$l_4 = \tilde{S}_{11}\mu^4 - 2\tilde{S}_{16}\mu^3 + (2\tilde{S}_{12} + \tilde{S}_{66})\mu^2 - 2\tilde{S}_{26}\mu + \tilde{S}_{22} \qquad \text{(c)}$$

The resulting characteristic equation is

$$l_4(\mu)l_2(\mu)-l_3^2(\mu) = 0 \qquad \text{(a)}$$

also (19)

$$\eta_k = -\frac{l_3(\mu_k)}{l_2(\mu_k)} = -\frac{l_4(\mu_k)}{l_3(\mu_k)} \qquad \text{(b)}$$

It has been shown by Lekhnitskii (1963) that the $\mu_k$ are complex conjugates where the real part vanishes for orthotropic materials. Solving the polynomial (19), and substituting for the stresses and displacements (9) and (7), respectively, yields the following results designated by (h) for the homogeneous part of the solution,

$$\sigma_{11}^{(h)} = \sum_{k=1}^{6} \mu_k^2 F''(Z_k) \qquad \text{(a)}$$

$$\sigma_{22}^{(h)} = \sum_{k=1}^{6} F''(Z_k) \qquad \text{(b)}$$

$$\sigma_{23}^{(h)} = -\sum_{k=1}^{6} \eta_k F''(Z_k) \qquad \text{(c)}$$

$$\sigma_{13}^{(h)} = \sum_{k=1}^{6} \eta_k \mu_k F''(Z_k) \qquad \text{(d)} \qquad (20)$$

$$\sigma_{12}^{(h)} = -\sum_{k=1}^{6} \mu_k F''(Z_k) \qquad \text{(e)}$$

$$u_1^{(h)} = \sum_{k=1}^{6} p_k F'(Z_k) \qquad (f)$$

$$u_2^{(h)} = \sum_{k=1}^{6} q_k F'(Z_k) \qquad (g)$$

$$u_3^{(h)} = \sum_{k=1}^{6} t_k F'(Z_k) \qquad (h)$$

where

$$p_k = \tilde{S}_{11}\mu_k^2 + \tilde{S}_{12} - \tilde{S}_{14}\eta_k + \tilde{S}_{15}\eta_k\mu_k - \tilde{S}_{16}\mu_k \qquad (a)$$

$$q_k = \tilde{S}_{12}\mu_k + \frac{\tilde{S}_{22}}{\mu_k} - \frac{\tilde{S}_{24}\eta_k}{\mu_k} + \tilde{S}_{25}\eta_k - \tilde{S}_{26} \qquad (b) \qquad (21)$$

$$t_k = \tilde{S}_{14}\mu_k + \frac{\tilde{S}_{24}}{\mu_k} - \frac{\tilde{S}_{44}\eta_k}{\mu_k} + \tilde{S}_{45}\eta_k - \tilde{S}_{46} \qquad (c)$$

Following the idea of Wang and Choi (1982), the functions $F_k(Z_k)$ are expressed in the form

$$F_k(Z_k) = c_k \frac{Z_k^{\delta+2}}{(\delta+1)(\delta+2)} \qquad (22)$$

By choosing this particular expression, it can be readily shown (by performing second-order derivatives) that the general form of the stresses can be represented in the form

$$\sigma = Kr^{\delta} \qquad (23)$$

It is obvious that, by solving for $\delta$, we obtain the exact order of the singularity as r approaches zero. Equation (22) followed by (23) have to satisfy all boundary conditions and governing equations for the homogeneous and particular parts of the solution. Substituting (22) into (20) provides the following:

$$\sigma_{11}^{(h)} = \sum_{k=1}^{3} [c_k \mu_k^2 Z_k^{\delta} + c_{k+3} \bar{\mu}_k^2 \bar{Z}_k^{\delta}] \qquad (a)$$

$$\sigma_{22}^{(h)} = \sum_{k=1}^{3} [c_k Z_k^{\delta} + c_{k+3} \bar{Z}_k^{\delta}] \qquad (b)$$

$$\sigma_{23}^{(h)} = - \sum_{k=1}^{3} [c_k \eta_k Z_k^{\delta} + c_{k+3} \bar{\eta}_k \bar{Z}_k^{\delta}] \qquad (c)$$

$$\sigma_{13}^{(h)} = \sum_{k=1}^{3} [c_k \eta_k \mu_k Z_k^{\delta} + c_{k+3} \bar{\eta}_k \bar{\mu}_k \bar{Z}_k^{\delta}] \qquad (d) \qquad (24)$$

$$\sigma_{12}^{(h)} = - \sum_{k=1}^{3} [c_k \mu_k Z_k^{\delta} + c_{k+3} \bar{\mu}_k \bar{Z}_k^{\delta}] \qquad (e)$$

$$u_1^{(h)} = \sum_{k=1}^{3} [c_k p_k Z_k^{\delta+1} + c_{k+3} \bar{p}_k \bar{Z}_k^{\delta+1}]/(\delta + 1) \qquad (f)$$

$$u_2^{(h)} = \sum_{k=1}^{3} [c_k q_k Z_k^{\delta+1} + c_{k+3} \bar{q}_k \bar{Z}_k^{\delta+1}]/(\delta + 1) \qquad (g)$$

$$u_3^{(h)} = \sum_{k=1}^{3} [c_k t_k Z_k^{\delta+1} + c_{k+3} \bar{t}_k \bar{Z}_k^{\delta+1}]/(\delta + 1) \qquad (h)$$

It should be noted that the present contribution (23) from the homogeneous solution involves the parameter $\delta$. This parameter depends on the specific geometry in the close vicinity of the edge as well as on the elastic constants of the two adjacent plies. Thus, (23) is valid at the hole as well as at the plate edge, and refers to the relevant ply pair in which $\delta$ was calculated.

Substituting (22) into the free edge boundary conditions (12), yields three equations for each of the two adjacent plies, resulting in a total of six equations. Similarly, substitution into the interfacial conditions, (14) (15), contributes an additional six equations. There are six unknown coefficients $c_k$, k = 1-6, for each layer and the additional unknown power $\delta$. This system of 12 algebraic equations can be presented in a matrix form:

$$[A]\{C\} = 0 \tag{25}$$

where [A] is a 12x12 matrix whose elements involve $\delta$ as a power. In addition,

$$\{c\} = [c_k^{(m)},\ c_k^{(m+1)}]^T \qquad k = 1,2,3,4,5,6$$

This system establishes a nonlinear eigenvalue problem for which {C} are the eigenvectors and $\delta_i$ are the corresponding eigenvalues determined from the requirement that [A] must vanish for a non-trivial solution:

$$\det[A] = 0 \tag{26}$$

The solution of Eqn. (26) is performed by a deflation technique as presented by Muller (1956). Since (26) is a transcendental equation, an infinite set of solutions for $\delta$ is obtained. The algebraically smallest eigenvalue is a real number in [-1,0] and is the order of the singularity as explained by Wang and Choi (1982). For the case of an angle-ply laminate, the higher eigenvalues are either integers or pairs of conjugate complex numbers. The properly truncated set of eigenvalues is used in the particular solution to ensure convergence. Once (25) is solved, the stresses and displacements are obtained from (24) using the expressions:

$$\sigma_\alpha^{(h)} = \sum_n d_n^{(h)} f_{\alpha n}(x_1, x_2; \delta_n) \qquad \alpha = 1,2,4,5,6 \qquad \text{(a)}$$

$$u_\beta^{(h)} = \sum_n d_n^{(h)} g_{\beta n}(x_1, x_2; \delta_n) \qquad \beta = 1,2,3 \qquad \text{(b)} \qquad (27)$$

$$\sigma_3^{(h)} = - \frac{S_{3j}\sigma_j^{(h)}}{S_{33}} \qquad \text{(c)}$$

where $f_{\alpha n}$ and $g_{\beta n}$ are the eigenfunctions which coincide with the right-hand side of Eqn. (24) and include the infinite set of $\delta_n$. The infinite set of coefficients $\{d_n^{(h)}\}$ is to be determined in conjunction with the particular solution. A computer program, called "SINGULAR", was developed on a personal computer to provide the list of eigenvalues and the order of singularity. See Appendix B for a description and explanations of that code.

2.2.2 The particular solution

A particular solution (denoted by superscript p) to Eqn. (10) is expressed in the form :

$$F^{(p)} = a_1x_1^3 + a_2x_1^2x_2 + a_3x_1x_2^2 + a_4x_2^3 + a_5x_1^2 + a_6x_1x_2 + a_7x_2^2$$

$$\Psi^{(p)} = a_8x_1^2 + a_9x_1x_2 + a_{10}x_2^2 + a_{11}x_1 + a_{12}x_2 \qquad (28)$$

Substitution of Eqn. (28) into Eqn. (9) yields

$$\sigma_{11}^{(p)} = 2a_3x_1 + 6a_4x_2 + 2a_7 \qquad (a)$$

$$\sigma_{22}^{(p)} = 6a_1x_1 + 2a_2x_2 + 2a_5 \qquad (b)$$

$$\sigma_{23}^{(p)} = -2a_8x_1 - a_9x_2 - a_{11} \qquad (c) \qquad (29)$$

$$\sigma_{13}^{(p)} = a_9x_1 + 2a_{10}x_2 + a_{12} \qquad (d)$$

$$\sigma_{12}^{(p)} = -2a_2x_1 - 2a_3x_2 - a_6 \qquad (e)$$

and

$$\sigma_{33}^{(p)} = (A_1x_1 + A_2x_2 + A_3) - \frac{S_{3j}\sigma_j^{(p)}}{S_{33}} \qquad (30)$$

The expression of the particular part of the displacements, $u_i^{(p)}$, follows exactly the form of Eqns. (5a-c), in which

$$U_1^{(p)} = \frac{1}{2} G_{11} x_1^2 + G_{12} x_1 x_2 + G_{13} x_1 + \frac{1}{2} (G_{62} - G_{21}) x_2^2 + \frac{1}{2} G_{63} x_2 \qquad (a)$$

$$U_2^{(p)} = G_{12} x_1 x_2 + \frac{1}{2} G_{22} x_2^2 + G_{23} x_2 + \frac{1}{2} (G_{61} - G_{12}) x_1^2 + \frac{1}{2} G_{63} x_1 \qquad (b) \quad (31)$$

$$U_3^{(p)} = \frac{1}{2} G_{51} x_1^2 + (G_{52} + A_4) x_1 x_2 + G_{53} x_1 + \frac{1}{2} G_{42} x_2^2 + G_{43} x_2 \qquad (c)$$

and

$$G_{j1} = 2\tilde{S}_{j1} a_3 + 6\tilde{S}_{j2} a_1 - 2\tilde{S}_{j4} a_8 + \tilde{S}_{j5} a_9 - \tilde{S}_{j6} a_2 + S_{j3} A_1 \qquad (a)$$

$$G_{j2} = 6\tilde{S}_{j1} a_4 + 2\tilde{S}_{j2} a_2 - \tilde{S}_{j4} a_9 + 2\tilde{S}_{j5} a_{10} - 2\tilde{S}_{j6} a_3 + S_{j3} A_2 \qquad (b) \quad (32)$$

$$G_{j3} = 2\tilde{S}_{j1} a_7 + 2\tilde{S}_{j2} a_5 - \tilde{S}_{j4} a_{11} + \tilde{S}_{j5} a_{12} - \tilde{S}_{j6} a_6 + S_{j3} A_3 \qquad (c)$$

$$j = 1,2,4,5,6$$

The coefficients in Eqn. (28) are determined by satisfaction of the governing equations (10), the traction-free boundary conditions Eqn. (12), and the interfacial conditions (14,15). To this end, a system of 34 linear algebraic equations is obtained for the 44 unknown coefficients in Eqns. (29)-(32). Equation (10) yields:

$$-6\tilde{S}_{24}a_1 + 2(\tilde{S}_{25} + \tilde{S}_{46})a_2 - 2(\tilde{S}_{14} + \tilde{S}_{56})a_3 + 6\tilde{S}_{15}a_4 + \tilde{S}_{44}a_8$$

$$- 2\tilde{S}_{45}a_9 + 2\tilde{S}_{55}a_{10} = - 2A_4 + A_1S_{34} - A_2S_{35} \qquad \text{(a)}$$

(33)

$$a_i^{(m),(m+1)} = 0 \qquad i = 3,4,6,7,10,12 \qquad \text{(b)}$$

and the following quantities are identical for the m and the m+1 plies:

$$a_j, \quad j = 1,2,5,8,11; \qquad A_jS_{33}, \quad i = 1,2,3; \qquad A_4;$$

$$G_{11}; \quad G_{13}; \quad G_{61}-G_{12}; \quad \tfrac{1}{2}G_{63} + \omega_3; \quad G_{51}; \quad G_{53}; \quad \text{(c) - (m)}$$

$$u_{i0}, \quad i = 1,2,3; \qquad \omega_k, \quad k = 1,2;$$

Using Eqn. (33 b,c), we can rewrite (33a) in the form

$$(\tilde{S}_{25}^{(k)} + \tilde{S}_{16}^{(k)})a_2 + \tilde{S}_{44}^{(k)}a_8 + 2A_4 = 0 \qquad k = m,\ m+1 \qquad (34)$$

Similar elimination will provide

$$G_{11} = 6\tilde{S}_{12}a_1 + \tilde{S}_{15}a_9 + S_{13}A_1 \qquad \text{(a)}$$

$$G_{13} = 2\tilde{S}_{12}a_5 + S_{13}A_3 \qquad \text{(b)}$$

$$G_{61} = - 2\tilde{S}_{64}a_8 - 2\tilde{S}_{66}a_2 \qquad \text{(c)}$$

$$G_{12} = 2\tilde{S}_{12}a_2 + S_{13}A_2 \qquad (d) \qquad (35)$$

$$G_{63} = -\tilde{S}_{64}a_{11} \qquad (e)$$

$$G_{51} = 6\tilde{S}_{52}a_1 + \tilde{S}_{55}a_9 \qquad (f)$$

$$G_{53} = 2\tilde{S}_{52}a_5 \qquad (g)$$

The use of Eqn. (35) in (33 d-k) assuming no rigid body translations and rotations, results in

$$a_1[6(\tilde{S}_{12}^{(m)} - \tilde{S}_{12}^{(m+1)})] + a_9[\tilde{S}_{15}^{(m)}] - a_9'[\tilde{S}_{15}^{(m+1)}]$$

$$+ A_1[S_{13}^{(m)} - S_{13}^{(m+1)}S_{33}^{(m)}/S_{33}^{(m+1)}] = 0 \qquad (36)$$

$$a_5[2(\tilde{S}_{12}^{(m)} - \tilde{S}_{12}^{(m+1)})] + A_3[S_{13}^{(m)} - S_{13}^{(m+1)}S_{33}^{(m)}/S_{33}^{(m+1)}] = 0 \qquad (37)$$

$$a_8[2(\tilde{S}_{64}^{(m)} - \tilde{S}_{64}^{(m+1)})] + a_2[2(\tilde{S}_{66}^{(m)} + \tilde{S}_{12}^{(m)} - \tilde{S}_{66}^{(m+1)} - \tilde{S}_{12}^{(m+1)})]$$

$$+ A_2[S_{13}^{(m)} - S_{13}^{(m+1)}S_{33}^{(m)}/S_{33}^{(m+1)}] = 0 \qquad (38)$$

$$a_{11}[\tilde{S}_{64}^{(m)} - \tilde{S}_{64}^{(m+1)}] = 0 \qquad (39)$$

$$a_1[6(\tilde{S}_{52}^{(m)} - \tilde{S}_{52}^{(m+1)})] + a_9[\tilde{S}_{55}^{(m)}] - a_9'[\tilde{S}_{55}^{(m+1)}] = 0 \qquad (40)$$

$$a_5[2(\tilde{S}_{52}^{(m)} - \tilde{S}_{52}^{(m+1)})] = 0 \qquad (41)$$

At this stage, we are left with 11 unknowns: $a_1$, $a_2$, $a_5$, $a_8$, $a_9$, $a_9'$, $a_{11}$, $A_1$, $A_2$, $A_3$, $A_4$ where $a_9$ and $a_9'$ are for the $m^{th}$ and $m^{th}+1$ plies respectively, and the rest of the coefficients are identical for both layers. These unknowns appear in the 8 equations; (34), (36)-(41). In order to impose the far-end conditions (13), the full expressions for the stresses (i.e., the sum of the homogeneous and particular parts) are needed. This adds the infinite number of unknowns $d_n^{(h)}$ (Eqn. (27)). It should be noted that although in practical computation this set of unknowns, $d_n^{(h)}$, is truncated, the system of equations is still over determined since some of the unknowns were eliminated by the additional equations. Next, the double integrals in (13) are exactly evaluated. The results are in App. A. Equations (A1 - A6) together with (34),(36)-(41), form a system of 14 equations in the above 11 unknowns and the additional unknowns $\{d_n\}$.

In order to incorporate the effect of the hole, the approach mentioned in (3.1.2.3) is applied. It should be noted that the calculated stresses using Lekhnitskii's theory for anisotropic plate with elliptical cavity are $\sigma_{13cal}^{(m)}$ and $\sigma_{33cal}^{(m)}$. Thus,

$$\sigma_{33}^{(m)}(x_1,x_2) = \sigma_{33cal}^{(m)}(x_1,x_2)$$

$$m = 1,2,....\text{no. of plies} \qquad (42)$$

$$\sigma_{13}^{(m)}(x_1,x_2) = \sigma_{13cal}^{(m)}(x_1,x_2)$$

The traction-free boundary conditions at the upper and lower surfaces of

the laminate are:

$$\sigma_{22}^{(k)}(x_1, x_2) = 0$$

$$\sigma_{23}^{(k)}(x_1, x_2) = 0 \qquad (43)$$

$$\sigma_{12}^{(k)}(x_1, x_2) = 0 \qquad k = 1,2; \quad x_2 = b, -c, \text{ respectively}$$

At the exterior free edge

$$\sigma_{11}^{(k)}(x_1, x_2) = 0$$

$$\sigma_{13}^{(k)}(x_1, x_2) = 0 \qquad (44)$$

$$\sigma_{12}^{(k)}(x_1, x_2) = 0 \qquad k = 1,2; \quad x_1 = a$$

For the symmetric laminate, the following relations are required at the plane of symmetry

$$u_{1,2}(x_1, x_2) = 0$$

$$u_{2,1}(x_1, x_2) = 0 \qquad (45)$$

$$u_{3,2}(x_1, x_2) = 0$$

The above conditions (42)-(45), are satisfied by minimization of the

error of the residuals in the sense of a weighting function technique. The stresses and the relevant derivatives of the displacements (as required in Eqn. (45)) have the general form

$$\mathbb{R} = \sum_{n} D_n \phi_n - f \tag{46}$$

where $D_n$ are the coefficients $a_i$, $A_j$, $d_k^{(h)}$, and $\phi_n$ are the trial functions to be identified with the eigenfunctions of the exact solution. The function f is either zero or consists of the solutions obtained from the hole effect, Eqn.(42). Orthogonalization of $\mathbb{R}$ with the trial functions, such that the inner product vanishes, is performed in the form

$$(\phi_j, [\sum_{i=1}^{n} D_i \phi_i - f]) = 0 \qquad j = 1,2,\ldots,n \tag{47}$$

The inner product yields n equations where n is the number of all unknowns taken into account. Thus

$$\sum_{i=1}^{n} D_i \int_{\mathbb{D}} (\phi_j \phi_i) dS = \int_{\mathbb{D}} (\phi_j f) dS \qquad j = 1,2,\ldots,n \tag{48}$$

where $\mathbb{D}$ is the domain in which the problem is treated and therefore it is where integration is performed. In our case, this domain is changed according to the line where the boundary condition takes place and that is where integration is carried out. The explicit form of Eqn. (48) is given by

$$D_i\Big[\int_0^a (F_{2i}^{(1)}F_{2j}^{(1)} + F_{4i}^{(1)}F_{4j}^{(1)} + F_{6i}^{(1)}F_{6j}^{(1)})dS\Big|_{x_2=b}$$

$$+ \int_0^b (F_{1i}^{(1)}F_{1j}^{(1)} + F_{5i}^{(1)}F_{5j}^{(1)} + F_{6i}^{(1)}F_{6j}^{(1)})dS\Big|_{x_2=a}$$

$$+ \int_{-c}^0 (F_{1i}^{(2)}F_{1j}^{(2)} + F_{5i}^{(2)}F_{5j}^{(2)} + F_{6i}^{(2)}F_{6j}^{(2)})dS\Big|_{x_1=a}$$

$$+ \int_t^{a-t} (F_{3i}^{(1)}F_{3j}^{(1)} + F_{5i}^{(1)}F_{5j}^{(1)})\,dS\Big|_{x_2=0}$$

$$+ \int_t^{a-t} (F_{3i}^{(2)}F_{3j}^{(2)} + F_{5i}^{(2)}F_{5j}^{(2)})\,dS\Big|_{x_2=0}$$

$$+ \int_0^a (L_{1i}^{(2)}L_{1j}^{(2)} + L_{2i}^{(2)}L_{2j}^{(2)} + L_{3i}^{(2)}L_{3j}^{(2)})dS\Big|_{x_2=CL} =$$

$$= \int_t^{a-t} (\sigma_{3cal}^{(1)}F_{3j}^{(1)} + \sigma_{5cal}^{(1)}F_{5j}^{(1)} + \sigma_{3cal}^{(2)}F_{3j}^{(2)} + \sigma_{5cal}^{(2)}F_{5j}^{(2)})dS\Big|_{x_2=0} \qquad (49)$$

in which j=1,2,... (no. of unknowns) and t is the laminate thickness. In Eqn. (49), $F_{\alpha i}(m)$ is defined by the homogeneous and particular parts of the solution, Eqns. (27) and (29) respectively.

The index $\alpha$ = 1,2,3,4,5,6 denotes the contracted Greek notation for the stresses. The functions $L_{\beta i}(m)$ ($\beta$ = 1,2,3) are defined by the derivatives (45). The integrals in (49) are performed numerically using Simpson's method. The number of points of integration is of great importance when convergence of the solution is considered. Equations (34),(36)-(41),(49) provide a set of linear algebraic equations

$$AD = \mathbb{B} \tag{50}$$

in which A is the coefficients matrix with order (qxn), q>n; q is the number of unknowns associated with the 14 equations from the elasticity solution (34),(36)-(41),(49),(A1)-(A6), and n is the total number of unknowns. In Eqn. (49) D is a vector (nx1) of the unknowns.

The over determined system may be solved in the least square sense as

$$A^{\dagger}AD = A^{\dagger}\mathbb{B} \tag{51}$$

in which $A^{\dagger}$ is the conjugate transpose of A. Eqn. (51) turns out to be solvable since $A^{\dagger}A$ is of the order (nxn) and $A\ \mathbb{B}^{\dagger}$is (nx1), but due to the nature of the general solution it appears that some rows and/or columns might be zero or show dependency which causes $A^{\dagger}A$ to be singular. Even if a mathematical singularity does not occur, due to the use of a computer, the solution of such a system might be strongly ill-conditioned, depending upon the properties of the plies which enter the equations. This ill-conditioned behavior may be treated by adopting the method of singular-value decomposition, Stewart (1973). According to this method, every matrix A (qxn), q>n, may be expressed as the multiplication of three matrices as follows

$$A = U\Sigma V^{T} \tag{52}$$

where U and V are (qxq) and (nxn) unitary matrices whose columns are the

orthonormalized eigenvectors of $AA^T$ and $A^TA$, respectively. The matrix $\Sigma$ is diag($\sigma$,0) which is an (qxn) matrix with $\sigma$ being the square roots of the non-zero eigenvalues of $A^TA$. Let $U'$ be denoted by

$$U' = AV\left[\begin{array}{c|c} \Sigma_r^{-1} & 0 \\ \hline 0 & 0 \end{array}\right] \tag{53}$$

in which $\Sigma_r^{-1}$ are the reciprocals of the non-zero components of $\Sigma$ in a descending order on the diagonal. Let us also define w by

$$w = U'^T B \tag{54}$$

and

$$v_i = \frac{w_i}{\sigma_i} \qquad i = 1,2,\ldots\ldots\ldots,n \tag{55}$$

The desired solution is determined from

$$\{D\} = [V]\{v\} \tag{56}$$

Having obtained {D}, the displacements and stresses are computed from Eqns. (27),(29) and (30). A description of the program "EDGSTR" is given in appendix C. This program follows the above analysis and calculates the stresses and displacements.

2.3. Convergence of the solution and examples

Consider the case of a $[\pm 45]_s$ laminate which was considered by Wang and Choi (1982), Wang and Crossman (1977), Pipes and Pagano (1970), and Lagace and Kassapoglou (1987). The properties of the unidirectional single ply as given by the above mentioned authors, for the graphite-epoxy system are:

$E_1$ = 20e6 psi, $E_2 = E_3$ = 2.1e6 psi, $G_{12} = G_{13} = G_{23}$ = 0.85e6 psi, and $\nu_{12} = \nu_{23} = \nu_{13}$.

As a case study, a circular hole is centrally located, and the laminate is subjected to a unit stress in the $x_3$ direction as shown in fig. 4a.

Results were obtained in three locations: in the vicinity of the hole and at the free edge of the laminate as well as far from these two locations where classical lamination theory or results of anisotropic plate analysis with a center hole are valid. Convergence of the obtained stresses was studied by examining the effect of the number of eigenvalues and the number of integration points on the results. The study of the effect of the number of eigenvalues was limited to the ability of the computer to provide accurate solutions when using the Muller (1956) deflation method since this method involves calculations of differences between numbers that converge to the point that multiplication by that difference results in computer underflow. Convergence was studied on all stresses. Predicted results for the normal stress $\sigma_{22}$ are exhibited for three different numbers of eigenvalues and 200 integration points as shown in fig. 3. Observing curves 1-5 in Fig. 3, we conclude that convergence is achieved using 25 eigenvalues with slight changes between the cases of 50, 100, and 200

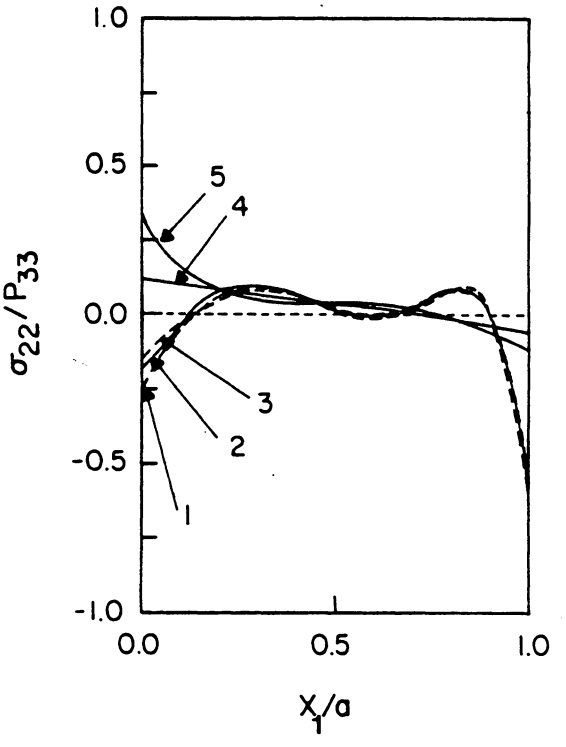


Figure No. 3: Examine convergence of $\sigma_{22}$ through various numbers of eigenvalues and points of integration

| curve #: | 1 | 2 | 3 | 4 | 5 |
|---|---|---|---|---|---|
| eigenvalues: | 25 | 25 | 25 | 15 | 7 |
| integration pnts: | 200 | 100 | 50 | 100 | 100 |

integration points. Curves 4 and 5 show results in which low number of eigenvalues are used and therefore result in wrong stress distribution. Curves 1-3 present close results in which the same number of 25 eigenvalues are used and show convergence. The results of curves 1-3 at $x_1/a = 1$, match the results presented by Wang and Choi (1982) for the similar case of a straight free edge. In order to investigate the effect of the hole on the stress distribution at various locations along its circumference, we present in fig. 4b all stress distributions along a cut made perpendicular to the laminate straight free edge, and in fig. 4c, the variation of the normal stress $\sigma_{22}$ along the cross sections which are radial to the hole at $\alpha = 0^\circ, 10^\circ, 30^\circ, 60^\circ$, and $80^\circ$. This figure exhibits well the fiber orientation dependence which provide various orders of singularities. The values of the orders of singularity are given by

$$\delta_1 = -.025575658 \qquad \text{for } \alpha = 0^\circ$$

$$\delta_1 = -.026100409 \qquad \text{for } \alpha = 10^\circ$$

$$\delta_1 = -.030274706 \qquad \text{for } \alpha = 30^\circ$$

$$\delta_1 = -.030274706 \qquad \text{for } \alpha = 60^\circ$$

$$\delta_1 = -.026100409 \qquad \text{for } \alpha = 80^\circ$$

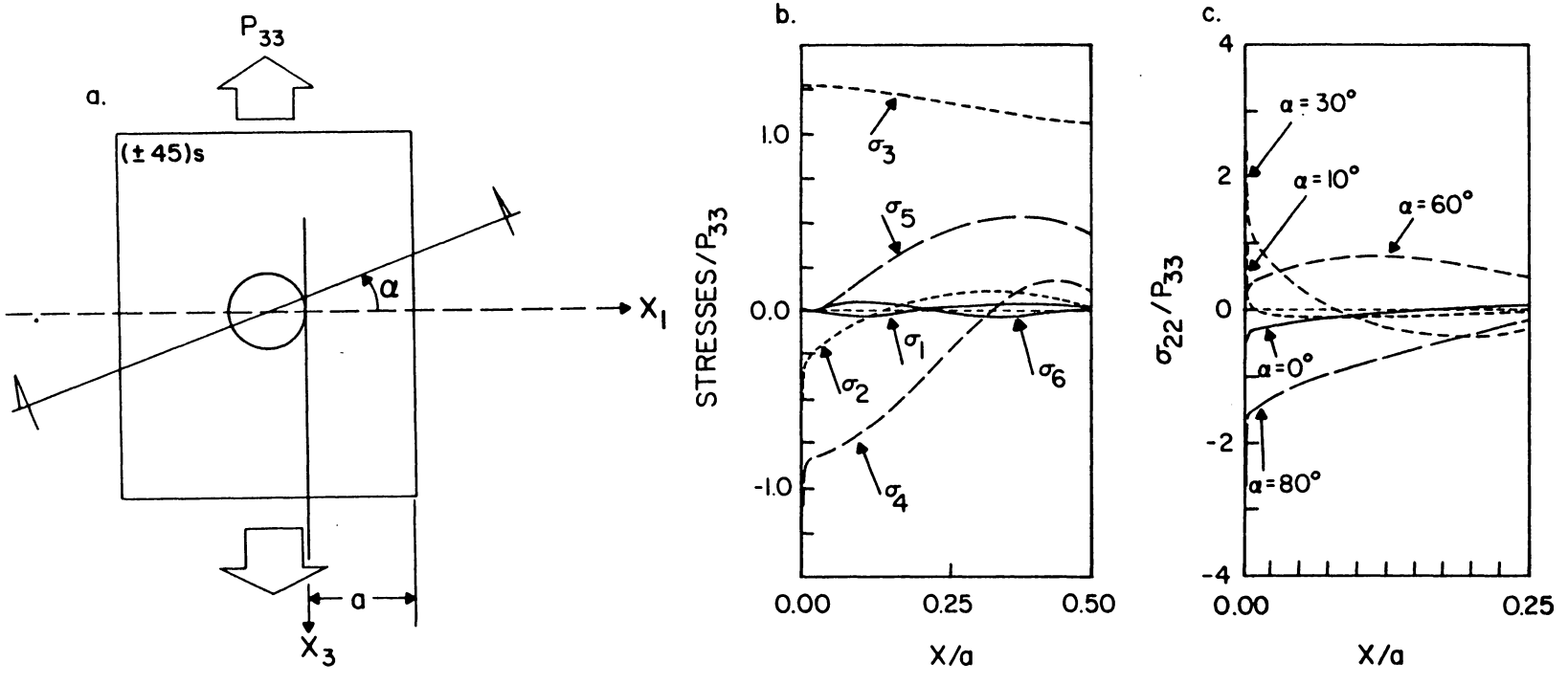


Figure No. 4: a: Geometry and description of cuts

b: Stress distribution at $\alpha = 0^{\circ}$;25 e.v., 200 int. pnts.

c: Comparison of normal stress $\sigma_{22}$ at various cuts

where $\delta_1$ for the cases of $\alpha = 10^\circ, 30^\circ, 60^\circ$ and $80^\circ$ is calculated for the direction tangential to the hole edge which provides an interface between [35/-55], [15/-75], [-15,75] and [-35/55] orientations, respectively. The latter analysis is done using a coordinate system transformed to match the direction tangential to the hole and to the radial cross section in order to satisfy the basic assumptions introduced in 2.1 and the traction-free boundary conditions at the hole edge as explained in 2.1.2.2. The validity of the results for the transformed configuration are limited to the vicinity of the hole within the region in which the stresses are controlled by the mathematical singularity.

# Chapter 3

## PREDICTION MODEL FOR THE ONSET OF DELAMINATION BASED ON THE BOUNDARY LAYER EFFECT

The prediction model is established in this chapter, based on the following understandings of the phenomenon of edge delamination.

1. Delaminations are controlled by strain energy and its rate of change during the delamination process which is the strain energy release rate. The latter is a well-defined mathematically quantity and is also experimentally measurable.
2. There is a region of influence of the edge effect within which strain energy should be examined.
3. Since the stress field changes its nature drastically in close vicinity to the edge, the phenomenon is localized and therefore one should consider the rate of changes in that region which is of the order of one laminate thickness.

Near the laminate edge (straight or at the hole), the stress field is completely governed by the singular term $K_i x^{\delta 1}$ as it appears in Eqn. (23). This expression consists of the coefficient $K_i$ which is called in the literature "the near-field parameter" or "free-edge stress intensity factor", and by the singularity which appears in the exponent. To compare the stresses at two locations (any of the six components of the stress tensor) while taking the limit as the distance r goes to zero, we obtain the following:

$$\frac{\sigma^{(1)}}{\sigma^{(2)}} = \frac{K^{(1)}\, r^{\delta i^{(1)}}}{K^{(2)}\, r^{\delta i^{(2)}}} \tag{57}$$

which is also

$$\frac{\sigma^{(1)}}{\sigma^{(2)}} = \frac{K^{(1)}}{K^{(2)}}\, r^{\delta i^{(1)} - \delta i^{(2)}} \tag{58}$$

in which the indices 1,2 designate two examined and compared interfaces.

We can not actually compare stresses at the edges because they result in infinite values, so we chose to compare the parameters which are a combination of the stress terms. There are three cases to be examined through Eqn. (58). The first occurs when the power $\delta_1^{(1)} - \delta_1^{(2)}$ is positive, the second when it is negative, and the third when it vanishes. Note that the value of $\delta$ is always negative and within the region [-1,0], and both $K^{(1)}$ and $K^{(2)}$ should be positive (negative sign indicates compression which implies no delamination problem). Thus, mathematic manipulation of Eqn. (58) offers the following criterion:

$$\delta_1^{(1)} < \delta_1^{(2)} \Rightarrow \lim_{r \to 0}\left[\frac{\sigma^{(1)}}{\sigma^{(2)}}\right] = 0 \Rightarrow \sigma^{(1)} < \sigma^{(2)} \qquad \text{(a)}$$

$$\delta_1^{(1)} > \delta_1^{(2)} \Rightarrow \lim_{r \to 0}\left[\frac{\sigma^{(1)}}{\sigma^{(2)}}\right] = \infty \Rightarrow \sigma^{(1)} < \sigma^{(2)} \qquad \text{(b)} \tag{59}$$

$$\delta_1^{(1)} = \delta_1^{(2)} \Rightarrow \frac{\sigma^{(1)}}{\sigma^{(2)}} = \frac{K^{(1)}}{K^{(2)}} \qquad \text{(c)}$$

Let us examine once again the expression for the stress fields as

reflected through Eqns. (24) and (29). We recognize the singular nature at the edge of the laminate. The asymptotic stress field is generally expressed by the combination of the above-mentioned equations as,

$$\sigma_\alpha = \sum_{k=1}^{3} \left[ \mathbb{C}_{\alpha k} Z_k^{\delta 1} + \mathbb{C}_{\alpha(k+3)} \bar{Z}_k^{\delta 1} \right] + o(\text{higher order, nonsingular terms}) \qquad (\alpha = 1,2,3,4,5,6) \quad (60)$$

in which the coefficients $\mathbb{C}_{\alpha k}$ are related to the homogeneous solution as presented by Eqn. (27) associated with the first eigenvalue,

$$\mathbb{C}_{\alpha k} = d_1 f^*_{\alpha k 1} \qquad (61)$$

the functions $f^*_{\alpha k 1}$ are the coefficients of the coordinate $Z_k$ as they appear in Eqn. (24) and the coefficient $d_1$ is the relevant component of the vector D in Eqn. (48), associated with the order of the singularity.

The near-field parameters, $K_i$, play the role of amplitudes in the singular edge stresses. These parameters are introduced by

$$K_i = \lim_{x_1 \to 0} x_1^{-\delta 1} \sigma_i(x_1, 0; \delta_1) \qquad i = 1,2,3,4,5,6 \qquad (62)$$

The coordinate $x_2$ is zero since the coordinate system is located at the intersection of the interface and the hole edge. Eqn. (62) is the reciprocal form of Eqn. (61). The coordinate $Z_k$, as explained in Eqn. (16), is

$$Z_k = x_1 + \mu_k x_2$$

but since $x_2$ is taken to be zero,

$$Z_k \equiv \bar{Z}_k \equiv x_1$$

Following Eqns. (60) & (61), we conclude

$$K_1 = d_1 \left( \sum_{k=1}^{3} [c_k \mu_k^2 + c_{k+3} \bar{\mu}_k^2] \right) \qquad (a)$$

$$K_2 = d_1 \left( \sum_{k=1}^{3} [c_k + c_{k+3}] \right) \qquad (b)$$

$$K_4 = - d_1 \left( \sum_{k=1}^{3} [c_k \eta_k + c_{k+3} \bar{\eta}_k] \right) \qquad (c) \qquad (63)$$

$$K_5 = d_1 \left( \sum_{k=1}^{3} [c_k \eta_k \mu_k + c_{k+3} \bar{\eta}_k \bar{\mu}_k] \right) \qquad (d)$$

$$K_6 = - d_1 \left( \sum_{k=1}^{3} [c_k \mu_k + c_{k+3} \bar{\mu}_k] \right) \qquad (e)$$

and

$$K_3 = \frac{S_{3j} K_j}{S_{33}} \qquad j = 1,2,4,5,6 \qquad (f)$$

In order to solve for the energy release rate quantity, the ideas of fracture mechanics are used. The solution for the problem of delamination crack is similar to the analysis presented in chapter 2.

The calculation of the stress singularity is done with the same tool, taking the angles of the edge faces $\theta$, as shown in fig. 2, as $180^{\circ}$ and $-180^{\circ}$, respectively. Again, the singularity is the number within the series of eigenvalues which is in the domain [-1,0]. The similarity to fracture mechanics enables us to denote the near-field parameters as "free-edge stress intensity factors" in equivalent terminology to the crack tip stress intensity factors as it appears in linear elastic fracture mechanics, Broek (1982). For the complete analogy to the field of fracture mechanics, we may present the three modes of stress intensities, $K_I$, $K_{II}$, and $K_{III}$ as presented by Erdogan (1965) and Rice (1965) for the case of cracks in dissimilar media. Here we refer to the interlaminar stresses $\sigma_2$, $\sigma_4$, and $\sigma_6$,

$$K_I = \lim_{x \to 0^+} \sum_{n=1}^{3} \sqrt{2\pi}\, x^{-\delta n}\, \sigma_{2n}(x,0;\ \delta n)$$

$$K_{II} = \lim_{x \to 0^+} \sum_{n=1}^{3} \sqrt{2\pi}\, x^{-\delta n}\, \sigma_{4n}(x,0;\ \delta n) \qquad (64)$$

$$K_{III} = \lim_{x \to 0^+} \sum_{n=1}^{3} \sqrt{2\pi}\, x^{-\delta n}\, \sigma_{6n}(x,0;\ \delta n)$$

As noted by Erdogan (1965), the stress intensities in Eqn. (60) are different than the ones in a homogeneous solid, and therefore its physical interpretation is different as well.

Following the concept of virtual crack extension, Irwin (1957), and adapting that into the problem of delamination cracking, Christensen (1979), we may write the expression for the energy release rate, based

on the displacements v,u, and w, and the length of the virtual crack extension, $\delta\beta$, as follows,

$$G_{total} = G_I + G_{II} + G_{III}$$

$$= \lim_{\delta\beta \to 0} \frac{1}{2\delta\beta} \int_0^{\delta\beta} \Big\{ \sigma_2(r,0) \left[ v^{(m)}(\delta\beta - r, \pi) - v^{(m+1)}(\delta\beta - r, -\pi) \right]$$

$$+ \sigma_6(r,0) \left[ u^{(m)}(\delta\beta - r, \pi) - u^{(m+1)}(\delta\beta - r, -\pi) \right]$$

$$+ \sigma_4(r,0) \left[ w^{(m)}(\delta\beta - r, \pi) - w^{(m+1)}(\delta\beta - r, -\pi) \right] \Big\} \qquad (65)$$

Observing Eqns. (63)-(65), we conclude that all the expressions presented are proportional, respectively. Therefore, for the purpose of comparisons, we may chose the most convenient term out of these three and, rather than using the physical expression of the strain energy release rate, we may use the relatively simple to calculate term of the near-field parameters.

To summarize the procedure of applying the prediction model, we first start with the analysis for the stress singularities at all the interfaces at different azimuthal angles. Next, we calculate the near-field parameters by the completion of the particular solution. The sign of the parameters determines the behavior, minus is compression and plus is tension. We may filter out the cases of negative values of the near-field parameters since obviously it indicates no delamination. For the case in which two similar interfaces are compared, we obtain similar

orders of singularity. Thus, a decision is made based upon comparison of energy release rate or the magnitude of the edge intensity.

# Chapter 4

# EXPERIMENTAL PROCEDURE

Experimental work is essential for the validation of any theory. Postulations and means of investigation may be examined and refined by the results of reality. With these facts in mind, a testing program was setup in an attempt to bring as much reality as possible into the theoretically based prediction model. The testing program with all its aspects is presented in this chapter.

The objective of the tests was to detect and locate the onset of delamination at the edge of a hole in a composite laminate. Two major factors were taken into consideration, the materials and loads. When one considers materials in conjunction with composites, there are two major elements, the combination of fibers/matrix, and the fiber direction as reflected in stacking sequence. The second factor, loading condition, covers the other major aspect of performance of a tested specimen. Therefore, both tension and compression were applied. The following sections give details about these as well as other points of interest, including the description of observations and results.

## 4.1 Specimens - materials and geometry

Two types of unidirectional systems were chosen. They differ in the type of matrix material but both have used the same fiber. They are the AS4/3501-6 , herein designated by "Z", and the AS4/1808 material designated by "Y". This choice of matrix systems provided an excellent

opportunity to examine the dependency of behavior upon matrix type and its performance sensitivity.

The stacking sequences chosen were $[(0/45/90/-45)_s]_4$ which is a quasi-isotropic, and $[(0/45/0/-45)_s]_4$ - an orthotropic layup. The first is designated by "A" and the other by "B".

The geometry of the specimens corresponded to the basis for the analysis and may be viewed in table 3 also referring to fig. 2. All specimens, three each of the Z-A, Z-B, Y-A, and Y-B types (which are the combinations of the two matrix systems and the two types of stacking sequences) for a total of twelve, were center-notched, finite-width coupons 6 inches long.

4.1.1 How specimens were made

All specimens were cut from large plates. The plates were Ultra Sonically scanned in order to detect possible voids and to eliminate extraneous and irrelevant disturbances. A diagram, describing the cutting process, was made. Each specimen was coded by its location within the parent plate. The coding system resulted in the addition of two digits to the two letters from the combination Z, Y, A, and B, and completed the "name" of each specimen. All these procedures were used to assist in isolating peculiar behavior due to irrelevant factors, and to assist in isolating the interpretation of damage.

4.1.2 Notched and unnotched properties

Properties of the unidirectional plates are given in table 1. Table 2 provides unnotched laminate properties for all four combinations of Z-A, Z-B, Y-A, and Y-B, as calculated by means of classical lamination theory, Jones (1975).

Geometrical properties of all specimens may be viewed in table 3. These properties were measured by a digital caliper and averaged over few measurements for each of the dimensions. Table 3 also provides the strength information for critical tensile and compressive stresses of the notched specimens as obtained by testing three specimens of each type. The ungripped length of the specimens was 2.5". For both, tension and compression loadings, a failure in which critical load was determined, was defined when the specimen could not sustain any more load. For the tension case, such failure occurred as the specimen was broken into two pieces. For the compression case, failure occurred when plies started to buckle.

## Table No. 1: Material Properties

| | AS4/3501-6 | | AS4/1808 | |
|---|---|---|---|---|
| | compression | tension | compression | tension |
| $E_1$ [Msi] | 21.1 | 20.7 | 17.0633 | 17.2395 |
| $E_2$ [Msi] | 2.0 | 2.0 | 1.226 | 1.164 |
| $\nu_{12}$ | 0.3 | 0.3 | 0.2866 | 0.304 |
| $G_{12}$ [Msi] | 0.835 | | 0.6937 | |
| t [in] | 0.005 | | 0.0058 | |

Table No. 2: Laminate Properties

| | $[(0/45/90/-45)_s]_4$ | | $[(0/45/0/-45)_s]_4$ | |
|---|---|---|---|---|
| | AS4/3501-6 | AS4/1808 | AS4/3501-6 | AS4/1808 |
| $E_1$ [Msi] | 8.371 | 6.668 | 12.19 | 9.86 |
| $E_2$ [Msi] | 8.371 | 6.668 | 3.874 | 2.096 |
| $G_{12}$ [Msi] | 3.179 | 2.558 | 3.179 | 2.558 |
| $\nu_{12}$ | 0.3169 | 0.3032 | 0.6568 | 0.6661 |

Table NO. 3: Test specimens - dimensions & strength

| type | dimensions [in] | | | | critical stress [ksi] | | critical load [kip] | |
|---|---|---|---|---|---|---|---|---|
| | e | $d_1$ | a | t | $S_T$ | $S_C$ | tension | compres. |
| Y-B 3-4 | 0.366 | 0.378 | 0.363 | 0.18 | 54.1 | -55.2 | 10.80 | 11.02 |
| Y-B 3-6 | 0.364 | 0.379 | 0.364 | 0.1787 | 54.1 | -55.2 | 10.71 | 10.93 |
| Y-A 6-9 | 0.363 | 0.379 | 0.364 | 0.1772 | 39.4 | -45.2 | 7.74 | 8.88 |
| Y-A 6-11 | 0.363 | 0.38 | 0.363 | 0.1773 | 39.4 | -45.2 | 7.75 | 8.89 |
| Z-B 7-1 | 0.558 | 0.38 | 0.561 | 0.1817 | 59.2 | -52.8 | 16.15 | 14.4 |
| Z-B 7-2 | 0.559 | 0.38 | 0.56 | 0.1802 | 59.2 | -52.8 | 15.99 | 14.26 |
| Z-A 7-6 | 0.561 | 0.378 | 0.561 | 0.1817 | 42.3 | -43.8 | 11.53 | 11.94 |
| Z-A 7-7 | 0.565 | 0.378 | 0.559 | 0.1813 | 42.3 | -43.8 | 11.51 | 11.92 |
| Y-B 3-8 | 0.364 | 0.38 | 0.367 | 0.1773 | 54.1 | -55.2 | 10.65 | 10.86 |
| Y-A 6-13 | 0.363 | 0.379 | 0.364 | 0.1728 | 39.4 | -45.2 | 7.55 | 8.66 |
| Z-B 7-3 | 0.557 | 0.38 | 0.56 | 0.18217 | 59.2 | -52.8 | 16.16 | 14.41 |
| Z-A 7-8 | 0.562 | 0.371 | 0.559 | 0.18166 | 42.3 | -43.8 | 11.52 | 11.93 |

note: refer to fig. 2 for dimensions designation

## 4.2 Testing procedure

To achieve the objectives of the testing program, the procedure consisted of quasi-static loading in both tension and compression. Eight specimens were tested in tension, and the remaining four specimens were tested in compression. A list of the specimens by their codes, divided into the two types of loads, follows:

Tension:

Y-B 3-4, Y-B 3-6, Y-A 6-9, Y-A 6-11, Z-B 7-1, Z-B 7-2, Z-A 7-6, Z-A 7-7

Compression:

Y-B 3-8, Y-A 6-13, Z-B 7-3, Z-A 7-8

The first load condition was chosen as 60% of the given critical load, as found in an early experimental study, for the relevant case. At the critical load level, failure of the specimens was observed. Then, the load was raised in steps of 5% at a time. After each loading step, the specimen was taken out of the testing machine and X-rayed, then put back to the machine to be reloaded. In the following few sections the details of that procedure are described.

### 4.2.1 Testing machines

For the tension test, an INSTRON screw-driven test machine was chosen. That machine is very convenient due to its simplicity of operation and calibration. The load rate was controlled.

For the compression test, the more complicated MTS servo-hydraulic machine was chosen. This machine is capable of carrying out a reliable compression test without risking the loss of specimens in possible

buckling. The test may be either strain, load, or stroke controlled as required to ensure a successful completion of the experiment.

### 4.2.2 Loading fixture and measurements during the test

The only measurements taken during the test were of the load level to ensure accuracy of the current load magnitude. In the tension test, two types of load cells were used. A 10-kip load cell was used for load levels under 10 kips. A 20-kip load cell was used for load levels above 10 kips. A Digital Volt Meter was used to measure the load level. For the 10-kip load cell, 1 volt indicated 1 kip loading, while for the 20-kip load cell 1 volt corresponded 2 kips. On the MTS machine, the range of 20 kips was used to provide the range of 1 volt for 2 kips.

### 4.2.3 X-ray detection technique

As mentioned, the specimens were taken out of the testing machine after each loading step and inspected for delaminations by the X-ray radiographic technique. The following is a full description of the procedure as carried out.

Before the removal of the specimen from the testing machine, the specimen was held under 50% of the testing load and a penetrant material was applied to the edges of the hole and the free edges of the specimen as well as all over the upper and lower surfaces. The type of penetrant used was Zinc Iodine which penetrates delamination areas and cracks of all kinds. When the specimens were X-rayed, the Zinc Iodine blocked the

X-ray beam and, by doing so, it created white spots in the shape of the defects on the film, which become black spots on the positive after being developed. That is the way we detected cracks and delaminations on the resulting pictures.

Once the Zinc Iodine was applied to the specimen, it was left for a couple of hours in order to penetrate as much as possible. Then, the outer surfaces of the specimen were cleaned very carefully with Acetone to prevent any direct contact of Zinc Iodine with the film (to prevent the film destruction).

The next stage was the actual X-ray process. There were two types of radiographs taken for each specimen. The so-called $0^{\circ}$, in which the specimen was X-rayed through its surface while lying on the film, and the $90^{\circ}$ in which the specimen was put on its edge resulting in a picture of a longitudinal section. The film used was a Kodak SR-5 single-sided X-ray film. For the $0^{\circ}$, the specimen was exposed for 3 minutes at an intensity of 43 mv. For the $90^{\circ}$, the exposure time was 4 minutes at an intensity of 80 mv. Next, the specimen was removed, and the film was soaked in a developer solution for 4 minutes, then rinsed for less than a minute in pure water and soaked in a fixer for another 4 minutes, then rinsed again and put aside to dry. That process was carried out eight times for the tension test and six time for the compression test, a total of 88 times !

## 4.3 Observations and results

After being X-rayed, the results were carefully observed in a

microfiche machine under 36X magnification. The purpose, of course, was to inspect for delaminations. Results of selective stages for each specimen are presented in figs. 5 - 20. The first figure of each specimen shows a scheme of the situation throughout the selected stages, while the second figure is a print of the X-ray of the last stage of both the $0^{\circ}$ and the $90^{\circ}$ exposures. Fig. 5a illustrates the views of specimens shown in figs. 5 - 20.

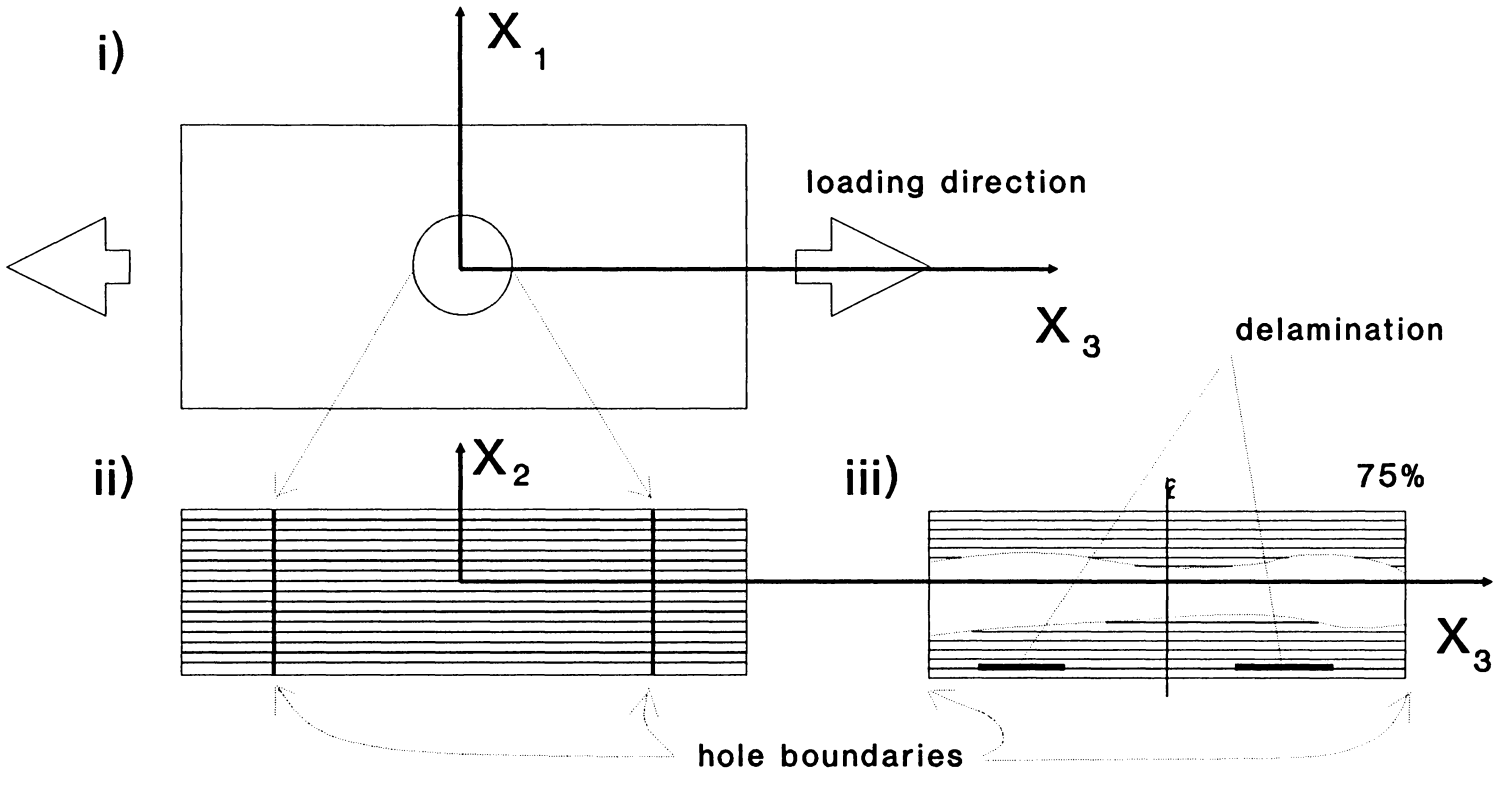


Figure No. 5a: i) top view of specimen, figures 6,8,10,12,14,16,18,20
ii) edge view, cut at $x_3$ axis, figures 6,8,10,12,14,16,18,20
iii) same view as ii), figures 5,7,9,11,13,15,17,19,29

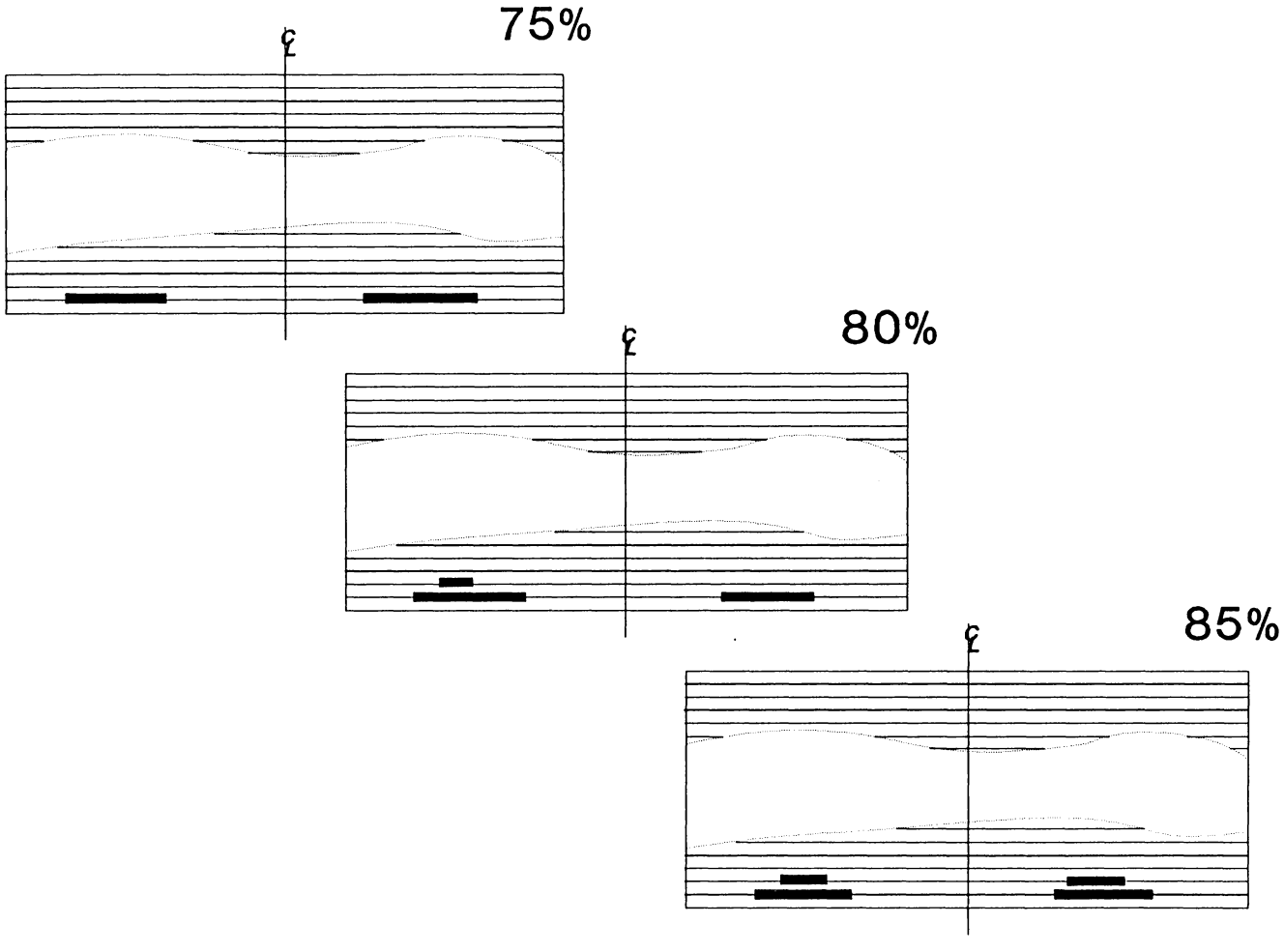


Figure No. 5: delamination process in Y-B 3-4, tension

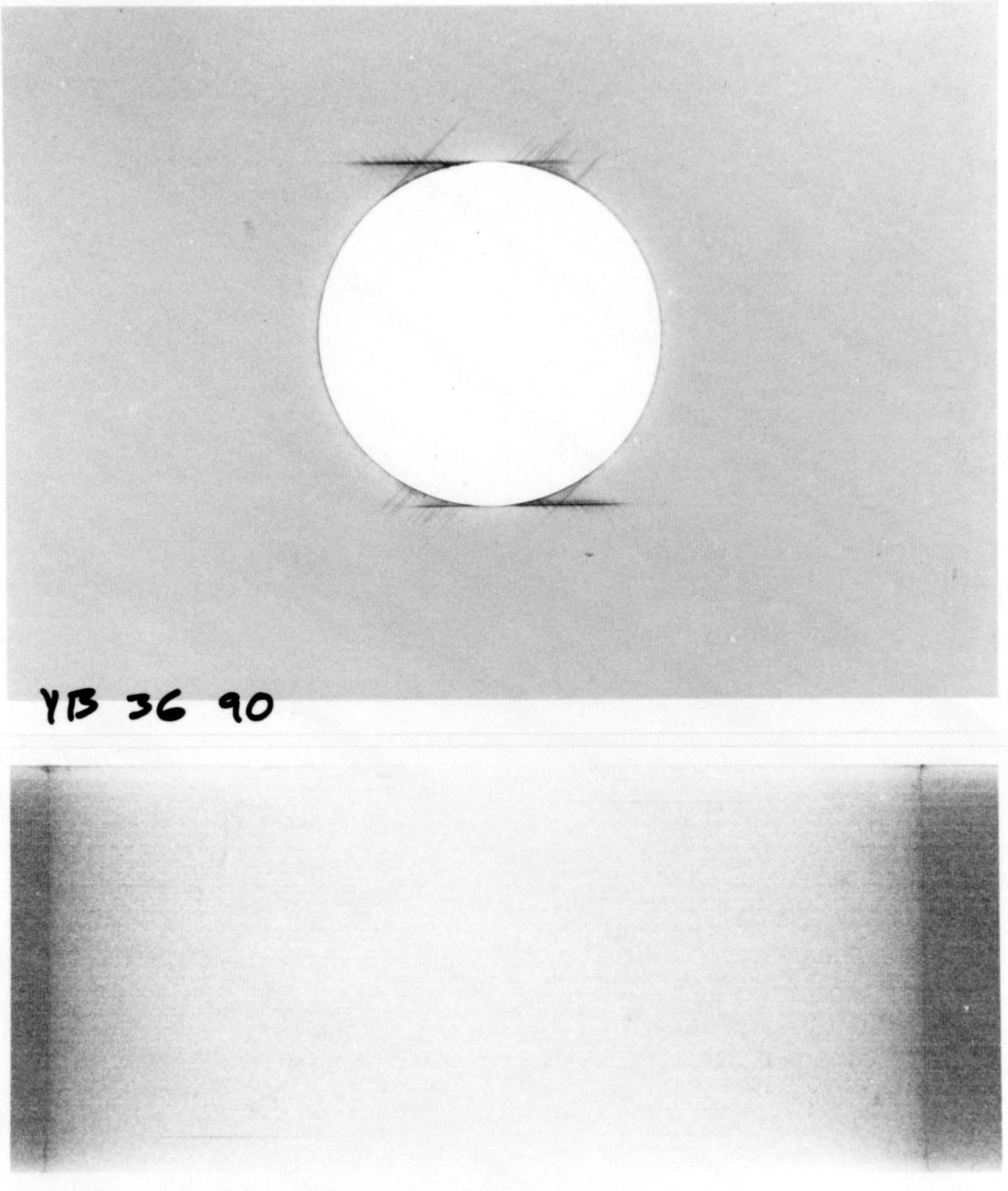


Figure No. 6: X-Ray of Y-B 3-4, 90% critical tensile load
specimen top view and cut shows hole surface

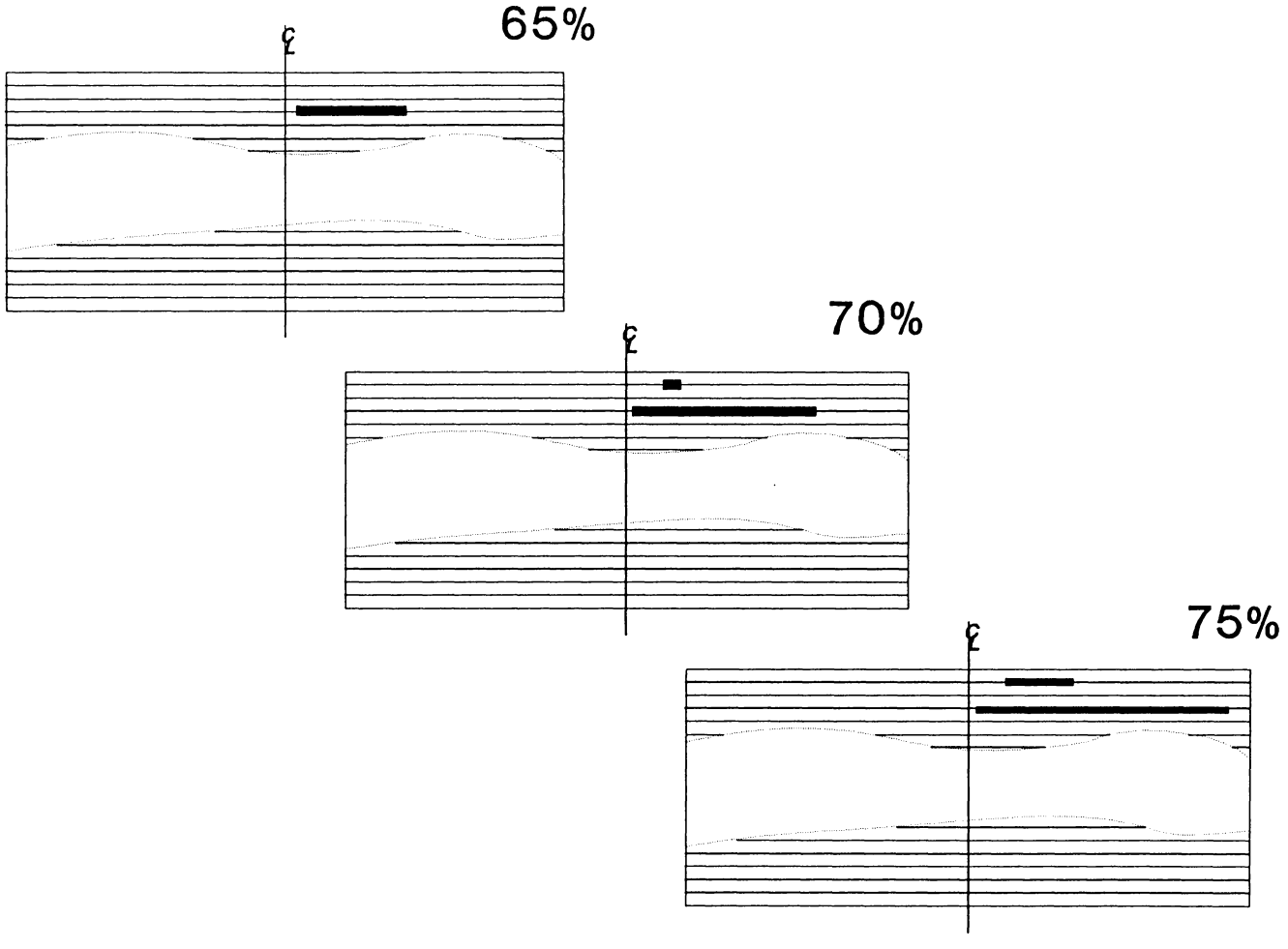


Figure No. 7: delamination process in Y-B 3-8 compression

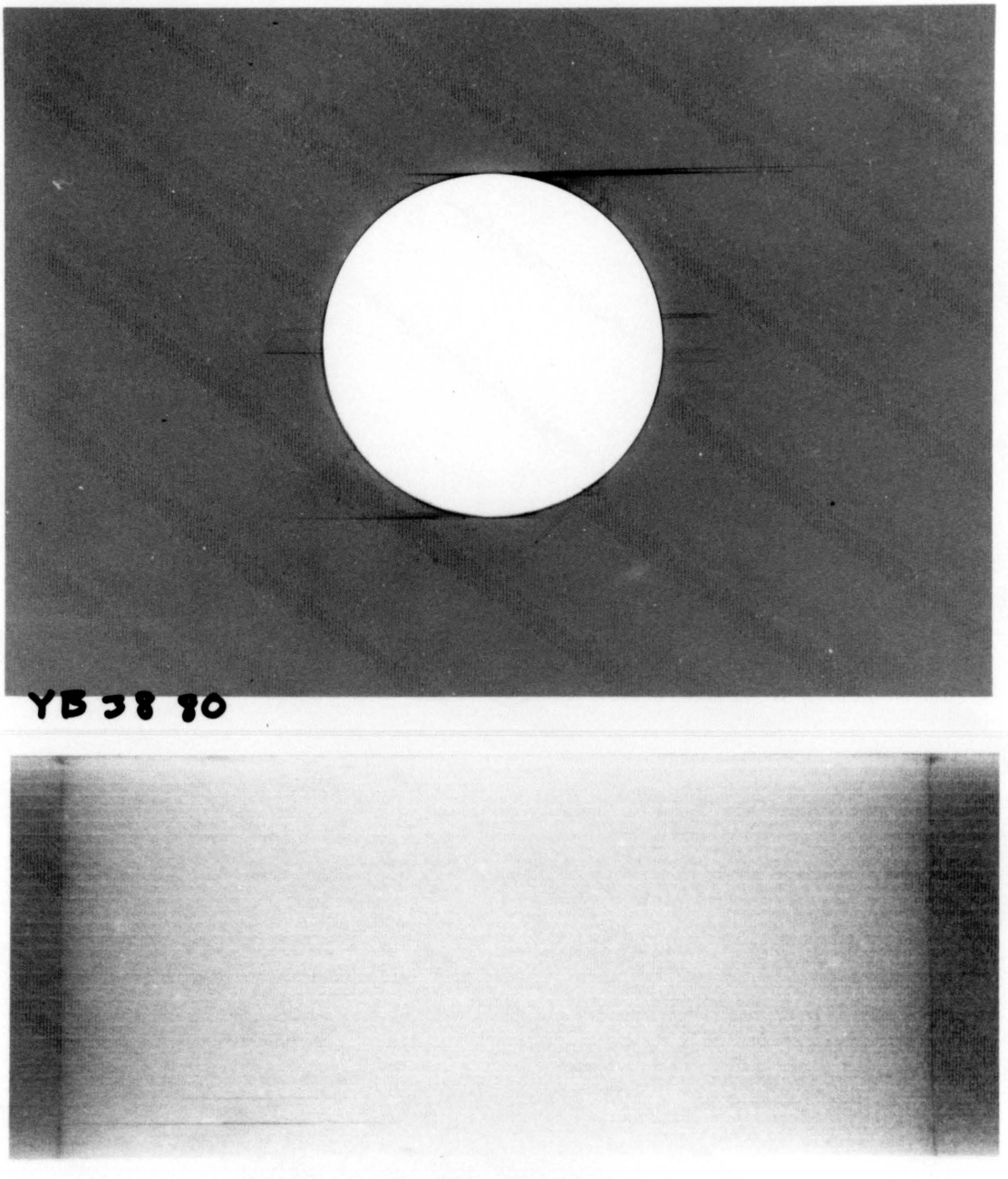


Figure No. 8: X-Ray of Y-B 3-8, 80% critical compress. load specimen top view and cut shows hole surface

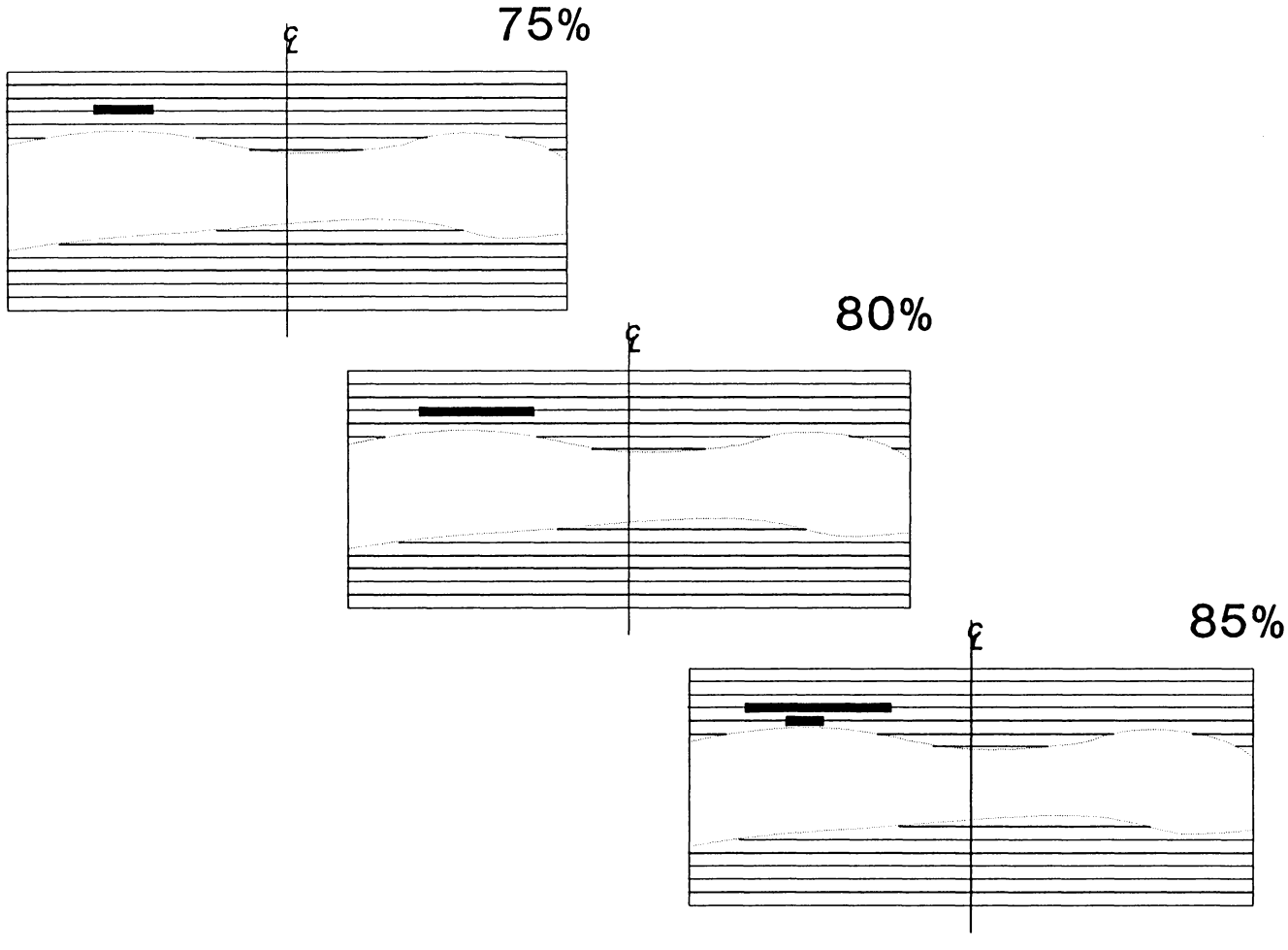


Figure No. 9: delamination process in Z-B 7-2, tension

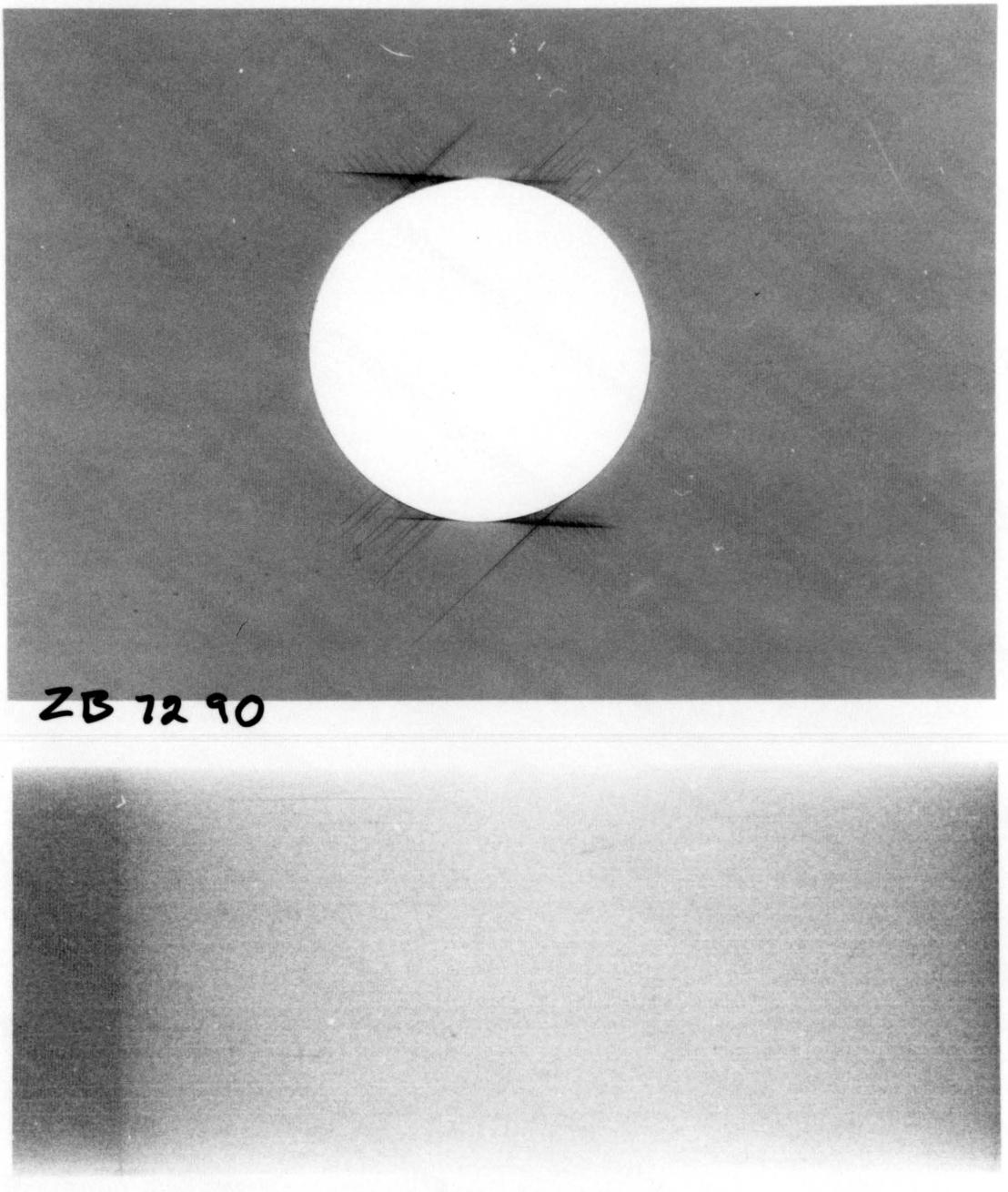


Figure No. 10: X-Ray of Z-B 7-2, 90% critical tensile load specimen top view and cut shows hole surface

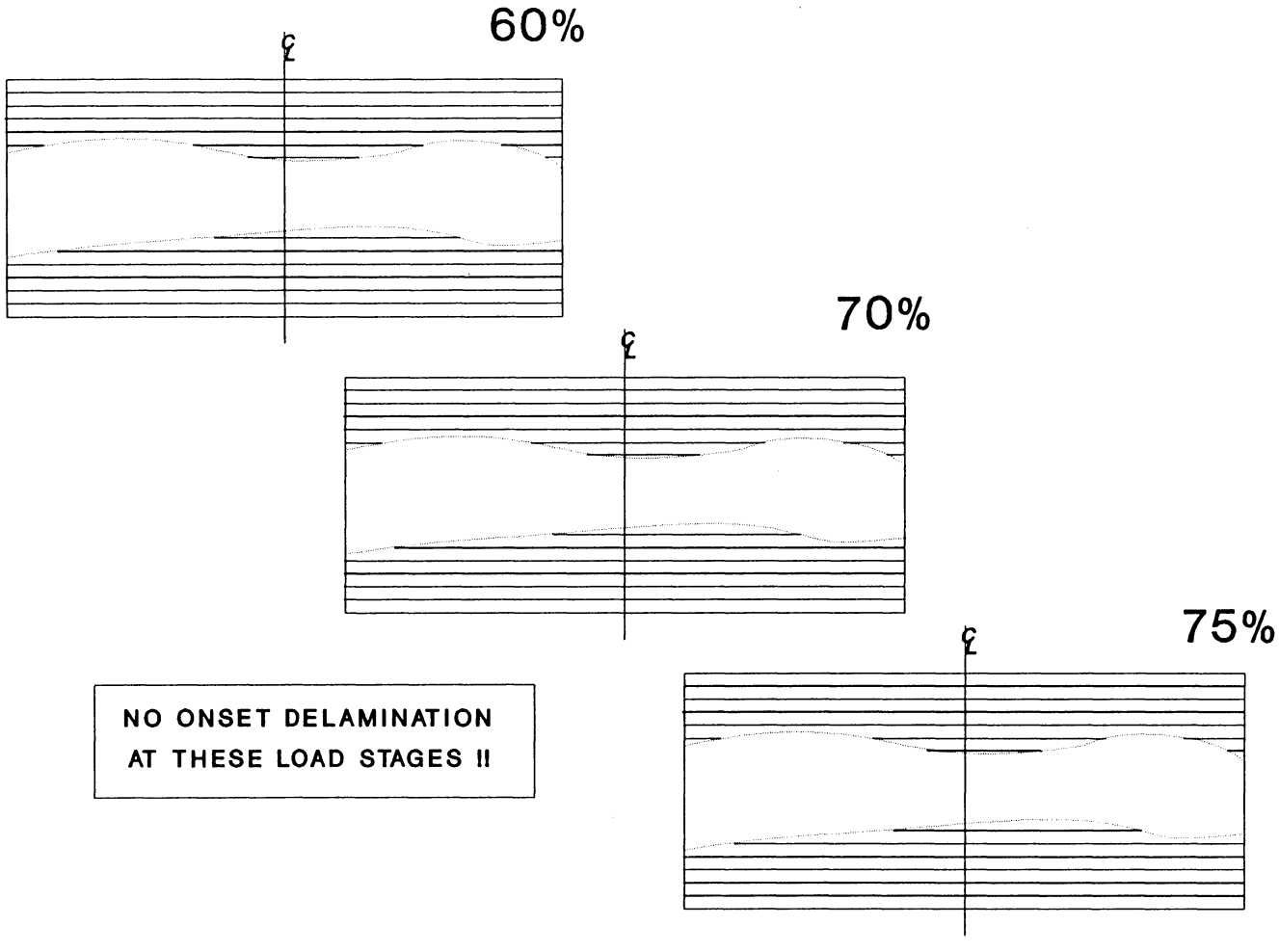


Figure No. 11: delamination process in Z-B 7-3 compression

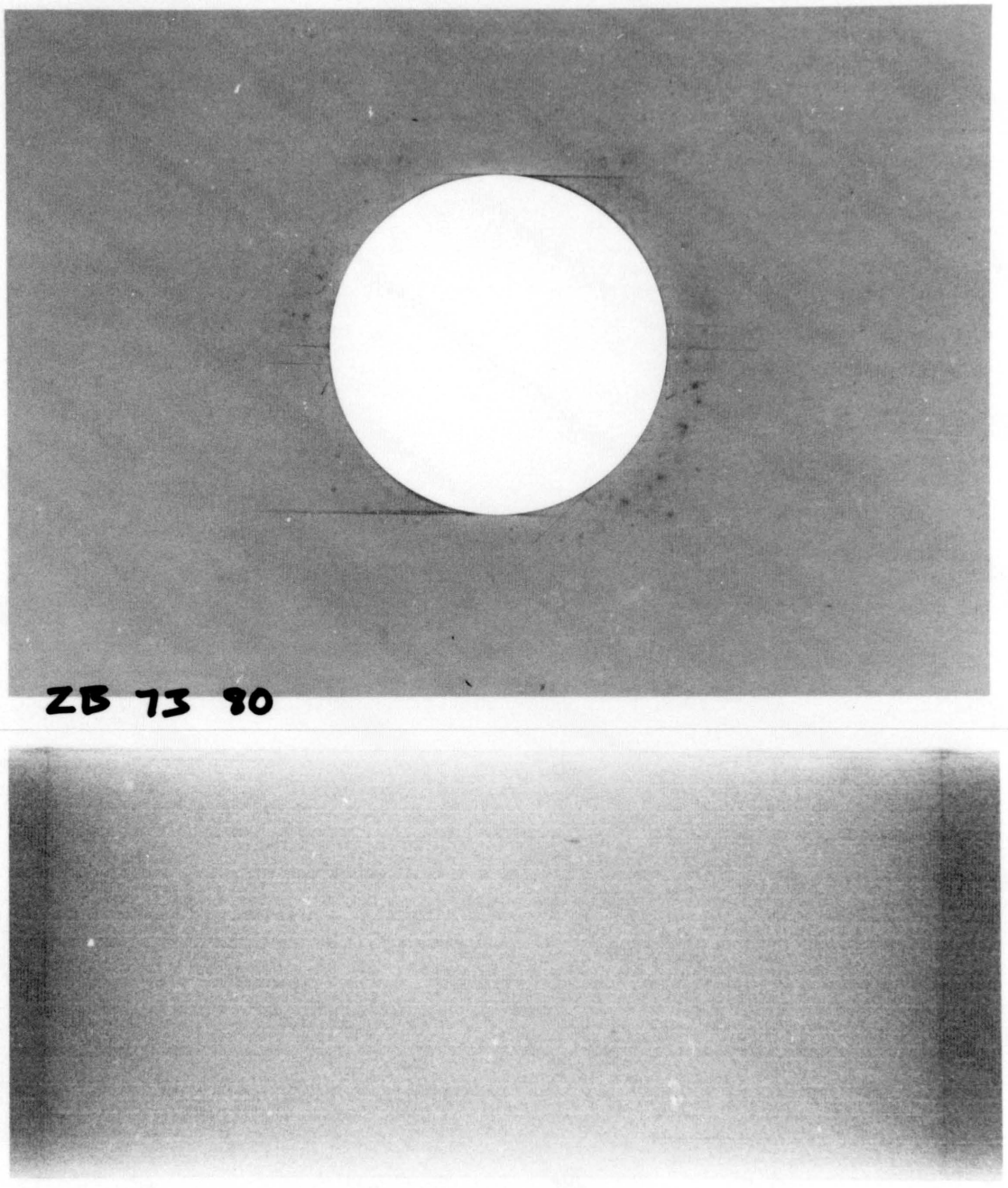


Figure No. 12: X-Ray of Z-B 7-3, 80% critical compress. load specimen top view and cut shows hole surface

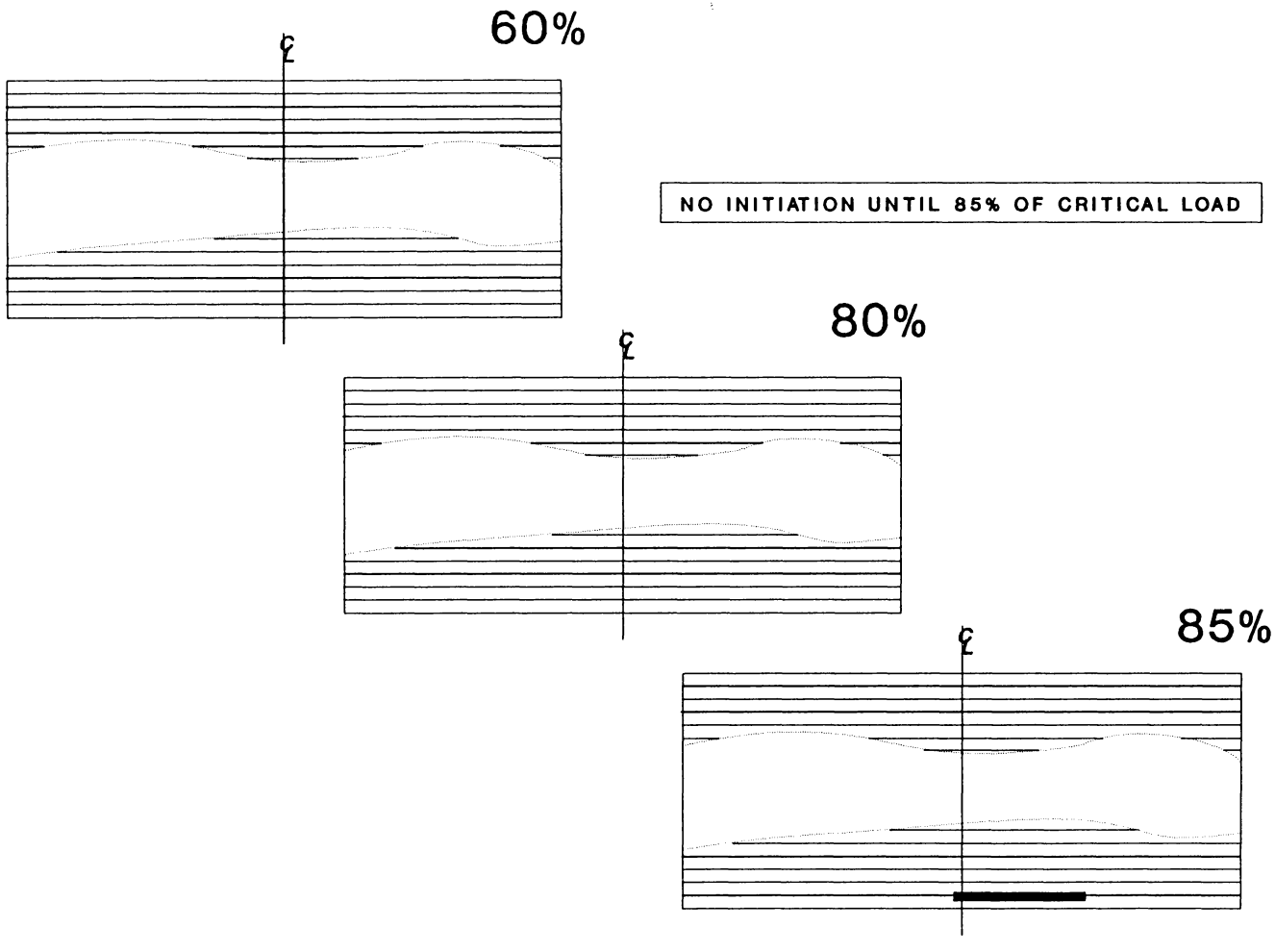


Figure No. 13: delamination process in Z-A 7-7, tension

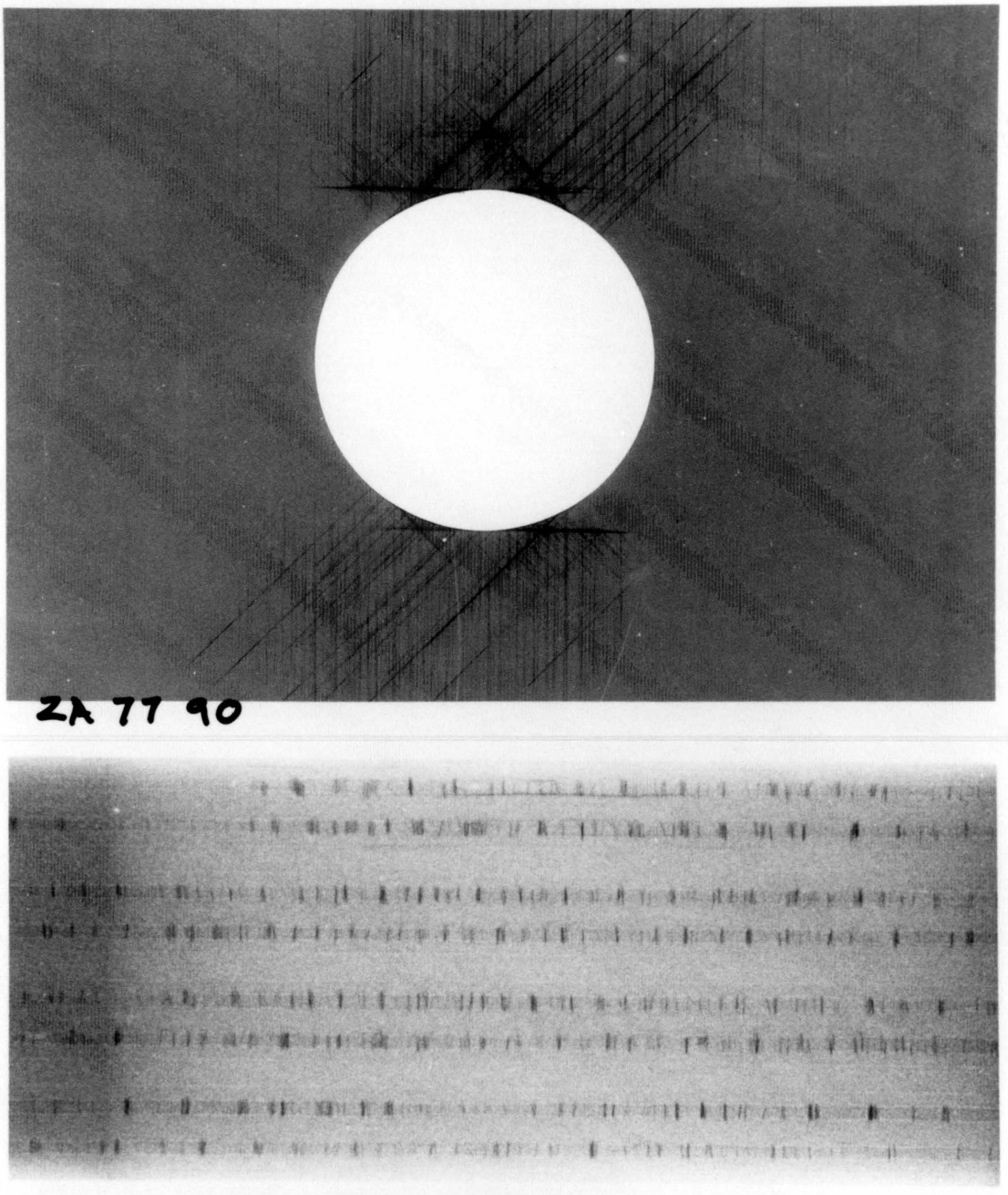


Figure No. 14: X-Ray of Z-A 7-7, 90% critical tensile load specimen top view and cut shows hole surface

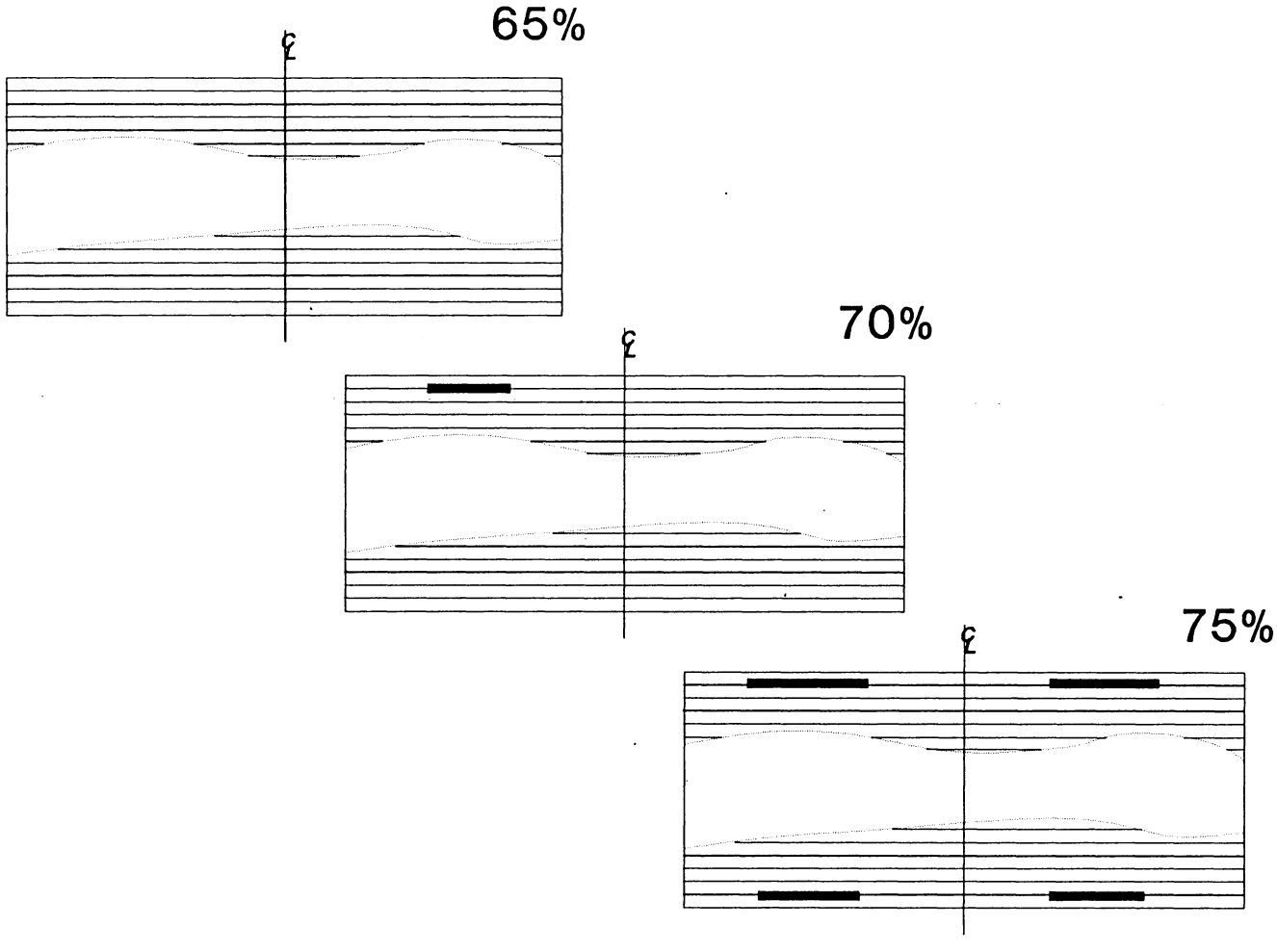


Figure No. 15: delamination process in Z-A 7-8, compression

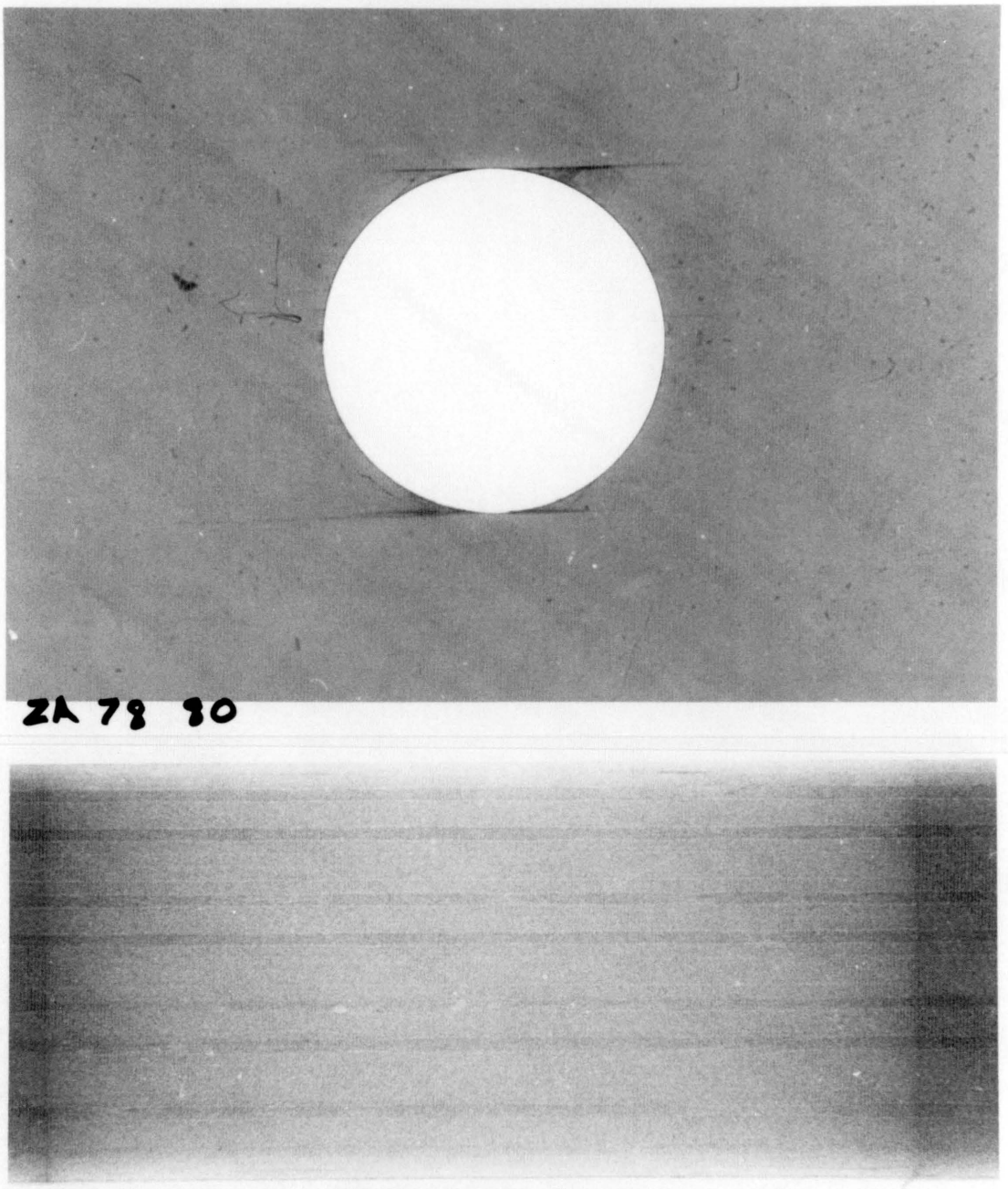


Figure No. 16: X-Ray of Z-A 7-8, 80% critical compress. load specimen top view and cut shows hole surface

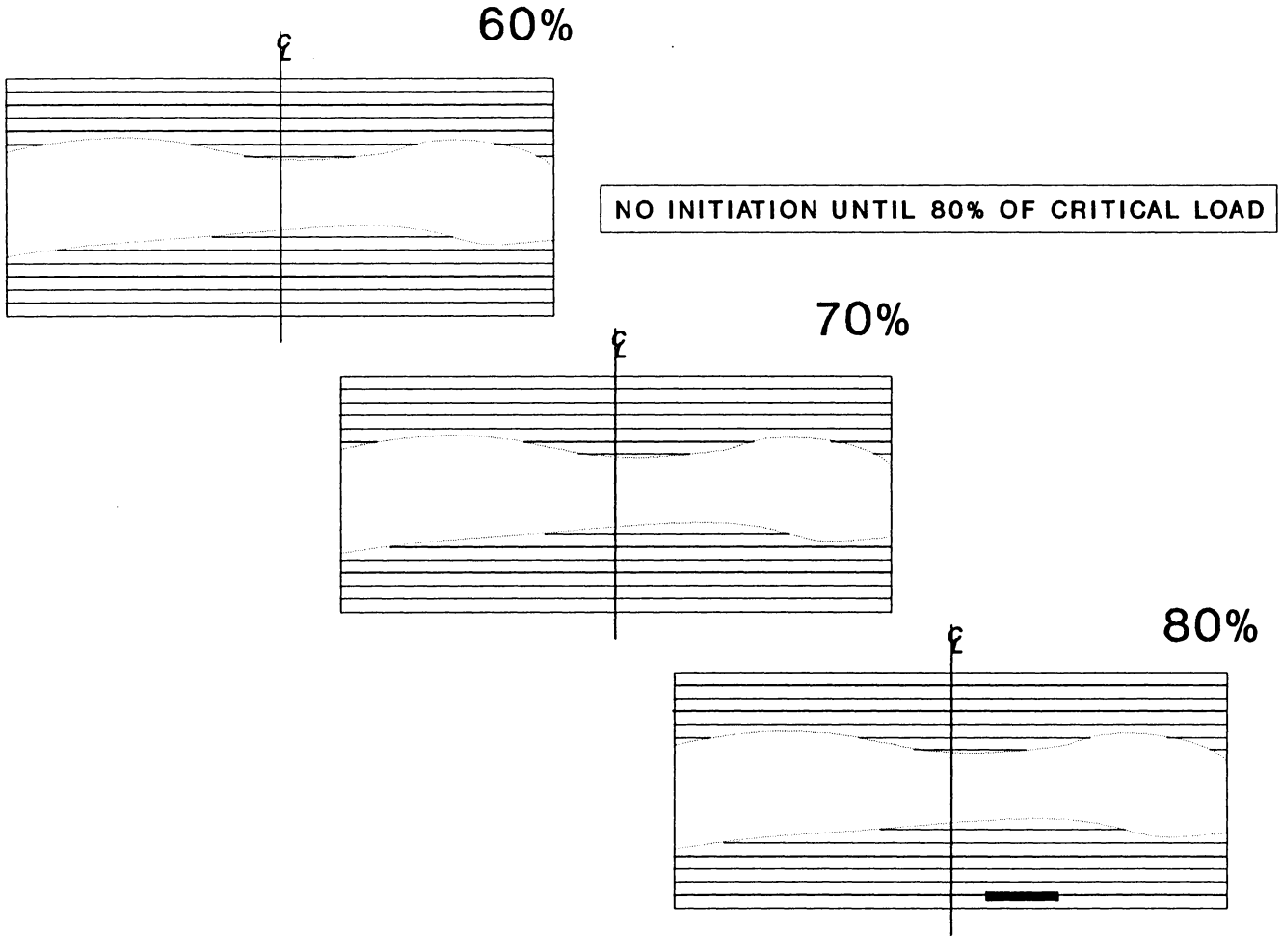


Figure No. 17: delamination process in Y-A 6-9, tension

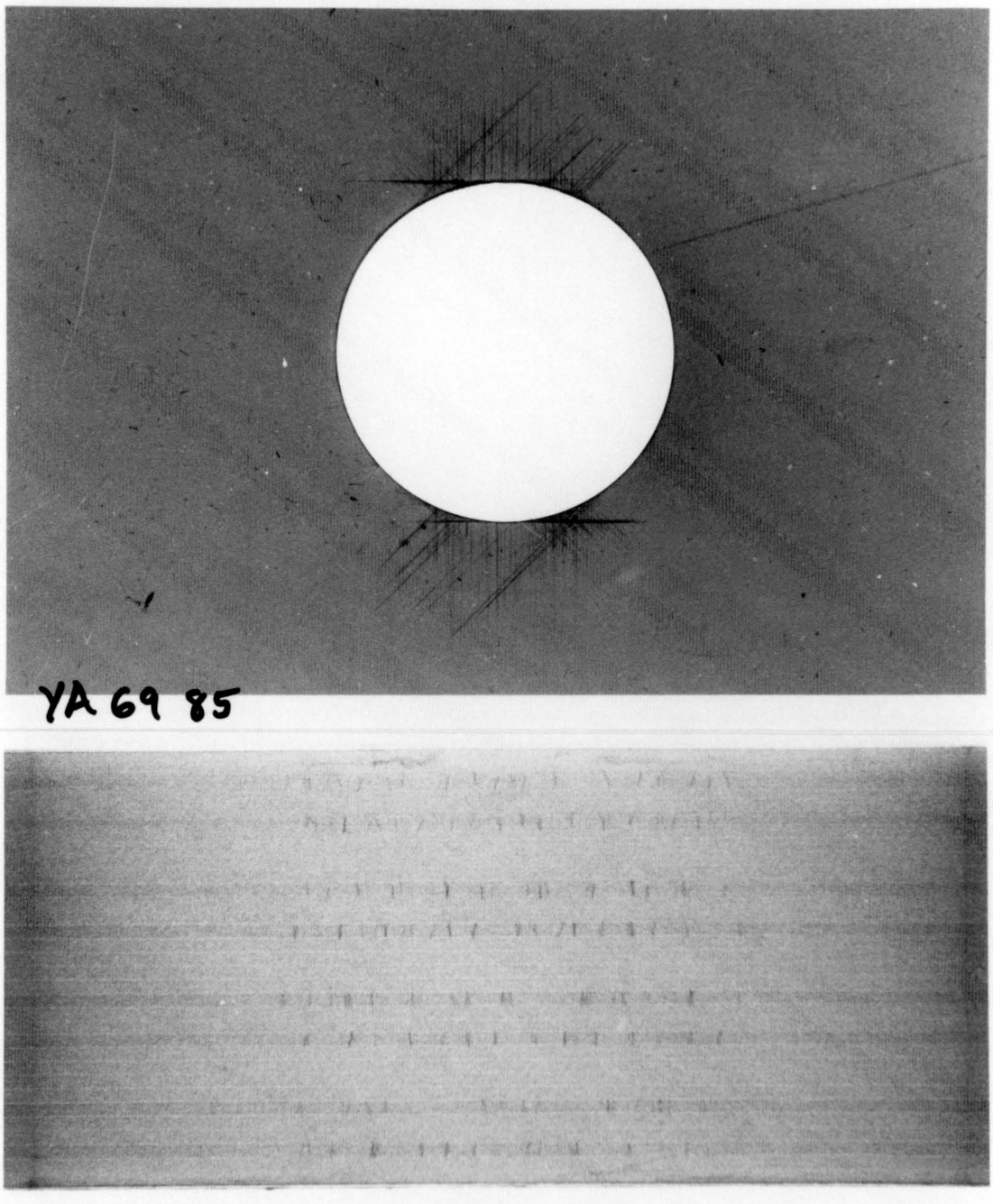


Figure No. 18: X-Ray of Y-A 6-9, 85% critical tensile load specimen top view and cut shows hole surface

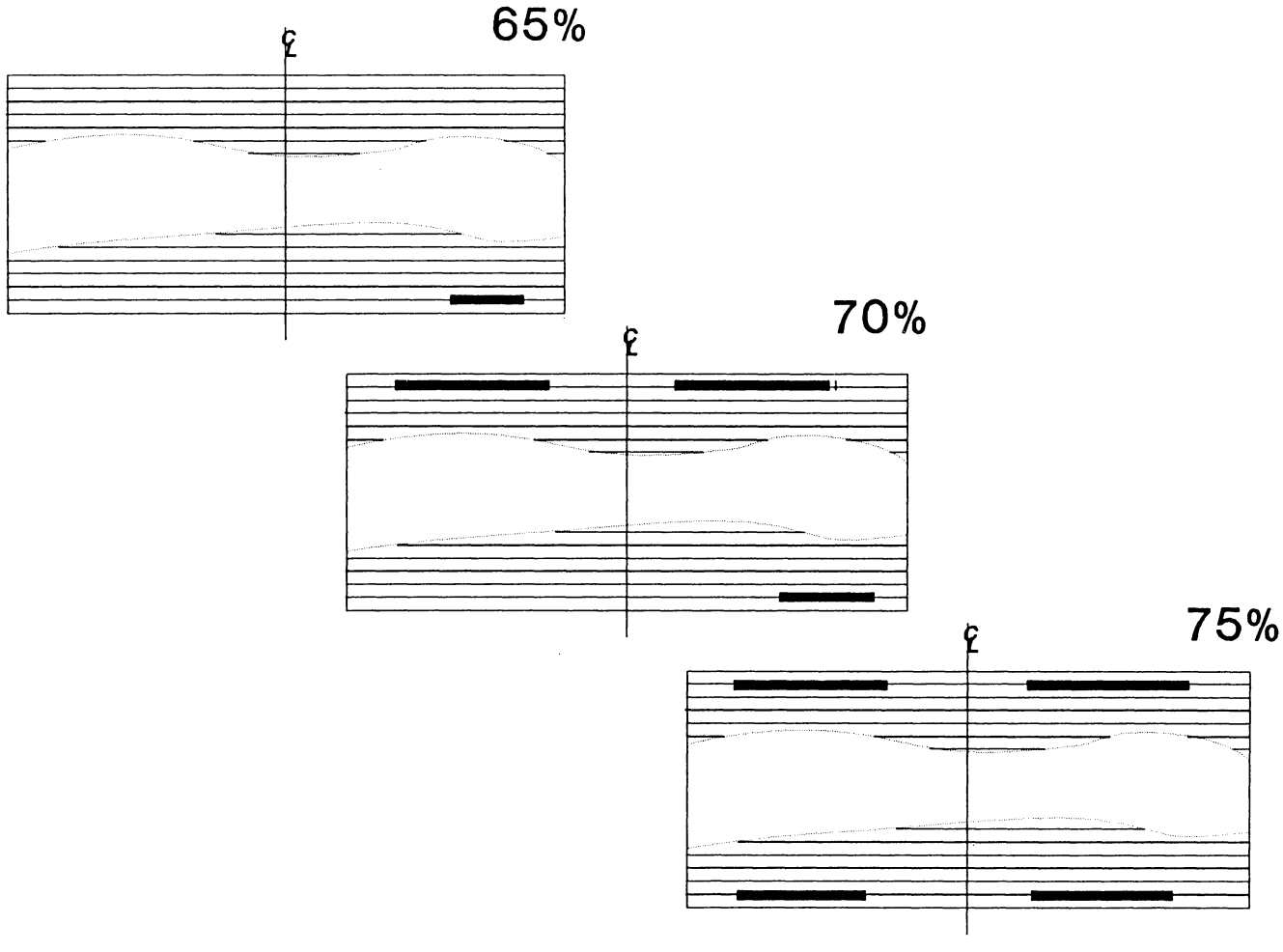


Figure No. 19: delamination process in Y-A 6-13, compression

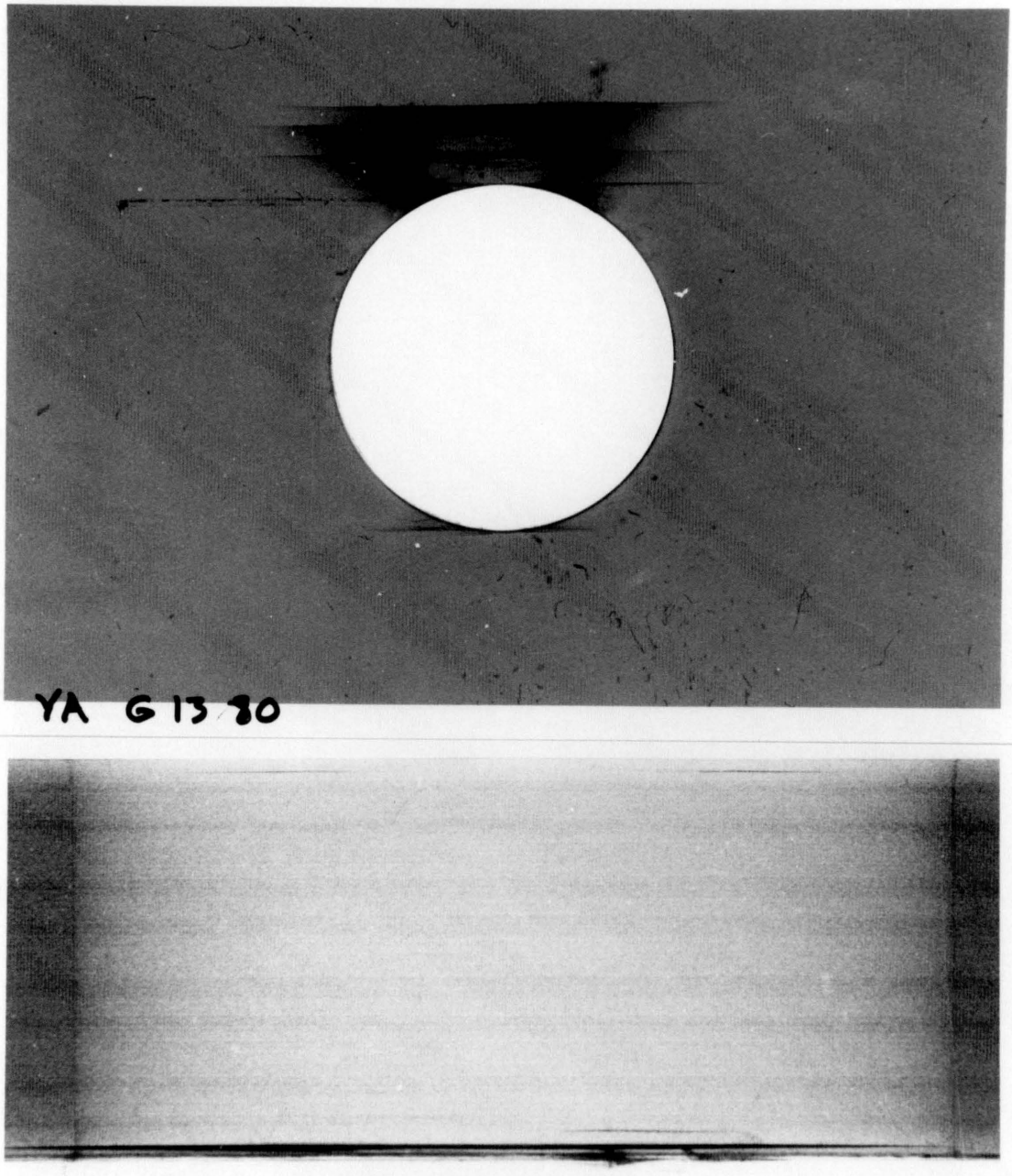


Figure No. 20: X-Ray of Y-A 6-13, 80% critical compres. load specimen top view and cut shows hole surface

The results as reflected in figs. 5 - 20 give rise to the following conclusions about the two types of materials and systems and their performance under tension as well as compression:

1. The 1808 matrix based laminate tended to delaminate more extensively under both tension and compression than did the 3501-6 matrix based laminate.
2. In compression, the 1808 matrix based laminate was more vulnerable to matrix cracking than the 3501-6, while in tension, the opposite was true.
3. All the cases in the above investigation show that delaminations occur always within the external "sub laminate", which is the basic repeating sequence, and are more likely to occur at one, or a combination of the first three interfaces.
4. Matrix cracks occur at low load levels in some cases, (60% and less) but they do not necessarily control delamination.
5. Azimuthal location of delaminations was similar for the cases examined.

# Chapter 5

# ANALYSIS OF TEST SPECIMENS

Following the investigation described in chapter 2, all test specimens were analyzed. Stages of analysis are correlated with the parameters needed for the prediction model. That consists of the calculation of the order of singularity through the homogeneous solution, and the calculation of the stress fields completing the solution with its particular part. In the following sections it will be shown how these analyses were done and provide results.

## 5.1 Order of singularity around the hole at all interfaces

The analysis of the order of singularity was performed with the computer program "SINGULAR". Description of the program and instructions are provided in App. B. Since the order of singularity depends on the two adjacent plies at the examined interface and is independent of the loads or the global geometry, there are several types of interfaces which represent all the cases of the two types of layer sequences. These interfaces are [0/45], [45/90], [90/-45], and [0/-45]. The hole was scanned for all cases at 0°, 20°, 40°, 60°, 80°, and 90° w.r.t. the longitudinal axis Z. When scanning the hole circumferencially, the coordinate system was reoriented as explained earlier. Therefore the fiber orientations of plies on both sides of the relevant interface, were calculated. Figs. 21 - 24 show the fiber direction and orientation of the sections around the hole for all the cases. Each cut provides a

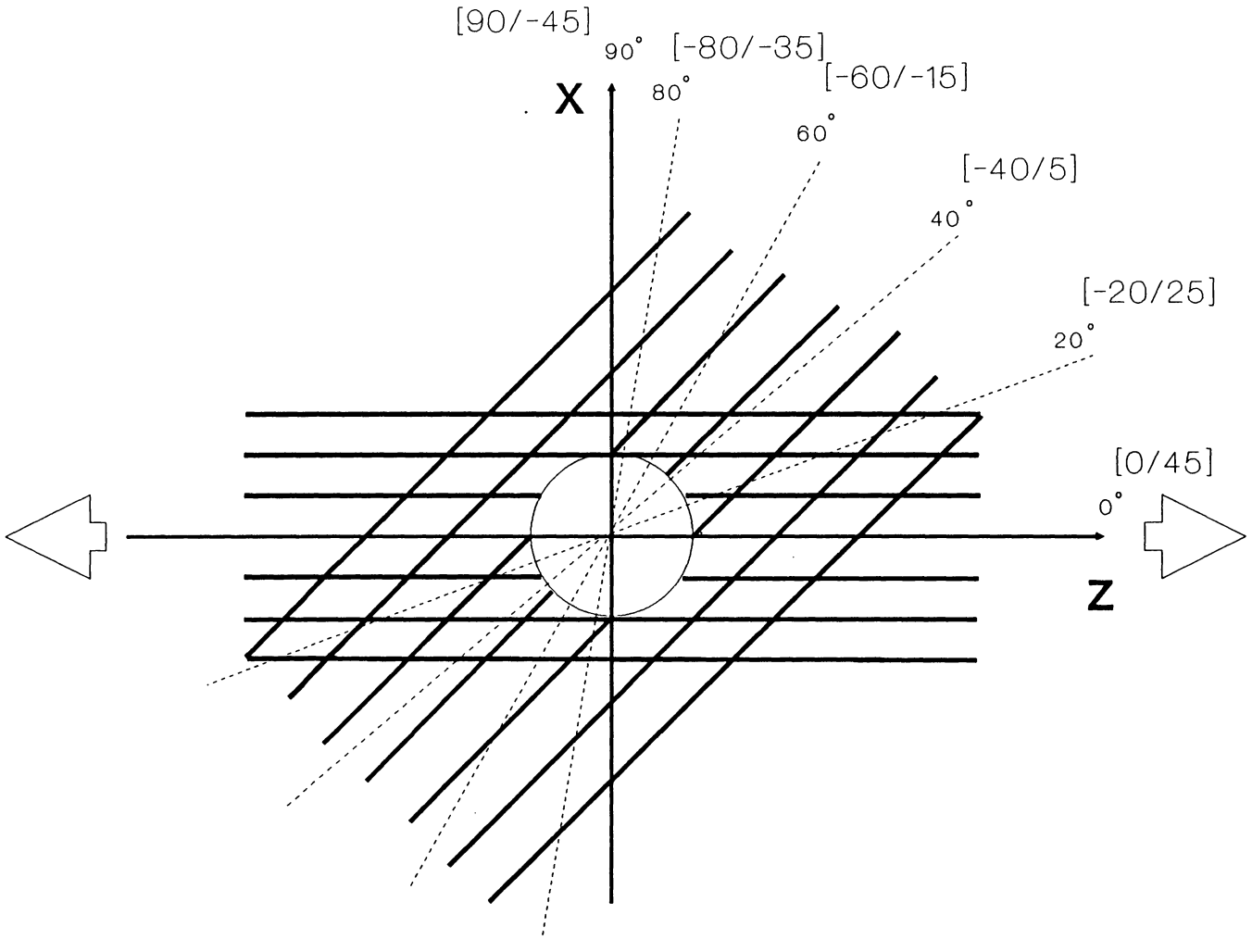


Figure No. 21: Interface [0/45], scan at 20,40,60,80,90 deg

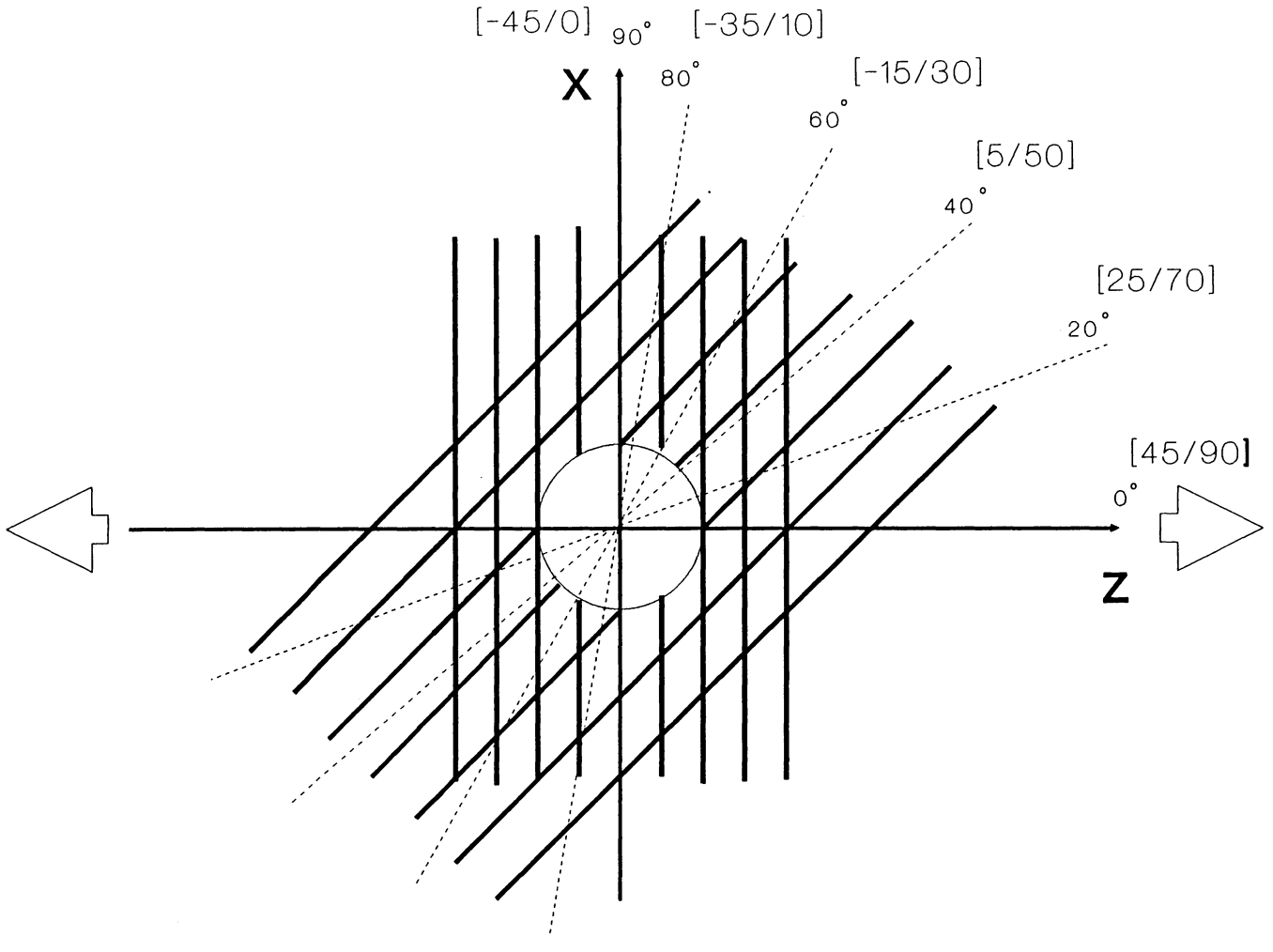


Figure No. 22: Interface [45/90], scan at 20,40,60,80,90 deg

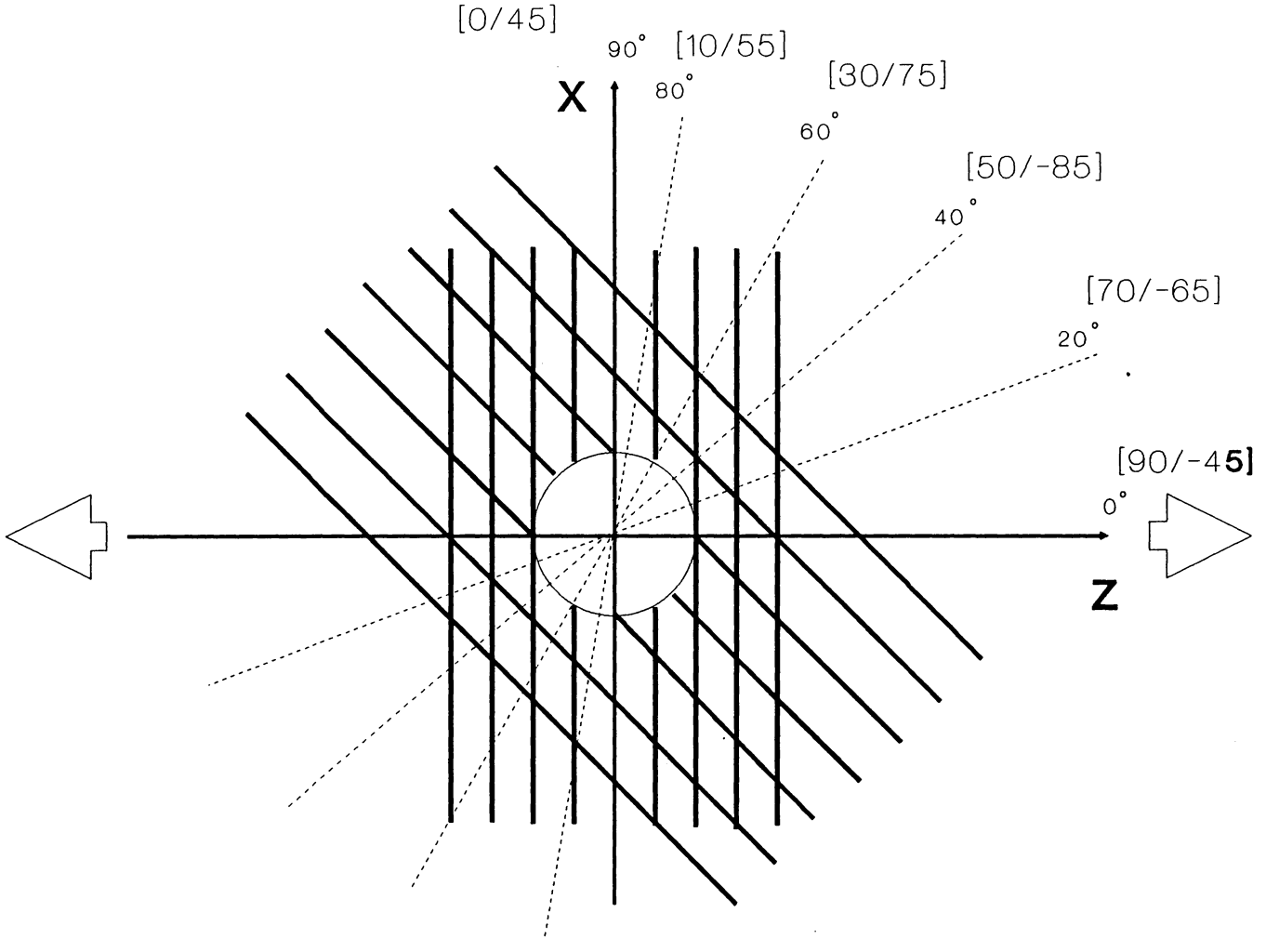


Figure No. 23: Interface [90/-45] scan at 20,40,60,80,90 deg

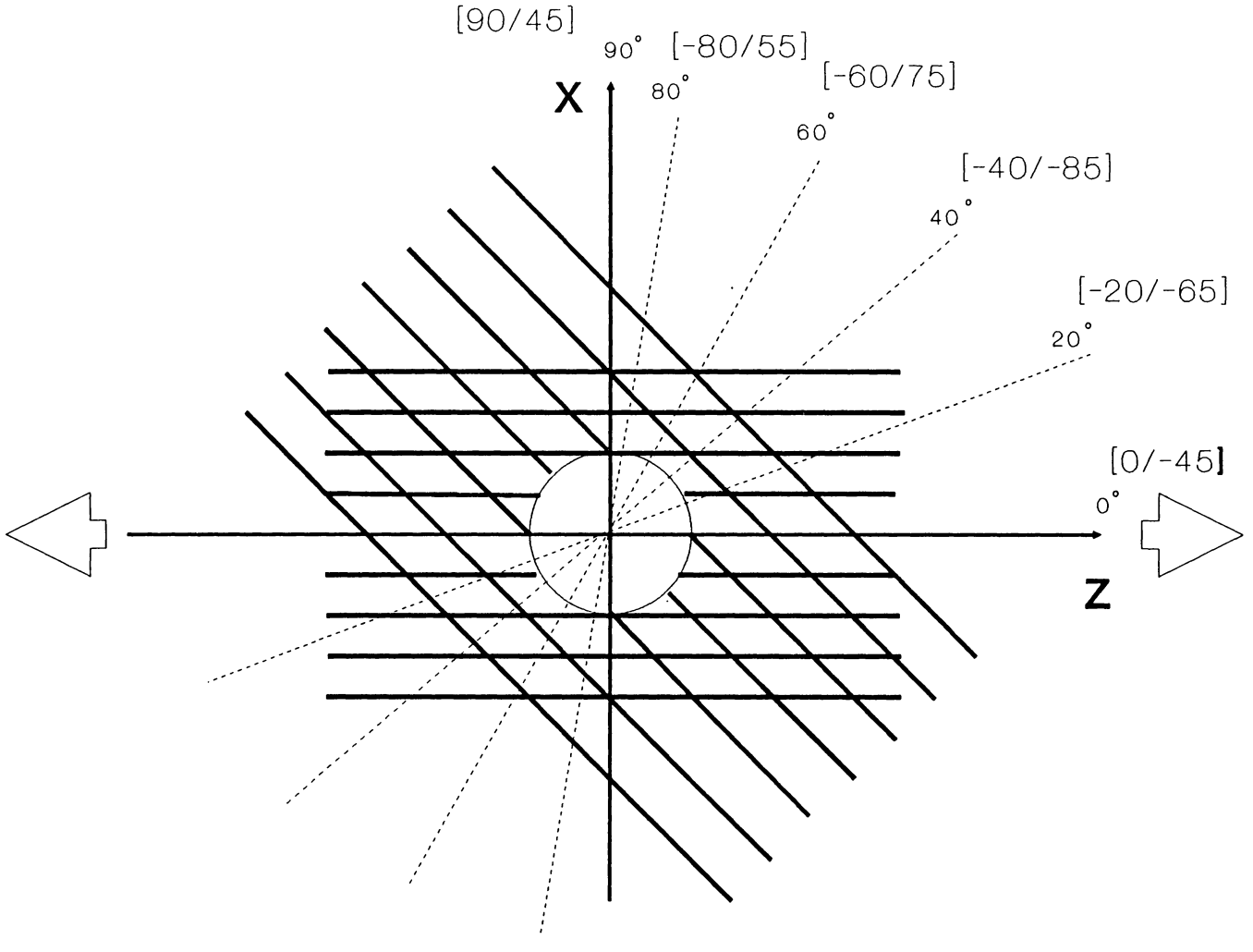


Figure No. 24: Interface [0/-45], scan at 20,40,60,80,90 deg

certain fiber orientation at the relevant interface. Table 4 summarizes all these rotated interfaces which are the subject of the analysis of the order of the singularity. The cases in Table 4 represent all the possibilities of fiber direction relations at all interfaces around the hole. With a proper input procedure, "SINGULAR" provided a series of eigenvalues for each case, and the order of the singularity was recognized by the demand that its real part has to be in the region [-1,0]. This requirement arises due to the fact that finiteness of displacement components at the origin is ensured only when $Re[\delta] > -1$, positive definiteness of strain energy of an elastic body, dictates the upper zero bound, Wang and Choi (1982). For an angle-ply system, the series of eigenvalues provide one number in that range and its imaginary part is always zero. For the other cases rather than an angle-ply, there might be more than one order of singularity and its imaginary part does not vanish. As mentioned above, for cases of non-angle-ply interfaces, there is more than one order of singularity, i.e., more than one eigenvalue within the region [-1,0]. For the case of several orders of singularities, Eqn. (60) is modified respectively. For example, for the case of two orders of singularities,

$$\sigma_\alpha = \sum_{k=1}^{6} \left[ K_{\alpha 1 k} Z_k^{\delta 1} + K_{\alpha 2 k} Z_k^{\delta 2} \right] + o(\text{higher order, nonsingular terms}) \qquad (\alpha = 1,2,3,4,5,6) \quad (66)$$

Results of analysis of all cases are summarized in Table 5. The largest, (algebraically smallest) dominant, order of singularity of each case is plotted in Figs. 25 - 28, as a function of the scanning angle

around the hole. These figures exhibit the distributions of the orders of singularity around the hole and assist to decide upon the location of the onset of delamination.

Table No. 4: rotated interfaces within the four types of interfaces in both A & B sequences

(in bold - nonrepeating interfaces for analysis)

| interface / angle | [0/45] | [45/90] | [90/-45] | [0/-45] |
|---|---|---|---|---|
| 0° | **0/45** | 45/90 | 90/-45 | 0/-45 |
| 20° | **-20/25** | **25/70** | **70/-65** | **-20/-65** |
| 40° | **-40/5** | **5/50** | **50/-85** | **-40/-85** |
| 60° | **-60/-15** | **-15/30** | **30/75** | **-60/75** |
| 80° | **-80/-35** | **35/10** | **10/55** | **-80/55** |
| 90° | **90/-45** | -45/0 | 0/45 | 90/45 |

Table No. 5: Dominant singularities, -Re[$\delta$], at examined interfaces for both materials Z & Y

| | AS4/3501-6 | AS4/1808 |
|---|---|---|
| [0/45] | 0.003644 , 0.007254, 0.01088 | ——— |
| [-20/25] | 0.0064, 0.01568, 0.132866 | ——— |
| [-40/5] | 0.00663, 0.013509, 0.131959 | 0.009961, 0.0161172, 0.482903 |
| [-60/-15] | 0.005, 0.0101, 0.64955, 0.86395 | ——— |
| [-80/-35] | 0.007144, 0.01652, 0.04107 | 0.0126138, 0.0221839, 0.887588 |
| [90/-45] | 0.010024, 0.037704 | 0.008782, 0.012355, 0.05234 |
| [25/70] | 0.012296, 0.16937 | ——— |
| [5/50] | 0.00243, 0.012543, 0.50632 | ——— |
| [-15/30] | 0.01037, 0.08328 | ——— |
| [35/10] | 0.01037084, 0.0463 | ——— |
| [70/-65] | 0.0233789 | 0.010932, 0.05368, |
| [50/-85] | 0.00044, 0.01364, 0.03646 | 0.001167, 0.010656, 0.223996 |
| [30/75] | 0.016546, 0.070888, 0.187593 | ——— |
| [10/55] | 0.0037487, 0.009875, 0.518072 | ——— |
| [-20/-65] | 0.0155814, 0.0789128 | ——— |
| [-40/-85] | 0.01537073, 0.05944 | 0.005, 0.01, 0.04, 0.14, 0.423, 0.85 |
| [-60/75] | 0.02409697 | 0.012, 0.023, 0.271, 0.43826 |
| [-80/55] | 0.0019114, 0.0180756, 0.23627 | 0.0095, 0.0104, 0.029, 0.5971 |

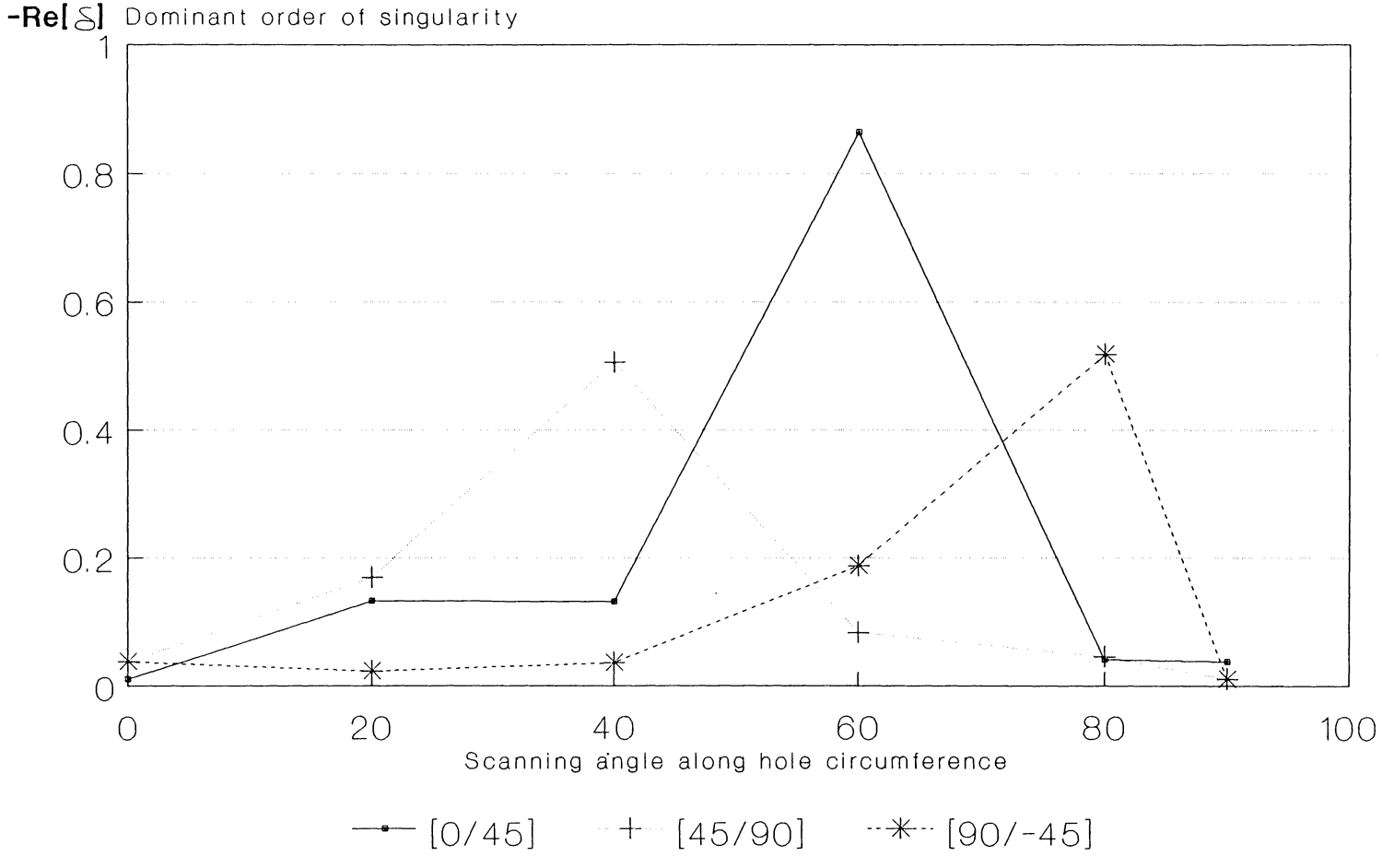


**Figure No. 25: Dominant singularities at interfaces around the hole for $[(0/45/90/-45)_S]_4$ - AS4/3501-6**

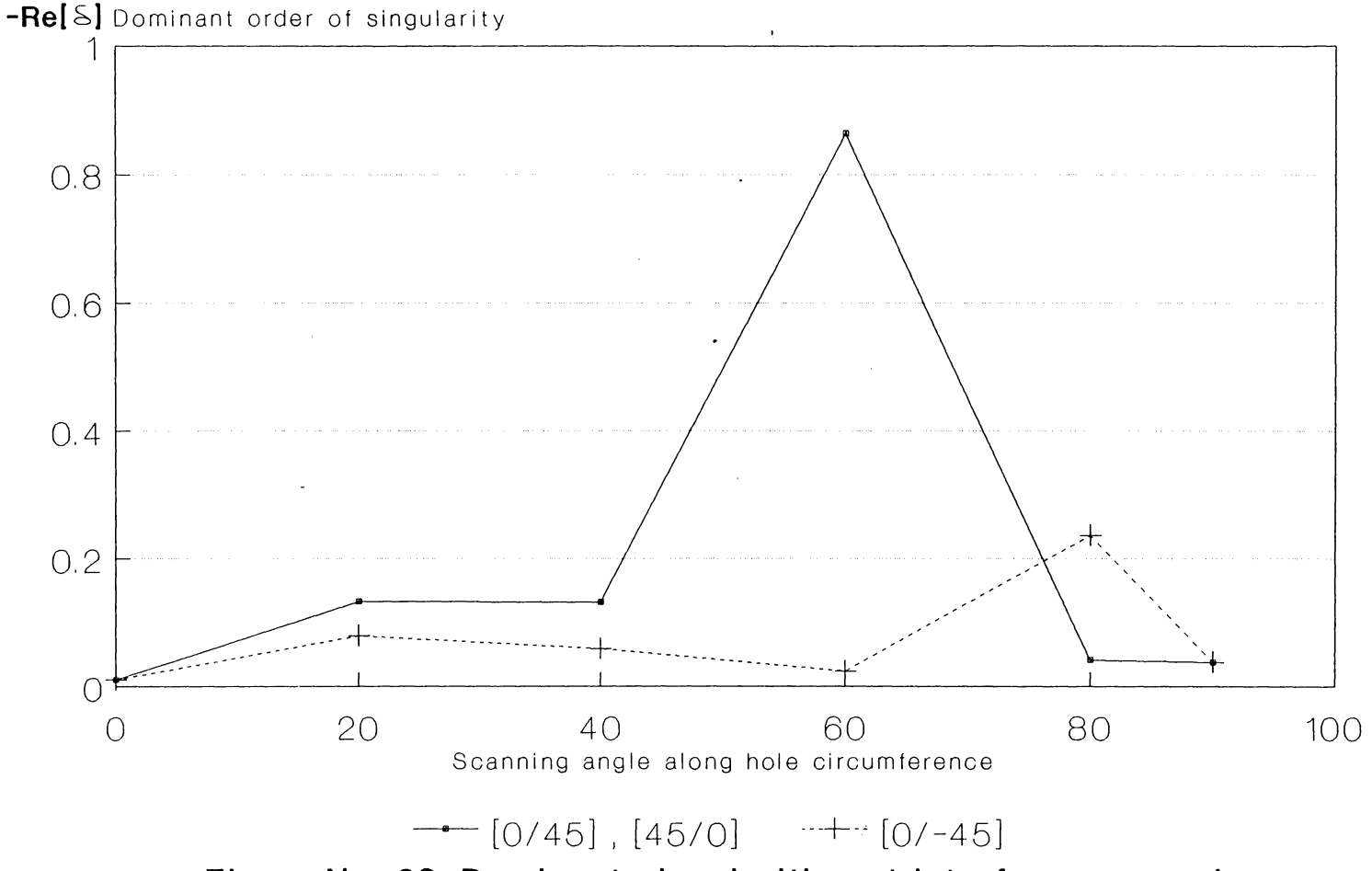


**Figure No. 26: Dominant singularities at interfaces around the hole for $[(0/45/0/-45)_S]_4$ - AS4/3501-6**

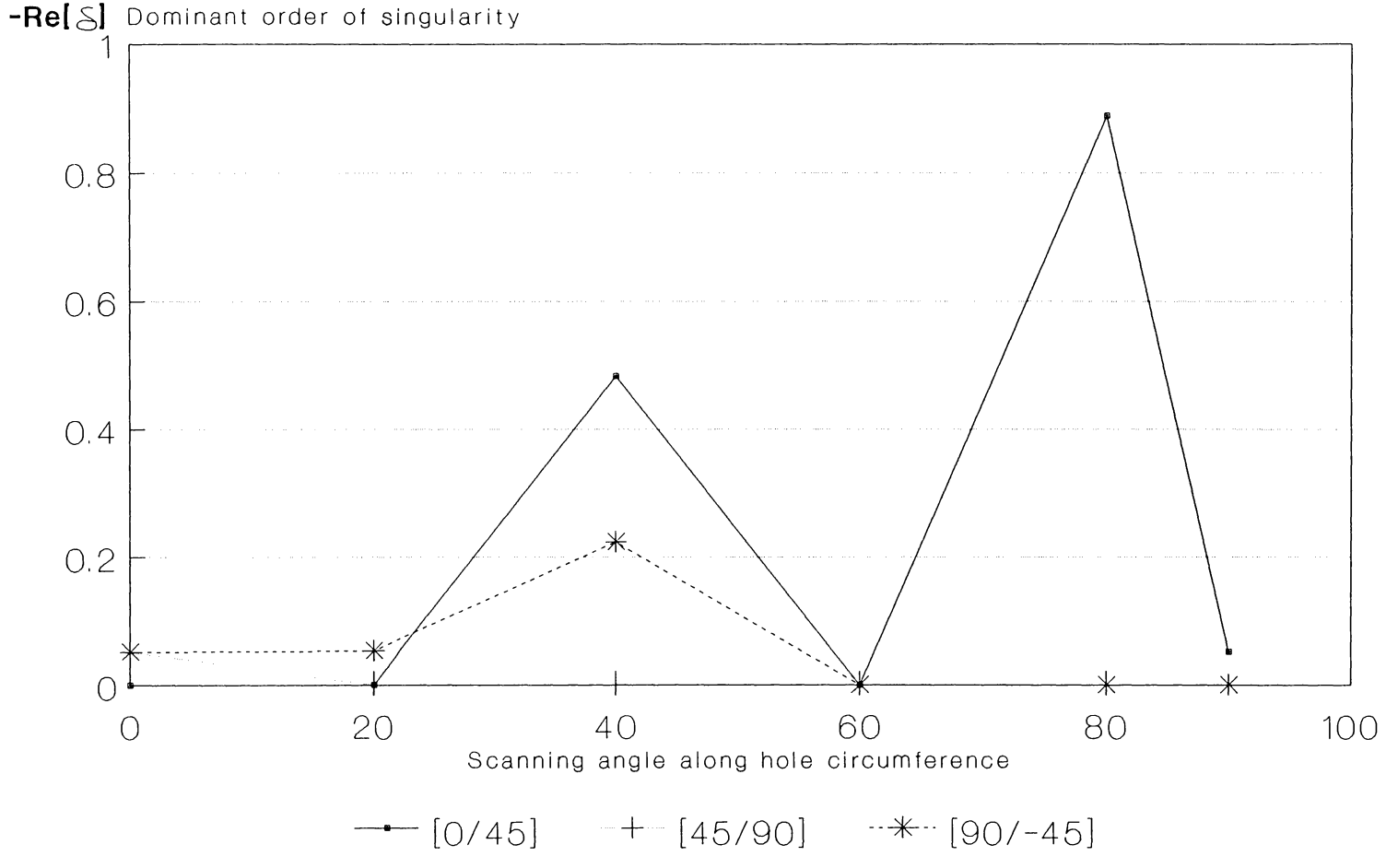


**Figure No. 27: Dominant singularities at interfaces around the hole for $[(0/45/90/-45)_S]_4$ - AS4/1808**

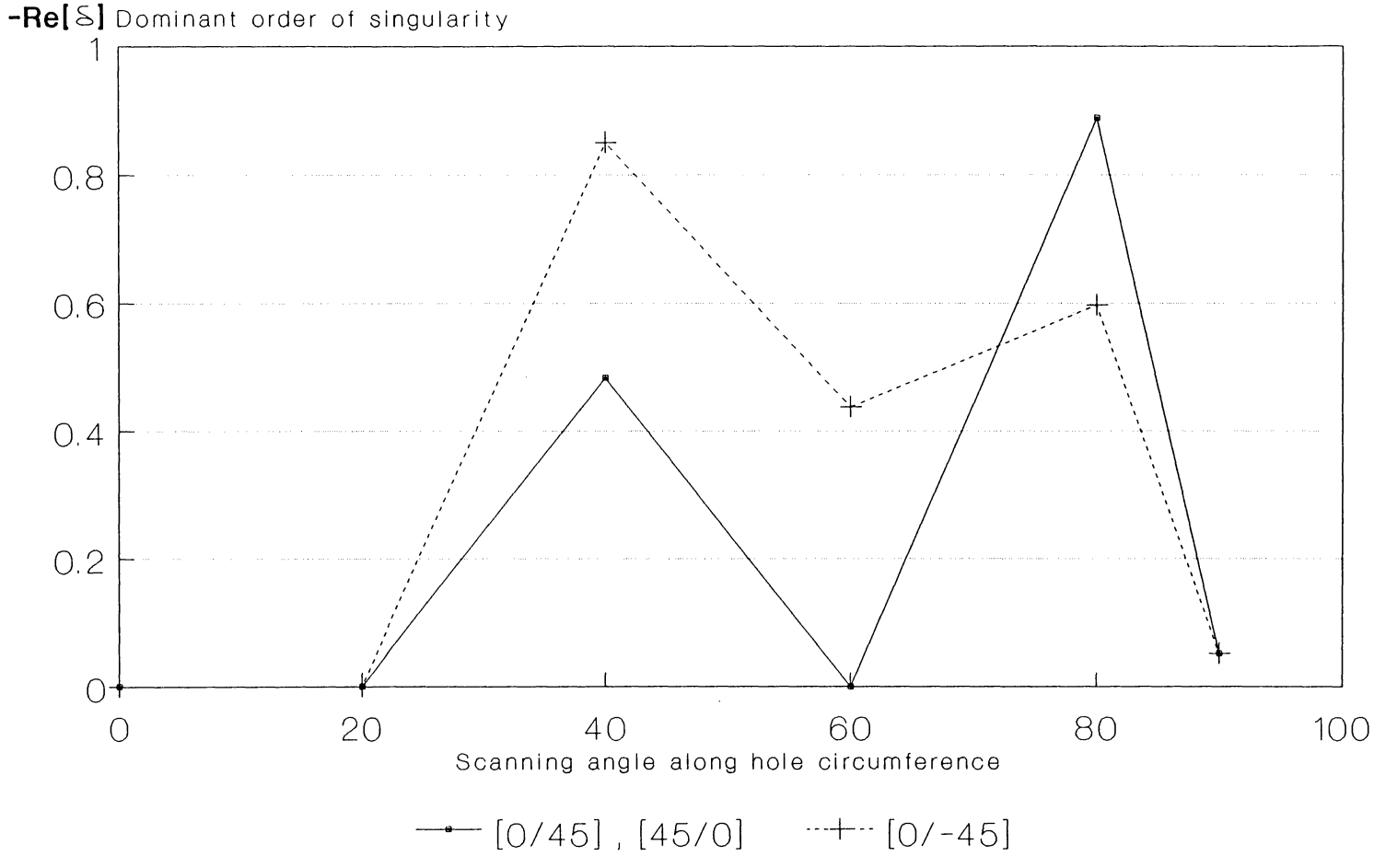


**Figure No. 28: Dominant singularities at interfaces around the hole for $[(0/45/0/-45)_S]_4$ - AS4/1808**

## 5.2 Stress fields and free edge intensities

Following the ideas drawn in chapter 3, we combine the two major parameters which the prediction model consists of. First, we use the analysis for the order of singularity to determine the interface and locations of interest, and than make final decisions upon the calculation of the energy release rate related parameters, i.e., the near-field parameters $K_1$. This process shortens the overall analysis and saves computer time as well. Figs. 25-28 show clearly the variety of locations in which the second choice has to be made, by the peaks of the curves which mean largest values of the plotted orders of singularity along the hole circumference. Analysis of the near-field parameters is made for both tension and compression. The analyzed locations are shown in table 6. The analysis is made using computer program "EDGSTR" which is described in App. C. The results are given in table 7. The analysis was done with positive remote loads which means that positive values indicate tension for the tension case and compression for the compression case, while negative values indicate tension for the case of compression loading, and compression for the case of tension remote load.

Table No. 6: Locations predicted by the order of singularity

| type | interface | scanning angle | oriented interface |
|---|---|---|---|
| Z-A | 0/45 | 20 ↙ | -20/25 |
| | 0/45 | 60 ← | -60/-15 |
| | 45/90 | 40 ← | 5/50 |
| | 90/-45 | 80 ← | 10/55 |
| Z-B | 0/45 | 60 ← | -60/-15 |
| | 45/0 | 60 ← | -60/-15 |
| Y-A | 0/45 | 80 ← | -80/-35 |
| | 0/45 | 40 ↙ | -40/5 |
| Y-B | 0/-45 | 40 ← | -40/-85 |
| | 0/45 | 80 ← | -80/-35 |

Table No. 7: Last stage analysis for selected locations - near field parameters

| material | AS4/3501-6 | | | | | | AS4/1808 | | | |
|---|---|---|---|---|---|---|---|---|---|---|
| sequence | A | | | | B | | A | | B | |
| interface | 0/45 | 0/45 | 45/90 | 90/-45 | 0/45 | 45/0 | 0/45 | 0/45 | 0/-45 | 0/45 |
| scan angle | 20 | 60 | 40 | 80 | 60 | 60 | 80 | 40 | 40 | 80 |
| $K_1$ | 0.783 | 0.946 | | | 2.439 | -0.200 | 0.445 | -2.661 | -3.438 | -4.449 |
| $K_2$ | 0.351 | -0.088 | | | -0.227 | 1.834 | -0.480 | 2.661 | -1.548 | 0.480 |
| $K_3$ | 2.363 | -0.298 | - 0 | - 0 | -0.769 | 0.511 | -0.060 | 0.881 | -6.588 | 0.060 |
| $K_4$ | -0.022 | 0.059 | | | 0.153 | -0.024 | 0.307 | - 0 | 5.090 | -0.306 |
| $K_5$ | -1.544 | 0.597 | | | 1.54 | -0.198 | 0.529 | - 0 | 9.125 | -0.529 |
| $K_6$ | 13.29 | -0.140 | | | -0.362 | -0.333 | -0.015 | -1.663 | -9.115 | 0.015 |

## 5.3 Application of the analytical results to the prediction model

Since the locations for the analyses were chosen according to the values of the order of the singularities, final decision upon the location of the onset of delamination was made based on the results of the analysis for the near-field parameters as shown in table 7. The process is very simple. First, we omit the negative magnitudes as they stand for compression which prevents the occurrence of delamination. Then, we look for the largest values which correspond to highest strain energy release rates. A physically related decision has to be made on the subject of which component dominates the phenomenon. Obviously, the out-of-plane component is a good candidate , though, a combination of all components is an option as well. Since there are solid arguments for both, final decision is accepted by observation of the experiments in relation with the analysis. Application of the analytical results to the prediction model will be examined visually in conjunction with the comparison of the analytical and the experimental results in the next chapter.

## Chapter 6

## COMPARISON OF ANALYTICAL AND EXPERIMENTAL RESULTS

As mentioned in a previous section, the prediction process is carried out in two stages. The first stage is to locate vulnerable spots by high singularities, and then the second stage consists of the decision based on the values of the-near field parameters which are energy-related coefficients. Once the most vulnerable locations are chosen by values of orders of singularity, final decision is made following the results in table 7. The predicted locations are chosen by the largest values of $K_2$, yet a further study might be performed in order to find a more realistic influence by a combination of modes involving shear components, i.e., $K_4$,$K_5$, and $K_6$. These locations are compared to the experimental results as shown in Fig. 29. It seems that good agreement is achieved by utilizing the largest values of the out-of-plane component of the near-field parameters. In none of the cases was there a disagreement about the interface. The center of the delaminated area as obtained by the experiments, does not match exactly the analytically based results in every case. In the case of Y-B in tension the location is off by $40^{\circ}$. Nevertheless, it seems that the agreement is generally good, and applicable as a tool upon which engineering decisions can be made, such as making necessary changes to ensure safety of laminate element in its conditions to the examined configuration.

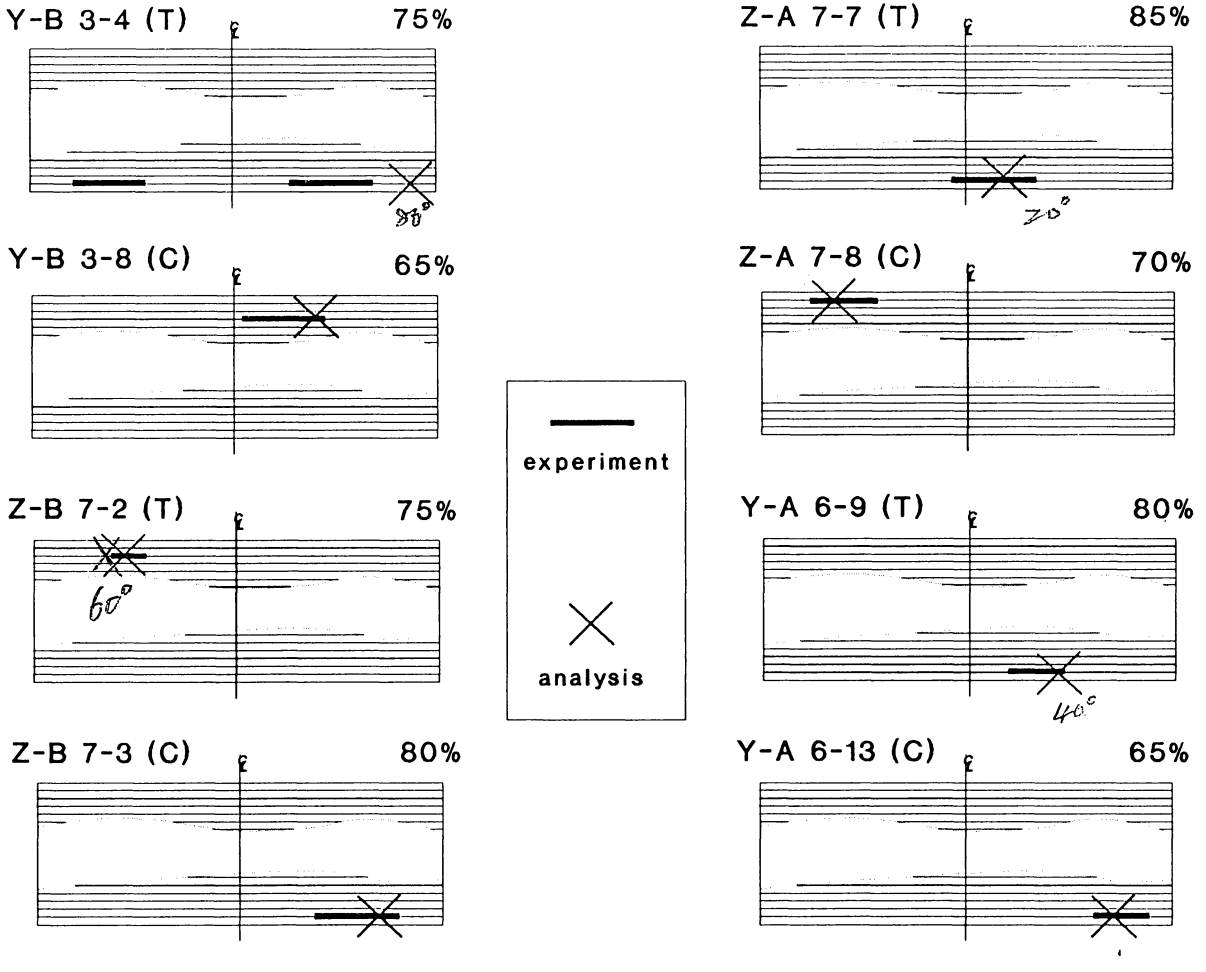


Figure no. 29: locations of the onset of delamination, analysis vs. experimental results

# Chapter 7

## SUMMARY AND CONCLUSIONS

The goal of this study was to investigate the behavior of the onset of delamination in a composite plate, focusing on the case of a hole in a coupon. The investigation was carried out in two parts, analytical and experimental, both combined to create a prediction model for the studied phenomenon.

The mission of establishing a prediction model and validating it by experiments is extremely difficult in this case. This is not a process of matching entities in the sense of curve fitting; here the task is to match the occurrence of a phenomenon at a point, which means that it is either valid or not.

As explained above, the analytically based prediction model consists of two major components. (1) The order of singularity of the stress field at the edge of the laminate, and (2) the near-field parameters which are the major components in the expression of the energy release rate which is linearly dependent upon them. Observation of the analytical results in conjunction with the experimental results, it seems that the nature of the singularity of the solution plays a major role in the mechanism of the delamination. Since that singularity is a result of a mathematical process, it is easy to ignore its physical importance. Indeed, we know that the mathematical singularity leads to infinite values of stresses which are not real, of course. The correct interpretation, however, rather than looking at the point stress values at the edge, is to consider the region of influence of the singular

stress field at a certain distance from the edge. The order of the mathematical singularity indicates the rate of change of stresses, or in its more physical interpretation, the energy release rate if delamination occurs. As in plasticity effects, the stress distribution is prone to a cutoff as dictated by the material performance, but the vicinity of that cutoff behaves in a certain way upon which qualification of the phenomenon is available.

The question of which of the components of the energy plays the major part in the delamination process, or is it the total quantity that should be considered, is partially answered here. It seems that relying on the out-of-plane component is enough to consider for the prediction process, yet this is a possible issue for further investigation in which a massive testing program should be done, probably resulting in statistically based conclusions.

Throughout the experiments, it was found that the type of matrix is a major issue in the subject of delamination, as was reflected through the analytical results as well. In fact, the analysis is capable of emphasizing that point since we obtain results all around the hole and as such we are able to compare and qualify such differences. In our case, we had two types of materials examined through two types of stacking sequences under two types of loads - tension and compression. The two types of materials consisted of the same fiber and differed by the matrix only. That isolated the matrix as an individually investigated parameter. The findings, as reflected throughout different tables and figures in previous chapters, show clearly that a system which consists of a matrix of the type 1808 is more sensitive and

vulnerable to delamination than the type 3501.

The analysis which provides the singularities and the near field parameters as well as stresses and displacements distribution is utilized through the programs "SINGULAR" and "EDGSTR". The first provides the series of eigenvalues which are used later by the second program to utilize the near-field parameters. It is very important to ensure convergence of the solution. Therefore, a series of runs should be performed, using different numbers of eigenvalues, choosing different numbers of integration points, and observing the results until convergence is achieved. The calculation process for the eigenvalues involves a deflation method which may result in division by relatively small numbers. That may lead to computationally ill conditions due to the limitations of the computers. Therefore, a suitable hardware should be selected to carry out the process. The best compiler for the task is the Turbo-Pascal used on PC's. That compiler allows real numbers ranging from $-10^{-5000}$ to $10^{5000}$. That satisfied the needs of the analysis in cases where the IBM main-frame failed to do. The above dictates the usage of micro-computers which are relatively slow. Therefore, the recommended hardware is the new IBM PS/2 model 80 or a similar machine with a CPU that uses the new and revolutionary processor 80386 by INTEL. The architecture of that processor also enables it to carry out multi-tasking jobs, a process which saves significant time.

NOMENCLATURE

| | |
|---|---|
| $A$ | coefficients matrix |
| $A_i$ | constants of integration |
| $a_i$ | coefficients of polynomials in the particular solution |
| $a$ | distance from hole to laminate edge |
| $B$ | cross sectional area at cut perpendicular to load direction |
| $B_F$ | free edge surface |
| $B_I$ | interface plane |
| $\mathbb{B}$ | results vector of set of linear equations |
| $b$ | out-of-plane coordinate of upper surface of laminate |
| $\mathbb{C}$ | coefficients vector, final description |
| $c_i$ | coefficients vector of homogeneous solution |
| $c$ | out-of-plane coordinate of lower surface of laminate |
| $D$ | vector of unknowns in the complete formulation |
| $\mathbb{D}$ | domain of integration |
| $d_1$, $d_3$ | elliptical hole axes in $x_1$ and $x_3$ directions respectively |
| $d_n^{(h)}$ | coefficients vector of the homogeneous solution |
| $ds$ | infinitesimal length |
| $E_1, E_2, E_3$ | unidirectional material properties |
| $E_x, E_y, E_z$ | laminate properties |
| $e$ | distance from hole to laminate edge |
| $F$ | Lekhnitskii's stress potentials |
| $F_k$ | Stress function used for the homogeneous solution |
| $f_{\alpha n}$ | stress eigenfunctions of the homogeneous solution |
| $G_I, G_{II}, G_{III}$ | strain energy release rates, mode I, II, and III |
| $G_{ij}$ | functions of the compliance and coeff. of part. solution |

| | |
|---|---|
| $g_{\beta n}$ | displacements eigenfunctions of the homogeneous solution |
| $(\ )^{(h)}$ | magnitude related to the homogeneous solution |
| $K_I, K_{II}, K_{III}$ | stress intensity factors, mode I, II, and III |
| $K_i$ | near-field parameters |
| $(\ )_k$ | magnitude related to the characteristic equation |
| $L_i$ | differential operator |
| $l_i$ | differential operator |
| $M_{ij}$ | remote loading - moment w.r.t. the indices |
| $(\ )^{(m)}$ | magnitude related to the $m^{th}$ ply |
| n | no. of unknowns ≡ no. of columns in the coefficients matrix |
| $p_k$ | function related to the homogeneous solution |
| $(\ )^{(p)}$ | magnitude related to the particular solution |
| $q_k$ | function related to the homogeneous solution |
| $P_{33}$ | uniaxial remote load in the $x_3$ direction |
| p | order of matrix - no. of rows |
| $\mathbb{R}$ | residual when utilizing a weighting technique |
| r | polar coordinate starts at the origin of the Cartesian sys |
| $S_{ij}$ | tensorial compliance matrix |
| $\tilde{S}_{ij}$ | reduced tensorial compliance matrix |
| S.V.D | the method of singular value decomposition |
| $(\ )^{(T)}$ | transpose |
| t | laminate thickness |
| $t_k$ | function related to the homogeneous solution |
| U | matrix of orthonormalized eigenvectors |
| $U_i$ | function related to the process of governing equations |
| $u_i$ | displacements vector |

| | |
|---|---|
| $u_{io}$ | rigid body displacements |
| V | matrix of orthonormalized eigenvectors |
| v | vector related to the singular value decomposition method |
| w | vector related to the singular value decomposition method |
| $x_i$ | directions |
| X | planner transverse direction of laminate |
| Y | out-of-plane direction of laminate |
| Z | longitudinal direction of laminate |
| $Z_k$ | argument of Lekhnitskii's stress functions |
| $\alpha$ | scanning azimuth at the hole |
| $( )_\alpha$ | Greek notation: 1-6 |
| $\delta_i$ | series of eigenvalues |
| $\delta_i^{(m)}$ | series of eigenvalues at interface m |
| $\delta\beta$ | virtual delamination length |
| $\varepsilon$ | nominal strain |
| $\varepsilon_{ij}$ | strain tensor |
| $\eta_k$ | coefficients related to the characteristic equation |
| $\Psi$ | Lekhnitskii's stress potential |
| $\phi$ | trial function related to the weighting technique |
| $\mu_k$ | roots of the characteristic equation |
| $\nu_{ij}$ | poisson's ratio |
| $\Theta^{(m)}$ | fiber direction at $m^{th}$ ply |
| $\theta^{(m)}$ | polar coordinate starts from the examined interface |
| $\Sigma$ | diagonal matrix of eigenvalues, related to the S.V.D |
| $\sigma_i$ | stresses in Greek notation |
| $\sigma_{ij}$ | stress tensor |

| | |
|---|---|
| $\sigma_{ijcal}$ | stress tensor computed for the anisotropic plate with hole |
| $\varphi$ | angle measured from the interface to $B_F$ |
| $\omega_i$ | rigid body rotations |
| $\bar{(\ )}$ | conjugate of complex number |
| $(\ )'$, $(\ )''$ | first and second differentiation |
| $\partial$ | partial differentiation |
| $\dagger$ | transpose of the conjugates |
| det[ ] | determinant |
| { } | vector |
| [ ] | matrix |

## REFERENCES


Broek, D. (1982). "Elementary engineering fracture mechanics", Martinus Nijhoff

Christensen, R. M. (1979). "Mechanics of composite materials", John Wiley & Sons, New-York.

Erdogan, F. (1965). "Stress distributions in bonded dissimilar materials with cracks", J. of Applied mechanics, 32, 403-410.

Hyer, M. W. and Klang E. C., (1985). "Contact stresses in pin-loaded orthotropic plates", Int. J. Solids Structures Vol. 21, No. 9, pp. 957-975.

Hyer, M. W. and Klang E. C., (1985). "Damage initiation at curved free edges: Application to uniaxially loaded plates containing holes and notches.", Recent advances in composites in the United States and Japan. ASTM STP 864, J. R. Vinson and M. Taya Eds., pp. 62-90.

Irwin, G. R. (1957). "Analysis of stresses and strains near the end of a crack transversing a plate. J. of Applied mechanics, 24, 361-364.

Jones, R. M. (1975). "Mechanics of composite materials", Scripta, Washington D.C.

Kassapoglou, C., and Lagace, A. P., (1987). "Closed form solutions for the interlaminar stress field in angle-ply and cross-ply laminates", Journal of composite materials, Vol. 21, pp. 292-308.

Kim, R. Y. and Soni, S. R., (1984). "Experimental and analytical studies on the onset of delamination in laminated composites", Journal of composite materials, Vol. 18.

Lekhnitskii, S. G., (1981). "Theory of elasticity of an anisotropic body", Mir Publishers, Moscow.

Muller, D. E., (1956). "A method for solving algebraic equations using an automatic computer", Mathematical tables and computations, Vol. 10, Oct. pp. 208-215.

O'Brien, T. K., (1982). "Characterization of Delamination Onset and Growth in a Composite Laminate", Damage in composite materials, ASTM STP 775, K. L. Reifsnider, Ed., pp. 140-167.

Pagano, N. J. and Pipes, B. R., (1973). "Some observations on the interlaminar strength of composite laminates", Int. J. Mech. Sol., Pergamon Press, Vol. 15 pp. 679-688.

Pipes, R. B., and Pagano, N. J. (1970). "Interlaminar stresses in composite laminates under uniform axial extension", Journal of composite materials, Vol. 4, pp. 538-548.

Rice, J. R. (1965). "Plane problems of cracks in dissimilar media" J. of Applied mechanics, 32, 418-423.

Stewart, G. W., (1973). "Introduction to matrix computations", Academic Press, Orlando, pp. 317-325.

Wang, A. S. D., and Crossman, F. W., (1977). "Some new results on edge effects in symmetric composite laminates", Journal of composite materials, Vol 11, pp. 92-106.

Wang, S. S. and Choi, I., (1982a). "Boundary-layer effects in composite laminates: Part 1 - Free edge stress singularities", ASME Journal of applied mechanics, Vol. 49, pp. 541-549.

Wang, S. S. and Choi, I., (1982b). "Boundary-layer effects in composite laminates: Part 2 - Free edge stress solutions and basic characteristics", ASME Journal of applied mechanics, Vol. 49, pp. 549-560.

Appendix A

INTEGRATION OF THE FAR END CONDITIONS EQUATIONS

$$a_9\left[\frac{x_1^2x_2}{2}\right] + \sum_n d_n\left\{\sum_{k=1}^{3}\left[C_k\eta_k\frac{Z_k^{\delta_n+2}}{(\delta_n+1)(\delta_n+2)}\right.\right.$$

$$\left.\left. + C_{k+3}\bar{\eta}_k\frac{\bar{Z}_k^{\delta_n+2}}{(\delta_n+1)(\delta_n+2)}\right]\right\} = 0 \qquad \text{(A1)}$$

$$a_8[x_1^2x_2] + a_9\left[\frac{x_1x_2^2}{2}\right] + a_{11}[x_1x_2]$$

$$+ \sum_n d_n\left\{\sum_{k=1}^{3}\left[C_k\eta_k\frac{Z_k^{\delta_n+2}}{\mu_k(\delta_n+1)(\delta_n+2)} + C_{k+3}\bar{\eta}_k\frac{\bar{Z}_k^{\delta_n+2}}{\bar{\mu}_k(\delta_n+1)(\delta_n+2)}\right]\right\} = 0$$

(A2)

$$A_1\left[\frac{x_1^2x_2}{2}\right] + A_2\left[\frac{x_1x_2^2}{2}\right] + A_3[x_1x_2] + a_1\left[-\frac{S_{32}}{S_{33}}3x_1^2x_2\right]$$

$$+ a_2\left[-\frac{S_{32}}{S_{33}}x_2^2x_1 + \frac{S_{36}}{S_{33}}x_1^2x_2\right] + a_5\left[-\frac{S_{32}}{S_{33}}2x_1x_2\right] + a_8\left[\frac{S_{34}}{S_{33}}x_1^2x_2\right]$$

$$+ a_9\left[\frac{S_{34}}{S_{33}}\frac{x_2^2x_1}{2} - \frac{S_{35}}{S_{33}}\frac{x_1^2x_2}{2}\right] + a_{11}\left[\frac{S_{34}}{S_{33}}x_1x_2\right]$$

$$+ \sum_n d_n\left\{-\frac{S_{31}}{S_{33}}\sum_{k=1}^{3}\left[C_k\mu_k\frac{Z_k^{\delta_n+2}}{(\delta_n+1)(\delta_n+2)} + C_{k+3}\bar{\mu}_k\frac{\bar{Z}_k^{\delta_n+2}}{(\delta_n+1)(\delta_n+2)}\right]\right.$$

$$-\frac{S_{32}}{S_{33}}\sum_{k=1}^{3}\left[C_k\frac{Z_k^{\delta_n+2}}{\mu_k(\delta_n+1)(\delta_n+2)} + C_{k+3}\frac{\bar{Z}_k^{\delta_n+2}}{\bar{\mu}_k(\delta_n+1)(\delta_n+2)}\right]$$

$$+\frac{S_{34}}{S_{33}}\sum_{k=1}^{3}\left[C_k\frac{\eta_k}{\mu_k}\frac{Z_k^{\delta_n+2}}{(\delta_n+1)(\delta_n+2)} + C_{k+3}\frac{\bar{\eta}_k}{\bar{\mu}_k}\frac{\bar{Z}_k^{\delta_n+2}}{(\delta_n+1)(\delta_n+2)}\right]$$

$$-\frac{S_{35}}{S_{33}}\sum_{k=1}^{3}\left[C_k\eta_k\frac{Z_k^{\delta_n+2}}{(\delta_n+1)(\delta_n+2)} + C_{k+3}\bar{\eta}_k\frac{\bar{Z}_k^{\delta_n+2}}{(\delta_n+1)(\delta_n+2)}\right]$$

$$\left.+\frac{S_{36}}{S_{33}}\sum_{k=1}^{3}\left[C_k\frac{Z_k^{\delta_n+2}}{(\delta_n+1)(\delta_n+2)} + C_{k+3}\frac{\bar{Z}_k^{\delta_n+2}}{(\delta_n+1)(\delta_n+2)}\right] = P_{33}\right.$$

(A3)

$$A_1\left[\frac{x_1^2x_2^2}{4}\right] + A_2\left[\frac{x_1x_2^3}{3}\right] + A_3\left[\frac{x_1x_2^2}{2}\right] + a_1\left[-\frac{S_{32}}{S_{33}}\frac{3x_1x_2^2}{2}\right]$$

$$+ a_2\left[-\frac{S_{32}}{S_{33}}\frac{2x_1x_2^2}{3} + \frac{S_{36}}{S_{33}}\frac{x_1x_2^2}{2}\right] + a_5\left[-\frac{S_{32}}{S_{33}}x_1x_2^2\right] + a_8\left[\frac{S_{34}}{S_{33}}\frac{x_1^2x_2^2}{2}\right]$$

$$+ a_9\left[\frac{S_{34}}{S_{33}}\frac{x_2^3x_1}{3} - \frac{S_{35}}{S_{33}}\frac{x_1^2x_2^2}{4}\right] + a_{11}\left[\frac{S_{34}}{S_{33}}\frac{x_1x_2^2}{2}\right]$$

$$+ \sum_n d_n\left\{\sum_{k=1}^{3}\left[C_k\left[\frac{x_2}{\mu_k}\frac{Z_k^{\delta_n+2}}{(\delta_n+1)(\delta_n+2)} - \frac{1}{\mu_k^2}\frac{Z_k^{\delta_n+3}}{(\delta_n+1)(\delta_n+2)(\delta_n+3)}\right]\right.\right.$$

$$\times\left[-\frac{S_{31}}{S_{33}}\mu_k^2 - \frac{S_{32}}{S_{33}} + \frac{S_{34}}{S_{33}}\eta_k - \frac{S_{35}}{S_{33}}\eta_k\mu_k + \frac{S_{36}}{S_{33}}\mu_k\right]$$

$$C_{k+3}\left[\frac{x_2}{\bar{\mu}_k}\frac{\bar{Z}_k^{\delta_n+2}}{(\delta_n+1)(\delta_n+2)} - \frac{1}{\bar{\mu}_k^2}\frac{\bar{Z}_k^{\delta_n+3}}{(\delta_n+1)(\delta_n+2)(\delta_n+3)}\right]$$

$$\left.\left.\times\left[-\frac{S_{31}}{S_{33}}\bar{\mu}_k^2 - \frac{S_{32}}{S_{33}} + \frac{S_{34}}{S_{33}}\bar{\eta}_k - \frac{S_{35}}{S_{33}}\bar{\eta}_k\bar{\mu}_k + \frac{S_{36}}{S_{33}}\bar{\mu}_k\right]\right]\right\}$$

$$= M_{11} \qquad \text{(A4)}$$

$$A_1\left[\frac{x_1^3x_2}{3}\right] + A_2\left[\frac{x_1^2x_2^2}{4}\right] + A_3\left[\frac{x_1^2x_2}{2}\right] + a_1\left[-\frac{S_{32}}{S_{33}}\,2x_1^3x_2\right]$$

$$+ a_2\left[-\frac{S_{32}}{S_{33}}\,\frac{x_1x_2^2}{2} + \frac{S_{36}}{S_{33}}\,\frac{2x_1x_2^2}{3}\right] + a_5\left[-\frac{S_{32}}{S_{33}}\,x_1^2x_2\right] + a_8\left[\frac{S_{34}}{S_{33}}\,\frac{2x_1^3x_2}{3}\right]$$

$$+ a_9\left[\frac{S_{34}}{S_{33}}\,\frac{x_1^2x_2^2}{4} - \frac{S_{35}}{S_{33}}\,\frac{x_1^3x_2}{3}\right] + a_{11}\left[\frac{S_{34}}{S_{33}}\,\frac{x_1^2x_2}{2}\right]$$

$$+ \sum_n d_n\left\{\sum_{k=1}^{3}\left[C_k\left(\frac{x_1}{\mu_k}\,\frac{Z_k^{\delta_n+2}}{(\delta_n+1)(\delta_n+2)} - \frac{1}{\mu_k}\,\frac{Z_k^{\delta_n+3}}{(\delta_n+1)(\delta_n+2)(\delta_n+3)}\right)\right.\right.$$

$$\times\left(-\frac{S_{31}}{S_{33}}\,\mu_k^2 - \frac{S_{32}}{S_{33}} + \frac{S_{34}}{S_{33}}\,\eta_k - \frac{S_{35}}{S_{33}}\,\eta_k\mu_k + \frac{S_{36}}{S_{33}}\,\mu_k\right)$$

$$C_{k+3}\left(\frac{x_1}{\bar{\mu}_k}\,\frac{\bar{Z}_k^{\delta_n+2}}{(\delta_n+1)(\delta_n+2)} - \frac{1}{\bar{\mu}_k}\,\frac{\bar{Z}_k^{\delta_n+3}}{(\delta_n+1)(\delta_n+2)(\delta_n+3)}\right)$$

$$\left.\left.\times\left(-\frac{S_{31}}{S_{33}}\,\bar{\mu}_k^2 - \frac{S_{32}}{S_{33}} + \frac{S_{34}}{S_{33}}\,\bar{\eta}_k - \frac{S_{35}}{S_{33}}\,\bar{\eta}_k\bar{\mu}_k + \frac{S_{36}}{S_{33}}\,\bar{\mu}_k\right)\right]\right\}$$

$$= M_{22} \qquad \text{(A5)}$$

$$a_8\left[\frac{2x_1^3x_2}{3}\right] + a_9\left[\frac{x_1^2x_2^2}{2}\right] + a_{11}\left[\frac{x_1^2x_2}{2}\right]$$

$$+ \sum_n d_n \left\{ \sum_{k=1}^{3} \left[ C_k \eta_k \right. \right.$$

$$\times \left( \left[ \frac{x_1}{\mu_k} + x_2 \right] \frac{Z_k^{\delta_n+2}}{(\delta_n+1)(\delta_n+2)} - \frac{1}{\mu_k} \frac{Z_k^{\delta_n+3}}{(\delta_n+1)(\delta_n+2)(\delta_n+3)} \right)$$

$$+ C_{k+3}\bar{\eta}_k$$

$$\times \left( \left[ \frac{x_1}{\bar{\mu}_k} + x_2 \right] \frac{\bar{Z}_k^{\delta_n+2}}{(\delta_n+1)(\delta_n+2)} - \frac{1}{\bar{\mu}_k} \frac{\bar{Z}_k^{\delta_n+3}}{(\delta_n+1)(\delta_n+2)(\delta_n+3)} \right)$$

$$= - M_{12} \qquad \text{(A6)}$$

Appendix B

PROGRAM "SINGULAR"

Program "SINGULAR" was developed on a PC using a Turbo Pascal compiler, Ver. 4.0. This compiler enables to use the large range of real numbers $\left[1.9\times10^{-4951}, 1.1\times10^{4932}\right]$. This extraordinary range enables the application of the deflation method, Muller (1956), when solving for the eigenvalues of the transcendental form matrix.

B1 Interactive input process

The following figures are the sequence of screens as appear in the process of input data into "SINGULAR". The program is self explanatory, and menu driven. Fig. B1 is the opening logo. Fig. B2 provides the user the choice of using a pre-defined input file or using the interactive on-screen input process. If the choice is a pre-defined file, then fig. B3 is the next screen to appear, asking for the input file name and verifying its existence. Also, this screen gives the exact data needed to be include in the pre-defined file. For the other choice of on-screen input process, fig. B4 views the relevant screen. This screen is self-explanatory and guides the user with a definition of each field shown on a line which is the lower side of the frame. This instruction line changes respectively with the cursor movements from one field to another.

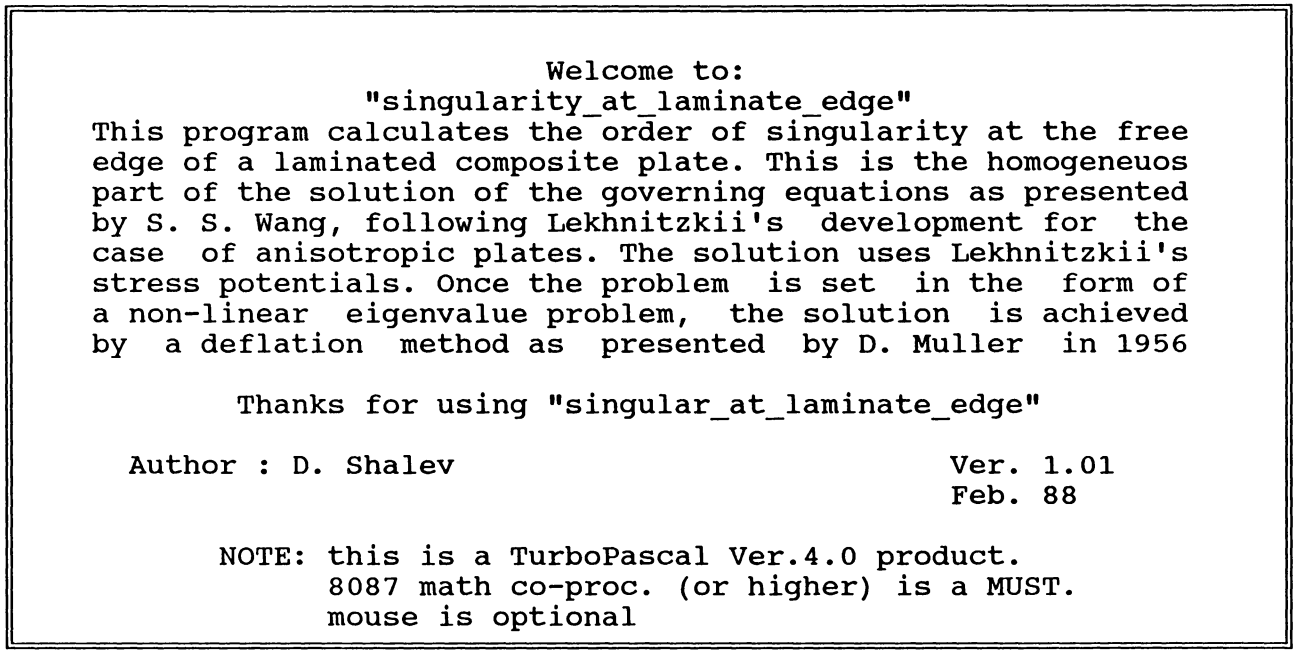


Figure No. B1: program "SINGULAR" - opening logo

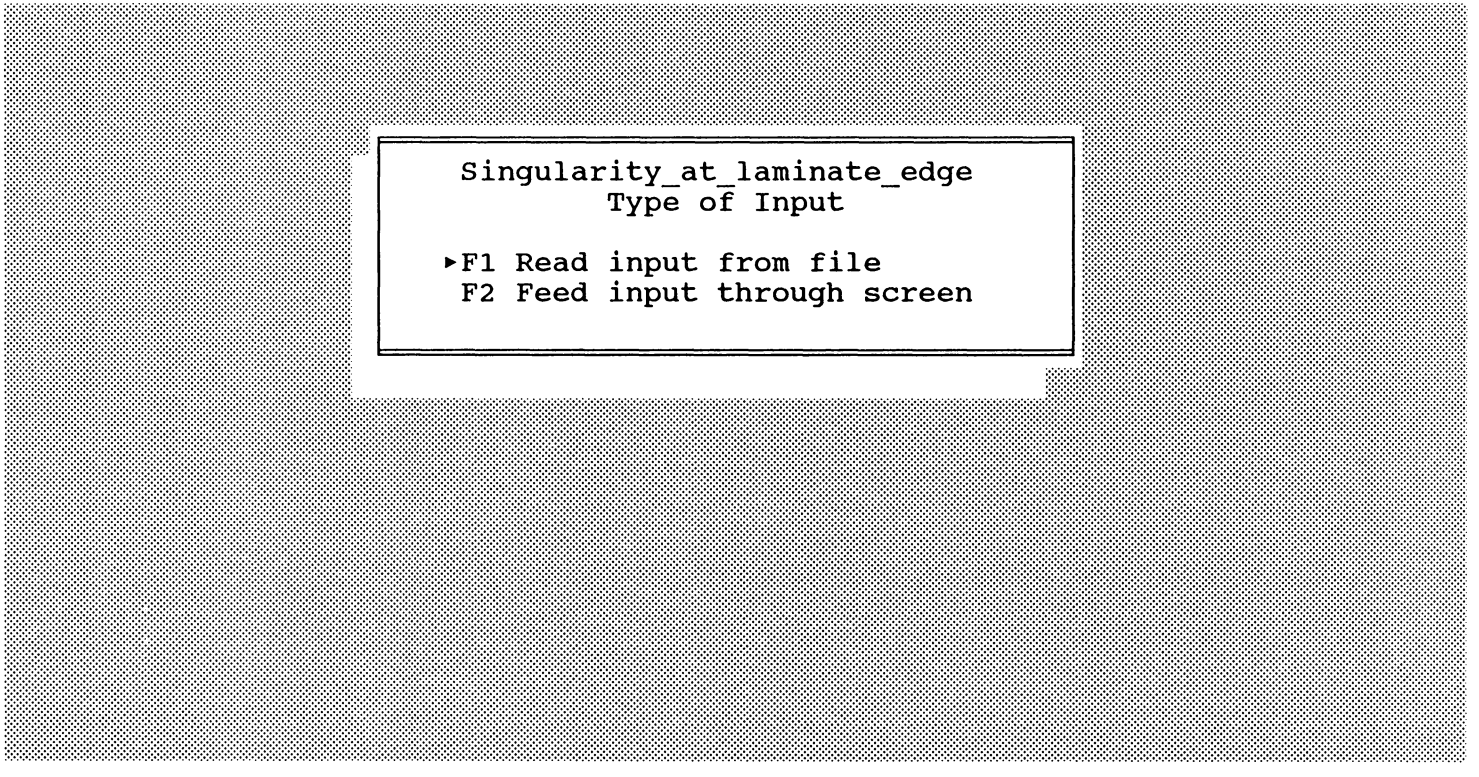


Figure No. B2: Chose input form

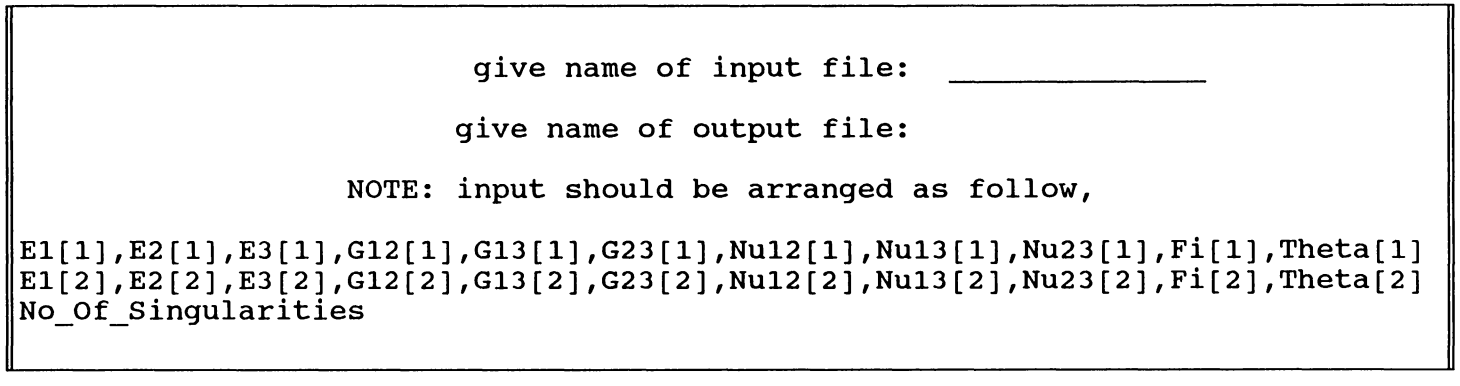


Figure No. B3: Chose input/output file names

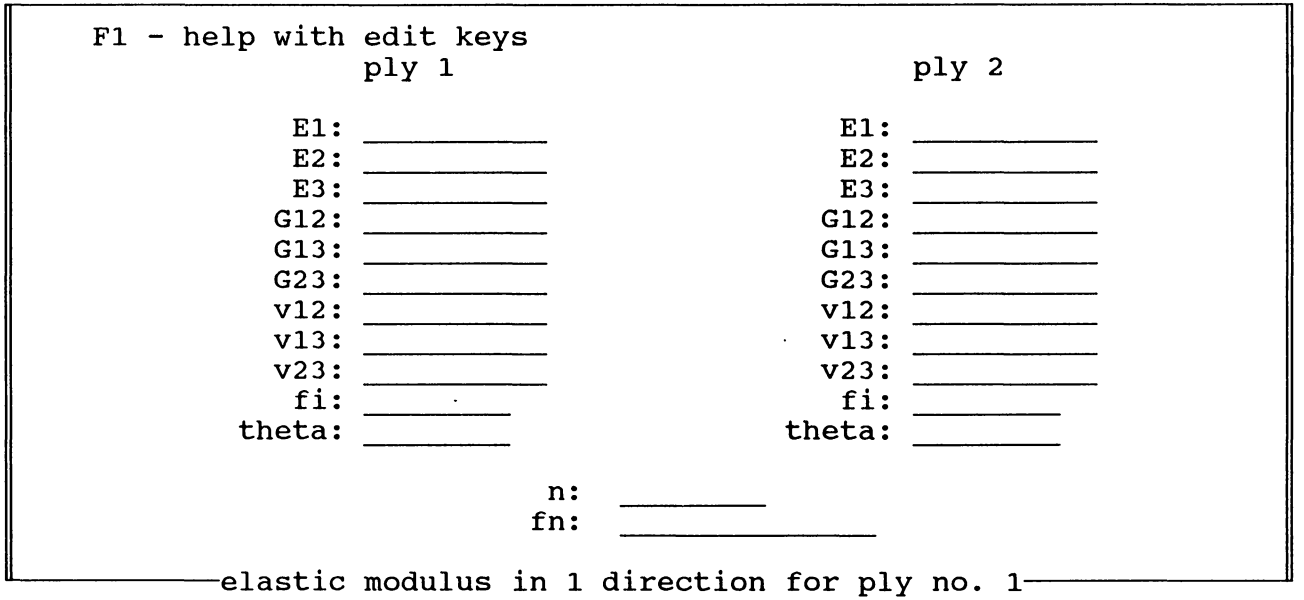


Figure No. B4: On-screen input process

B2 The output

Program "SINGULAR" results in one output file which contains a list which is the series of eigenvalues. The orders of singularity, following the above-described requirements, are marked for convenience.

Appendix C

PROGRAM "EDGSTR"

Program "EDGSTR" was developed on the Virginia Tech main-frame which is an IBM machine, using its vectorized option. The compiler used was a FORTRAN77 $2^{nd}$ generation called FORTVS2. This program uses the results of the analysis done by "SINGULAR", in terms of the series of eigenvalues, all the necessary materials and geometrical properties, and certain coefficients in a matrix form as obtained by "SINGULAR".

C1. Input file

The following is the structure of the input file for program "EDGSTR". Most of the input file is obtained automatically as an output file of the main-frame version of "SINGULAR". Few additions are required. The following is the complete structure.

| NDEL | INTEG |
|---|---|

NDEL - Number of eigenvalues to be used

INTEG - Number of integration points

| EE1 | EE2 | GG12 | NNI12 |
|---|---|---|---|

EE1 - effective modulus of the equivalent anisotropic laminate, dir. 1

EE2 - effective modulus of the equivalent anisotropic laminate, dir. 2

GG12 - effective modulus of the equivalent anisotropic laminate, dir. 12

NNI12 -effective poisson of the equivalent anisotropic laminate, dir. 12

| SZ | SX | SXZ | MZ | MX | MT |
|---|---|---|---|---|---|

SZ - external load in the longitudinal direction

SX - external load in the transverse direction

SXZ - external shear load

MZ - external longitudinal moment

MX - external transverse moment

MT - external torsional moment

| X1 | X2 | Y1 | Y2 | D | ALFA | XINIT |
|---|---|---|---|---|---|---|

note: refer to fig. 2 !

X1 - coordinate of -(e+2A)

X2 - coordinate of a

Y1 - Coordinate of b

Y2 - Coordinate of -c

D - hole diameter = 2A

ALFA - angle shows location around the hole w.r.t. the Z axis

XINIT - the distance from the edge were first value is to be calculated

The rest of the input is provided automatically as an output of "SINGULAR".

| E1 | E2 | E3 | G12 | G13 | G23 | NI12 | NI13 | NI23 | FI | THETA |
|---|---|---|---|---|---|---|---|---|---|---|

E1,E2,E3,G12,G13,G23,NI12,NI13,NI23 - elastic properties of the

unidirectional material of ply m

FI - fiber direction of ply m

THETA - angle of the free edge

S(i,j)

stiffness matrix of ply m

SBAR(i,j)

reduced stiffness matrix of ply m

MIU(i)

roots of the characteristic equation of ply m

ETA(i)

the ratios related to MIU(i) OF PLY M

H(i,j)

coefficients resulting from the analysis - refer to chapter 2

OMG(i)

coefficients resulting from the analysis - refer to chapter 2

the above curled parentheses are for ply m = 1,2

AKS(i,j)

transformation matrix which turns the problem from order of 12 to order of 6

| NDEL(i) |
|---|

the series of eigenvalues from the homogeneous solution.

The above is the structure of the input file. The next four pages are an example of such a file for the example illustrated in figs. 3 & 4.

```
27     100
.296359D+7 .296359D+7 .532918D+7 .743289
100.D0 0.D0 0.D0 0.D0 0.D0 0.D0
-10.5 9.5 -.015 .005 1.  0.00   1.D-8
   2.0000E+07    2.1000E+06    2.100E+06
   8.5000E+05    8.5000E+05    8.500E+05
   2.1000E-01    2.1000E-01    2.100E-01
   7.8563E-01    1.5707E+00
   0.8408E+01   -0.1105E+01   -0.3356E+01    0.0000E+00    0.4261E+01    0.0000E+00
  -0.1105E+01    0.9523E+01   -0.1105E+01    0.0000E+00   -0.1790E+01    0.0000E+00
  -0.3356E+01   -0.1105E+01    0.8408E+01    0.0000E+00    0.4261E+01    0.0000E+00
   0.0000E+00    0.0000E+00    0.0000E+00    0.2352E+02    0.0000E+00   -0.4441E-15
   0.4261E+01   -0.1790E+01    0.4261E+01    0.0000E+00    0.1094E+02    0.0000E+00
   0.0000E+00    0.0000E+00    0.0000E+00   -0.4441E-15    0.0000E+00    0.2352E+02
   0.7068E+01   -0.1544E+01    0.0000E+00    0.0000E+00    0.5963E+01    0.0000E+00
  -0.1546E+01    0.9378E+01    0.0000E+00    0.0000E+00   -0.1229E+01    0.0000E+00
   0.0000E+00    0.0000E+00    0.0000E+00    0.0000E+00    0.0000E+00    0.0000E+00
   0.0000E+00    0.0000E+00    0.0000E+00    0.2352E+02    0.0000E+00   -0.4440E-15
   0.5963E+01   -0.1229E+01    0.0000E+00    0.0000E+00    0.8783E+01    0.0000E+00
   0.0000E+00    0.0000E+00    0.0000E+00   -0.4440E-15    0.0000E+00    0.2352E+02
   0.0000E+00    0.3444E+01
   0.0000E+00    0.1035E+01
   0.0000E+00    0.8097E+00
   0.0000E+00   -0.3444E+01
   0.0000E+00   -0.1035E+01
   0.0000E+00   -0.8090E+00
   0.0000E+00   -0.3072E+01
   0.0000E+00    0.5584E+00
   0.0000E+00    0.2335E+00
   0.0000E+00    0.3072E+01
   0.0000E+00   -0.5584E+00
   0.0000E+00   -0.2335E+00
  -0.1186E+02    0.1201E-14   -0.1058E+02    0.5358E-15    0.2243E-14    0.3444E+01
  -0.1071E+01    0.3610E-15    0.5780E+00   -0.9738E-16    0.3612E-15    0.1035E+01
  -0.6545E+00    0.2821E-15    0.1881E+00   -0.4073E-16    0.2885E-15    0.8090E+00
  -0.1186E+02   -0.1201E-14   -0.1058E+02   -0.5358E-15    0.2243E-14   -0.3444E+01
  -0.1071E+01   -0.3610E-15    0.5780E+00    0.9738E-16    0.3612E-15   -0.1035E+01
  -0.6545E+00   -0.2821E-15    0.1889E+00    0.4074E-16    0.2885E-15   -0.8090E+00
   0.1743E-15    0.3444E+01
   0.1743E-15    0.1035E+01
   0.1743E-15    0.8090E+00
   0.1743E-15   -0.3444E+01
   0.1743E-15   -0.1035E+01
   0.1743E-15   -0.8090E+00
   2.0000E+07    2.1000E+06    2.1000E+06
   8.5000E+05    8.5000E+05    8.5000E+05
   2.1000E-01    2.1000E-01    2.1000E-01
  -7.8539E-01   -1.5707E+00
   0.8408E+01   -0.1105E+01   -0.3356E+01    0.0000E+00   -0.4261E+01    0.0000E+00
  -0.1105E+01    0.9523E+01   -0.1105E+01    0.0000E+00    0.1790E+01    0.0000E+00
  -0.3356E+01   -0.1105E+01    0.8408E+01    0.0000E+00   -0.4261E+01    0.0000E+00
   0.0000E+00    0.0000E+00    0.0000E+00    0.2352E+02    0.0000E+00    0.4440E-15
```

| | | | | | |
|---|---|---|---|---|---|
| -0.4261E+01 | 0.1790E+01 | -0.4261E+01 | 0.0000E+00 | 0.1094E+02 | 0.0000E+00 |
| 0.0000E+00 | 0.0000E+00 | 0.0000E+00 | 0.4440E-15 | 0.0000E+00 | 0.2352E+02 |
| 0.7068E+01 | -0.1546E+01 | 0.0000E+00 | 0.0000E+00 | -0.5963E+01 | 0.0000E+00 |
| -0.1546E+01 | 0.9378E+01 | 0.0000E+00 | 0.0000E+00 | 0.1229E+01 | 0.0000E+00 |
| 0.0000E+00 | 0.0000E+00 | 0.0000E+00 | 0.0000E+00 | 0.0000E+00 | 0.0000E+00 |
| 0.0000E+00 | 0.0000E+00 | 0.0000E+00 | 0.2352E+02 | 0.0000E+00 | 0.4440E-15 |
| -0.5963E+01 | 0.1229E+01 | 0.0000E+00 | 0.0000E+00 | 0.8783E+01 | 0.0000E+00 |
| 0.0000E+00 | 0.0000E+00 | 0.0000E+00 | 0.4440E-15 | 0.0000E+00 | 0.2352E+02 |
| 0.0000E+00 | 0.3444E+01 | | | | |
| 0.0000E+00 | 0.1035E+01 | | | | |
| 0.0000E+00 | 0.8090E+00 | | | | |
| 0.0000E+00 | -0.3444E+01 | | | | |
| 0.0000E+00 | -0.1035E+01 | | | | |
| 0.0000E+00 | -0.8090E+00 | | | | |
| 0.0000E+00 | 0.3072E+01 | | | | |
| 0.0000E+00 | -0.5584E+00 | | | | |
| 0.0000E+00 | -0.2335E+00 | | | | |
| 0.0000E+00 | -0.3072E+01 | | | | |
| 0.0000E+00 | 0.5584E+00 | | | | |
| 0.0000E+00 | 0.2335E+00 | | | | |
| -0.1186E+02 | -0.1201E-14 | -0.1058E+02 | -0.5358E-15 | -0.2243E-14 | 0.3444E+01 |
| -0.1071E+01 | -0.3610E-15 | 0.5780E+00 | 0.9738E-16 | -0.3612E-15 | 0.1035E+01 |
| -0.6545E+00 | -0.2821E-15 | 0.1889E+00 | 0.4073E-16 | -0.2885E-15 | 0.8090E+00 |
| -0.1186E+02 | 0.1201E-14 | -0.1058E+02 | 0.5358E-15 | -0.2243E-14 | -0.3444E+01 |
| -0.1071E+01 | 0.3610E-15 | 0.5780E+00 | -0.9738E-16 | -0.3612E-15 | -0.1035E+01 |
| -0.6545E+00 | 0.2821E-15 | 0.1889E+00 | -0.4073E-16 | -0.2885E-15 | -0.8090E+00 |
| 0.1743E-15 | -0.3444E+01 | | | | |
| 0.1743E-15 | -0.1035E+01 | | | | |
| 0.1743E-15 | -0.8090E+00 | | | | |
| 0.1743E-15 | 0.3444E+01 | | | | |
| 0.1743E-15 | 0.1035E+01 | | | | |
| 0.1743E-15 | 0.8090E+00 | | | | |
| 0.5840E-01 | 0.0000E+00 | 0.3702E+00 | 0.0000E+00 | 0.1881E+00 | 0.0000E+00 |
| 0.2220E-15 | 0.0000E+00 | 0.1991E+00 | 0.0000E+00 | 0.1165E+00 | 0.0000E+00 |
| 0.5800E+01 | 0.0000E+00 | -0.6210E+00 | 0.0000E+00 | -0.7720E+00 | 0.0000E+00 |
| -0.3119E+01 | 0.0000E+00 | -0.1221E-14 | 0.0000E+00 | -0.9468E-01 | 0.0000E+00 |
| -0.4571E+01 | 0.0000E+00 | 0.1198E+01 | 0.0000E+00 | 0.1562E+01 | 0.0000E+00 |
| 0.2832E+01 | 0.0000E+00 | -0.1468E+00 | 0.0000E+00 | 0.5689E-15 | 0.0000E+00 |
| 0.3330E-15 | 0.0000E+00 | 0.1991E+00 | 0.0000E+00 | 0.1165E+00 | 0.0000E+00 |
| 0.5840E-01 | 0.0000E+00 | 0.3702E+00 | 0.0000E+00 | 0.1881E+00 | 0.0000E+00 |
| -0.3119E+01 | 0.0000E+00 | -0.1249E-14 | 0.0000E+00 | -0.9468E-01 | 0.0000E+00 |
| 0.5800E+01 | 0.0000E+00 | -0.6210E+00 | 0.0000E+00 | -0.7720E+00 | 0.0000E+00 |
| 0.2832E+01 | 0.0000E+00 | -0.1468E+00 | 0.0000E+00 | 0.1054E-14 | 0.0000E+00 |
| -0.4571E+01 | 0.0000E+00 | 0.1198E+01 | 0.0000E+00 | 0.1562E+01 | 0.0000E+00 |

| | |
|---|---|
| -0.02557566 | 0.00000000 |
| 0.00000000 | 0.00000000 |
| 0.88147184 | -0.23400497 |
| 0.88147184 | 0.23400497 |
| 1.00000000 | 0.00000000 |
| 1.51152634 | -0.79281732 |
| 1.51152634 | 0.79281732 |
| 2.00000000 | 0.00000000 |

| | |
|---|---|
| 2.33894332 | -1.11584015 |
| 2.33894332 | 1.11584015 |
| 3.00000000 | 0.00000000 |
| 3.09135317 | 1.73604639 |
| 3.09135317 | -1.73604639 |
| 3.95200232 | -2.02871459 |
| 3.95200232 | 2.02871459 |
| 4.00000000 | 0.00000000 |
| 4.74409286 | -2.56838712 |
| 4.74409286 | 2.56838712 |
| 5.00000000 | 0.00000000 |
| 5.60214568 | -2.85885102 |
| 5.60214568 | 2.85885102 |
| 6.00000000 | 0.00000000 |
| 6.39626347 | -3.36527066 |
| 6.39626347 | 3.36527066 |
| 7.00000000 | 0.00000000 |
| 7.25651744 | -3.65759372 |
| 7.25651744 | 3.65759372 |
| 8.00000000 | 0.00000000 |
| 8.04972367 | -4.14799835 |
| 8.04972367 | 4.14799835 |
| 8.91205666 | -4.44076090 |
| 8.91205666 | 4.44076090 |
| 9.00000000 | 0.00000000 |
| 9.73970143 | 4.82743595 |
| 9.73970143 | -4.82743595 |
| 10.00000000 | 0.00000000 |
| 10.56741699 | 5.21487347 |
| 10.56741699 | -5.21487347 |
| 11.00000000 | 0.00000000 |
| 11.35762857 | -5.69087082 |
| 11.35762857 | 5.69087082 |
| 12.00000000 | 0.00000000 |
| 12.22198471 | 5.98346243 |
| 12.22198471 | -5.98346243 |
| 13.00000000 | 0.00000000 |
| 13.01073907 | -6.45620072 |
| 13.01073907 | 6.45620072 |
| 14.00000000 | 0.00000000 |
| 15.00000000 | 0.00000000 |
| 16.00000000 | 0.00000000 |
| 16.31465057 | -7.98135589 |
| 16.31465057 | 7.98135589 |
| 17.00000000 | 0.00000000 |
| 17.96561409 | -8.74253387 |
| 17.96561409 | 8.74253387 |
| 18.00000000 | 0.00000000 |
| 19.00000000 | 0.00000000 |
| 20.00000000 | -0.00000039 |
| 21.00000000 | 0.00000001 |
| 22.00000000 | 0.00000000 |

| | |
|---|---|
| 23.00000000 | 0.00000000 |
| 24.00000000 | 0.00000000 |
| 25.00000000 | 0.00000000 |
| 26.00000000 | 0.00000000 |
| 27.00000000 | 0.00000000 |
| 28.00000000 | 0.00000000 |
| 30.00001594 | -0.00000364 |
| 31.00011385 | -0.00028805 |
| 31.99647973 | 0.00133420 |
| 33.00003421 | -0.00268296 |
| 33.99869664 | -0.09253746 |
| 35.01203137 | -0.01801228 |
| 35.45796921 | 1.11312978 |
| 35.51097827 | 0.36380948 |
| 35.89506577 | -1.61654381 |

C2 Output file

The output file consists of the following structure. First, there are all the unknown coefficients of the particular and homogeneous parts of the solution. Next are the eigenvectors of the homogeneous solution. Next are the near-field parameters which are the eigenvectors multiplied by the first coefficient of the homogeneous solution. Last listed the stresses. Each line consists of three numbers. The first is an integer indicates the stress following the Greek notation. The second number is the coordinate along the interface going from the hole outward. The third number is the magnitude of the relevant stress.

The vita has been removed from the scanned document